AMERICAN UNIVERSITY OF BEIRUT

EXPERIMENTAL AND THEORETICAL INVESTIGATION OF THE TRANSITION FROM BANDS TO 2D SQUARES/HEXAGONS AND 3D TURING PATTERNS IN THE CADMIUM SULFIDE PRECIPITATION REACTION-DIFFUSION SYSTEM

by

MALAK HASSAN DAYEH

A thesis
submitted in partial fulfillment of the requirements
for the degree of Master of Science
to the Department of Chemistry
of the Faculty of Arts and Sciences
at the American University of Beirut

Beirut, Lebanon
July 2014

AMERICAN UNIVERSITY OF BEIRUT

EXPERIMENTAL AND THEORETICAL INVESTIGATION OF THE TRANSITION FROM BANDS TO 2D SQUARES/HEXAGONS AND 3D TURING PATTERNS IN THE CADMIUM SULFIDE PRECIPITATION REACTION-DIFFUSION SYSTEM

by

MALAK HASSAN DAYEH

Approved by:

_____

Dr. Mazen Al-Ghoul, Professor   Advisor
Chemistry

_____

Dr. Rabih Sultan, Professor   Committee Member
Chemistry

_____

Dr. Michel Kazan, Assistant Professor   Committee Member
Physics

Date of thesis defense: July 31, 2014

AMERICAN UNIVERSITY OF BEIRUT

THESIS, DISSERTATION, PROJECT RELEASE FORM

Student Name: ___Dayeh_____Malak_____Hassan_____
Last   First   Middle

(X) Master's Thesis   ◯ Master's Project   ◯ Doctoral Dissertation

☐   I authorize the American University of Beirut to: (a) reproduce hard or electronic copies of my thesis, dissertation, or project; (b) include such copies in the archives and digital repositories of the University; and (c) make freely available such copies to third parties for research or educational purposes.

☐   I authorize the American University of Beirut, **three years after the date of submitting my thesis, dissertation, or project,** to: (a) reproduce hard or electronic copies of it; (b) include such copies in the archives and digital repositories of the University; and (c) make freely available such copies to third parties for research or educational purposes.

_Malak Dayeh_____August 8, 2014_____

Signature   Date

ACKNOWLEDGEMENTS

AN ABSTRACT OF THE THESIS OF

<u>Malak Hassan Dayeh</u>   for   <u>Master of Science</u>
<u>Major</u>: Chemistry

Title: <u>Experimental and theoretical investigation of the transition from bands to 2d squares/hexagons and 3d Turing patterns in the cadmium sulfide precipitation reaction-diffusion system</u>

Spatiotemporal pattern formation in precipitation reaction-diffusion (RD) systems was first observed as concentric rings by R. E. Liesegang in 1896. Later on, other structures have been reported, including: directly spaced rings, the unusual revert spacing, secondary structures, fractals, spirals (2D), helices (3D) and other features.

In our work, we study for the first time the formation of new precipitation patterns in two and three dimensions. Our system consists of diffusing sodium sulfide into a gel matrix containing dissolved cadmium (II) ions. When performed in a planar reactor (2D), the white cadmium hydroxide $Cd(OH)_2$ precipitation occurs parallel to the diffusion front and takes the form of spaced dots with squared/hexagonal symmetry. A yellow back front follows the evolution of the system due to the formation of the yellow cadmium sulfide CdS resulting from the anionic exchange between OH^- and S^{2-} ions. On the other hand, in (3D) the system exhibits more complex patterns due to the stacking of layers of the (2D) patterns along the third dimension. These (3D) patterns exhibit Turing-like behavior.

We intend to study the effect of different variables on the morphology of the patterns, including the concentration of inner and outer electrolytes, temperature, thickness of the gel, addition of capping agents, variation of ionic strength, and application of a static electric field. We also plan to investigate theoretically and numerically the spatiotemporal dynamics of the obtained patterns. In that regard, we will invoke the Cahn-Hilliard equation in the description of the precipitate pattern formation whereby the colloidal product resulting from the reaction of the diffusing electrolytes undergo spinodal decomposition followed by an Ostwald ripening scenario. The resulting evolution equations will be solved numerically using the Finite Element Method (FEM), which provides flexibility to solve these equations on domains with complex geometries.

CONTENTS

ILLUSTRATIONS

CHAPTER I

INTRODUCTION

A. Introduction

Pattern formation in self-organizing systems has been a subject of extensive research in many fields of science[1] and over a wide range of length scales[2]. It can be defined as the appearance of an array of organized macroscopic structures repeating with a defined or undefined symmetry[1], without the intervention of externally imposed conditions. This beautiful phenomenon has long intrigued scientists and triggered their curiosity to search for analogies in the real natural world (Fig. 1). It is broadly observed in chemistry (e.g. oscillating reactions and precipitating patterns)[3, 4, 5], physics (e.g. structure formation in astrophysics and convective patterns in fluids)[6, 7], biology (e.g. pattern formation in cells, nerve and cardiac systems, calcium waves)[8, 9, 10, 11], and geology (e.g. bands observed in a wide variety of rocks and the stratifications in the agate structure)[12, 13, 14]. Such organized patterns normally arise in open systems maintained far from equilibrium[15], and their study constitutes a new branch of research known as "Nonlinear Science".

An interesting example of self-organization in systems far from equilibrium is the periodic precipitation patterns formed in the wake of a moving chemical reaction front. This exciting observation was first discovered by the German chemist, Raphael Eduard Liesegang in 1896[16, 17], when he accidentally dropped a solution of silver nitrate ($AgNO_3$) on a thin layer of gelatin containing potassium dichromate ($K_2Cr_2O_7$). After a few hours, concentric rings of silver dichromate were produced[18] (Fig. 2). Although Liesegang realized that the formation of these patterns was related to the movement of molecules or ions with respect to one another, yet he was unable to explain the origin

1

of this surprising aspect, and his finding remained a scientific curiosity. Inspired by this result, scientists then tried other scarcely soluble electrolytes[19, 20], and different structures have been experimentally observed and reported; these include: bands with direct spacing[21], the unusual bands with revert spacing[22, 23, 24], bands with secondary structures[25], fractals[26], spirals[27], and 3D helices[28] (Fig. 3).
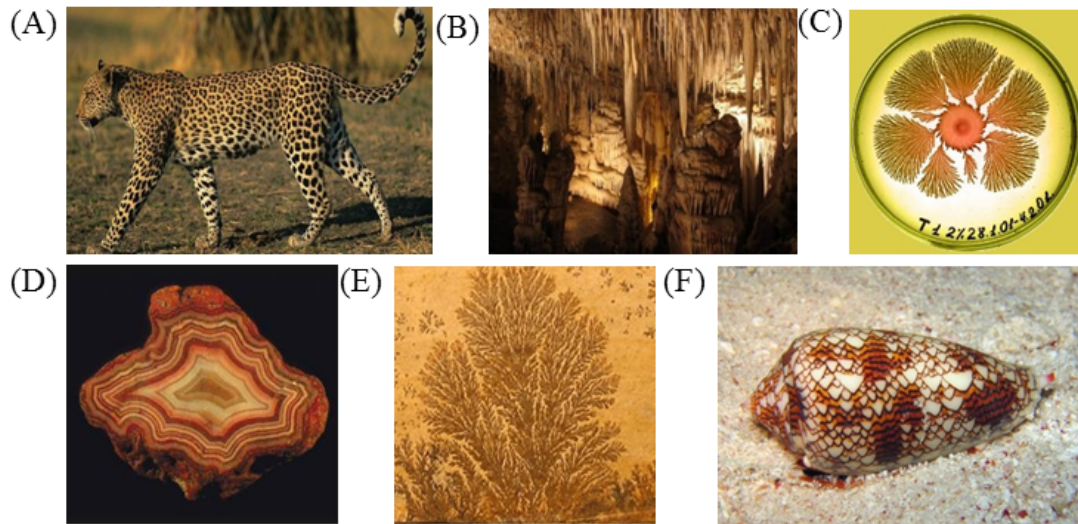
Figure 1: Examples of patterns obtained in nature that can be described in reaction-diffusion systems: (A) Turing patterns on a leopard [11]. (B) Jeita grotto stalactites (Courtesy of jeitagrotto.com). (C) Growth of a bacterial colony [2]. (D) A polished cross-section of a fortificated agate (Courtesy of agatelady.com). (E) Fractals formation on limestone [29]. (F) Patterns formed by reaction-diffusion on the seashell [30].

The ability to recreate life-like behavior in a test tube aroused the interest of chemists, biologists, physicists, mathematicians and engineers who teamed up to explore new type of reactions in motion[32]. Many theoretical studies then caught up, and new fields of science, particularly nonlinear chemical dynamics and kinetics, flourished. Computational resources and mathematical tools became also available to explain and model many puzzling phenomena, such as cave stalactites[33, 34], stripes or spots on animal surfaces[35], layered texture of agates [36], bacterial colonies[37], and several body activities including calcium signals travelling within cells and impulses within nervous system[11]. Such advances made reaction-diffusion systems a key element to the world evolution, and they were no more considered as a scientific oddity.
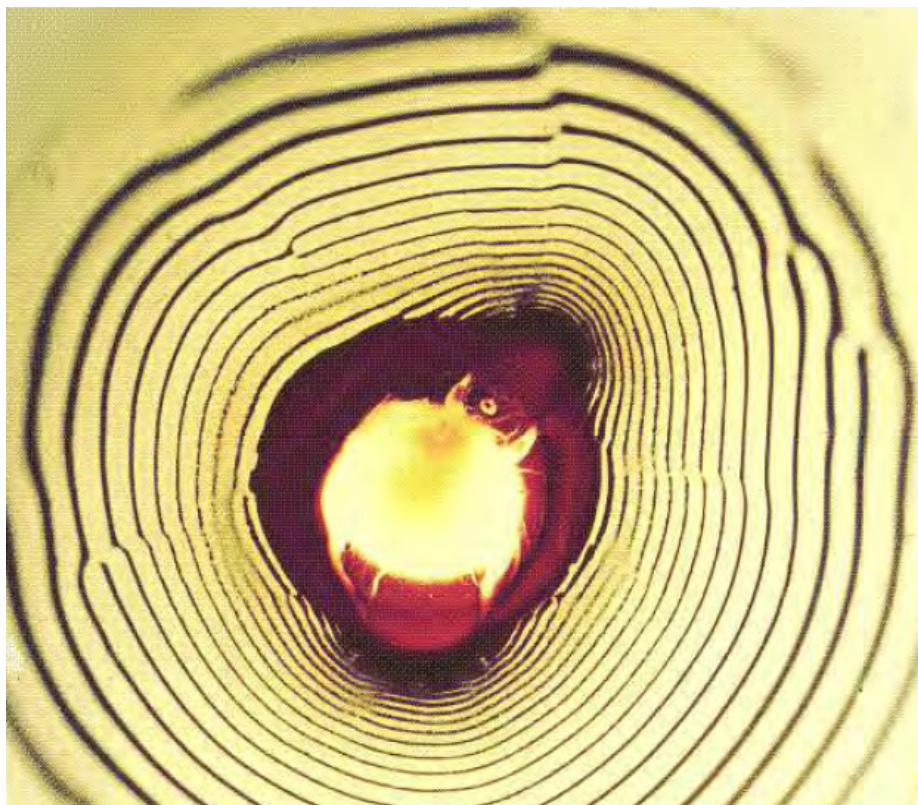
Figure 2: Periodic Liesegang rings appearing in silver dichromate system in gelatin gel[31].

Despite all this undeniable success, pattern formation in chemical systems has not been widely applied in modern technology due to the difficulty in bringing them under experimental control, especially at small scales. Reaction-diffusion systems have the ability to design new constructions and generate structures with significantly small dimensions, which makes them very suitable to be applied in micro- and nanotechnology. Therefore, applying and controlling chemistry in motion in a suitable way allows not only discoveries of new phenomena, but also designing practically important micro- and nano-structures without the interference of humans.

Although the interest in self-organization and pattern formation has been significantly increasing, and it has become a challenging task for scientists to present mechanisms to explain the dynamic laws governing their behavior, some scientists were not convinced. For them, the self-organization property of non-equilibrium systems constitutes a violation to the second law of thermodynamics, which states that the universe

3
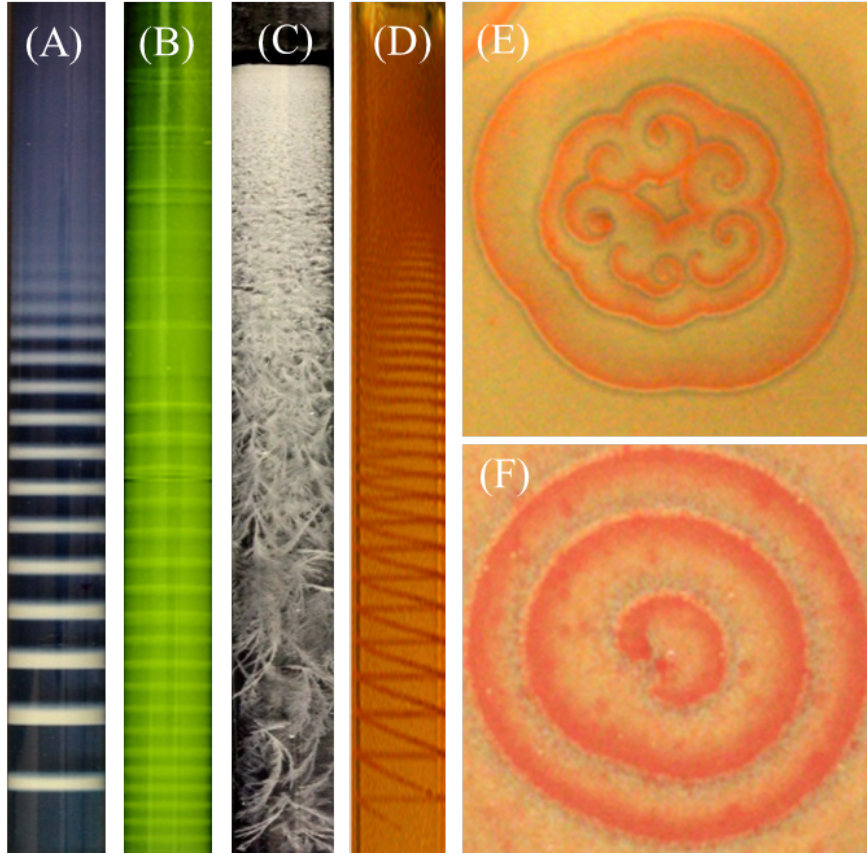
Figure 3: Different Liesegang patterns grown in gels for several sparingly soluble salts: (A) Direct spacing in $Ni(OH)_2$ system; (B) Revert spacing in CdS system; (C) Fractals in $La_2(C_2O_4)_3$ system; (D) Helicoidal pattern in $CuCrO_4$. (E) Spirals and (F) Ripples in HgI_2 system.

evolves towards a state of maximum entropy after any spontaneous change:

$$\Delta S_{total} = \Delta S_{system} + \Delta S_{surroundings} > 0. \tag{1}$$

In an attempt to explain the non-equilibrium behavior of chemical systems, Prigogine and his coworkers[15] in Brussels showed that self-organization phenomena are governed by the laws of non-equilibrium thermodynamics[5]. They pointed out that open systems exhibiting spontaneous self-organization are said to be dissipative systems due to the constant dissipation of free energy to the surroundings[38]. Hence, spatiotemporal patterns that form in an ordered fashion are called dissipative structures. The decrease in entropy of a system due to self-organization is therefore overcompensated by increasing the en-

tropy of the surroundings, and this refutes the doubt about the validity of the second law.

A wide spectrum of theoretical investigations was then proposed to study the evolution of Liesegang patterns. It can generally be classified into classes: the pre-nucleation and the post-nucleation theories. Both scenarios involve the essential processes of diffusion and precipitation, but each has its advantages and limitations.

B. Theories Governing Liesegang Phenomena

Many theories have been tailored to investigate the mechanism behind periodic precipitation phenomena and its complex dynamics; yet, there has never been any single universal theory able to explain comprehensively every experimental finding. However, it is possible to regroup the most thoroughly discussed theories into two main categories:

- Pre-nucleation theories based on Ostwald's supersaturation theory[39, 40, 41, 42]

- Post-nucleation theories based on Ostwald ripening[24, 43, 44]

1. Pre-Nucleation Theories

In 1897, shortly after the appearance of Liesegang's original paper[16], the first model attempting to explain periodic precipitation mechanism was published by the famous German chemist, Wilhelm Ostwald[45]. This model considers band formation as a spatially discontinuous nucleation process, whereby the interdiffusing reagents yield precipitation bands without the formation of any intermediate compound $(A + B \rightarrow P)$. According to this theory, precipitation is not an equilibrium process, and it does not form immediately upon the diffusion of the outer electrolyte (A) into the gel containing the inner electrolyte (B), until the solution is supersaturated. This means that at a certain position (x), the local concentration product of the reactants $a(x,t)b(x,t)$ has to reach the

so-called solubility product (K_{sp}) or the nucleation threshold of precipitation, p^*. The resulting equation from the supersaturation assumption at time t and position x can be written as follows:

$$a(x,t)\,b(x,t) \geq p^*$$ (2)

After supersaturation, nucleation of the precipitate P is initiated, and the nucleated particles grow and deplete the electrolytes A and B in the surroundings, thus allowing the formation of the first precipitate band and leaving a free space around it. Consequently, the local concentration product (ab) drops in the vicinity of the band, and nucleation is suppressed. As time proceeds, the diffusion of A continues until it again surpasses the threshold value at a certain position and triggers the formation of a new band. The repetition of this scenario, known as the Ostwald supersaturation-nucleation-depletion cycle, leads to the alternation of precipitate filled and precipitate void domains with increasing band spacing due to the dilution of the diffusing outer electrolyte (A) with time. Calculations based on Ostwald's supersaturation theory were carried out by Wagner[46], whose model was able to reproduce the obtained rhythmic precipitation banding and the spacing law to be described in the coming section. However, the first coherent mathematical formulations and semianalytical investigations of the problem were performed by Prager[39], and later reformulated and simplified by Zeldovich[47], as well as by Antal and Rácz[48]. A simple reaction-diffusion model resulting from the supersaturation assumption given in (1.2) can be described by the following evolution equations:

$$\frac{\partial a}{\partial t} = D_a \frac{\partial^2 a}{\partial x^2} - k\theta\,(ab - p^*) - \lambda abp,$$ (3)

$$\frac{\partial b}{\partial t} = D_b \frac{\partial^2 b}{\partial x^2} - k\theta\,(ab - p^*) - \lambda abp,$$ (4)

$$\frac{\partial p}{\partial t} = k\theta\,(ab - p^*) + \lambda abp,$$ (5)

where D_a and D_b are the diffusion constants of A and B, $\theta(x)$ is the step function describing an infinitely sharp threshold for precipitation with rate constant k, and λ is the rate constant of aggregation having large values to deplete B after a precipitation band formation.

The concentration profiles can be approximated as follows:

$$a(x,t) = a_0 \left(1 - \frac{x}{\sqrt{2D_a t}} \right),$$ (6)

$$b(x,t) = \frac{b_0}{\sqrt{2D_b(t-t_n)}}(x-x_n),$$ (7)

where x_n is the position of the band n, and t_n is the time required for its appearance. Figure 4 represents the concentration profiles of a and b, and their ion-product concentration ab after the appearance of the nth band, and just prior the formation of the $(n+1)^{th}$ band.
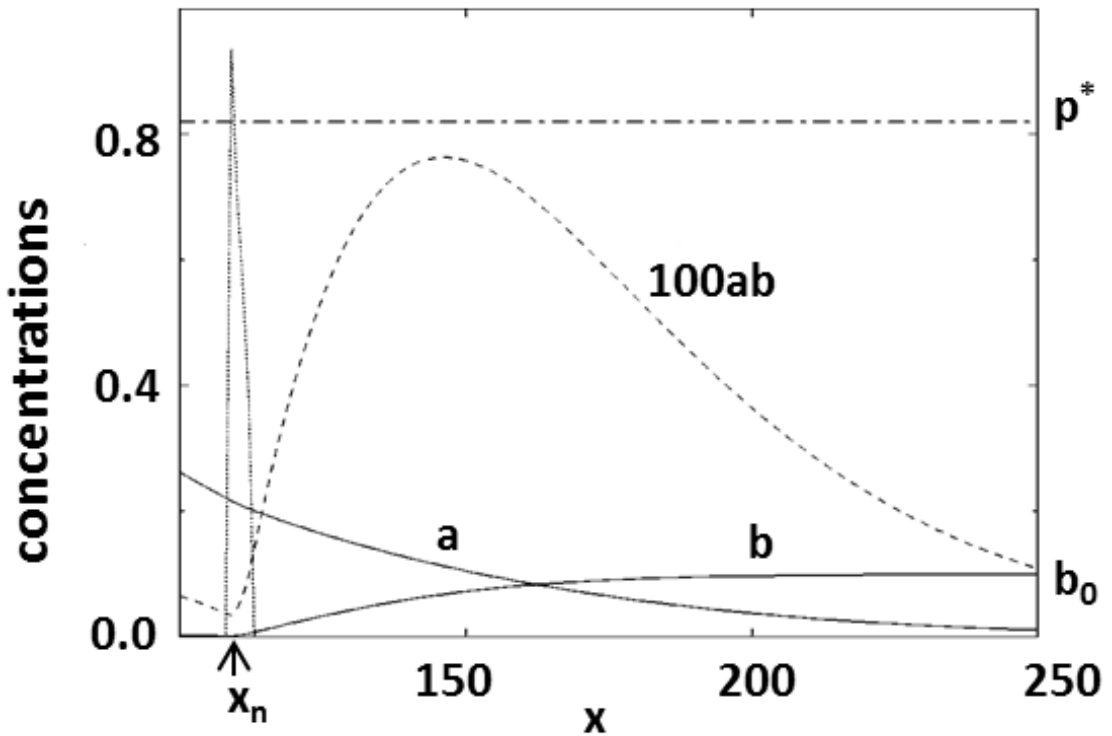
Figure 4: Computer simulation of the concentration profiles of a, b and the ion-product concentration ab in the supersaturation theory of the Liesegang banding. p^* represents the precipitation threshold, and x_n is the position of the band n[48].

At a first glance, Ostwald-Wagner-Prager theory appears to agree very well with the experimental observations, and it has been widely considered as the most accepted theory explaining Liesegang phenomena. However, some experimental observations in a broad class of precipitation systems raised some questions about its validity and applicability. One of the drawbacks in this theory is that it is unable to predict secondary banding[25] (rings break up into thinner ones) and to explain revert spacing[24] (decrease in band spacing away from the origin of an imposed gradient). Also it fails to explain the pattern formation obtained from an initially uniform dispersion of a precipitate in a gel medium[49].

2. Post-Nucleation Theories

a. Competitive Particle Growth

In order to overcome the difficulties outlined in the previous section, Feinn *et al.*[43, 50] proposed a new model based on chemical instability, generally referred to as the *Competitive Particle Growth model (CPG).* In this theory, the obtained sol after diffusion evolves through a competing mechanism between particles of different sizes, whereby large particles grow at the expense of smaller ones. This stems from the fact that small particles are more soluble than larger particles due to their higher surface energy. Thus, they tend to dissolve and diffuse towards the larger particles to decrease the total energy of the system. The evolution of the system will end up in a state of larger but fewer particles, and this is known as the Ostwald ripening scenario[45, 51]. The formation of periodic precipitation bands occurs through a focusing mechanism[52], where large particles aggregate, leaving clear zones that are depleted in small particles in the surrounding regions. In 1961, Lifshitz and Slyozov[51] provided a mathematical approach for the obtained phenomena in an attempt to find the average drop size of the growing particles.

The equation shows that the radius of the particle grows as one-third power of time:

$$R(t) \sim (D\gamma t)^{1/3}, \tag{8}$$

where $R(t)$ is the average radius of the particle, D represents the diffusion coefficient, γ is the interfacial tension of the particle, and t is the time.

b. Nucleation and Growth

Another often-applied theory in the post-nucleation mechanism is known as the theory of *Nucleation and Growth*[48]. The sequence of events proposed by this mechanism is that after the diffusion of the outer electrolyte (A) into the gel medium containing the inner electrolyte (B), and when the local concentration product $a(x,t)b(x,t)$ is greater than the solubility product (K_{sp}), the formation of a spatially homogeneous colloidal set of particles (C) takes place. The formation of colloids was also confirmed by Hedges and Henley[53] for many interacting salt systems. These created C molecules are then free to move until their local concentration c reaches a threshold value c^*. After that, nucleation starts, followed by the aggregation of C into an immobile precipitate P $(A + B \rightarrow C \rightarrow P)$. Precipitation continues until the concentration of C drops below another threshold p^*. This model is therefore characterized by two thresholds; one for nucleation and the other for droplet growth.

Although the mechanism of Liesegang pattern is explained based on the above-mentioned theories, Müller and Polezhaev[54, 55] proposed a model that takes into consideration all the processes of supersaturation, competition of nucleation rates, and the growth of large particles at the expense of dissolution of smaller ones. The strength of this model lies in its ability to explain non-trivial patterns obtained experimentally, such as radial dislocations of ring structures in a Petri dish[56], spirals[27] or helical patterns[28], and "Saturn-rings" in a test tube[39]. However, it fails to explain the formation of sec-

ondary structures within already formed bands and the stochastic pattern formation for low initial concentrations.

c. Turing Instability

Based on the same concept of nucleation of colloids prior to pattern formation, the *Autocatalytic Growth model*[24] was set forth by Flicker and Ross. They assumed that prior to band formation, a homogeneous solution of colloidal particles surrounded by electric double layers is obtained. The process can be summarized as:

$$pA + qB \overset{k_1}{\rightleftharpoons} C \tag{9}$$

where p and q are integers. Once C particles are formed they become charged. The primary charge of C is then neutralized by a diffuse layer of ions predominantly of a sign opposite to that of the primary layer, in addition to some ions with similar charges resulting from the interpenetrating distribution of ions. Using primes to symbolize colloidal particles with different ionic environments, the process can be written as:

$$C + B \underset{k_{-2}}{\overset{k_2}{\rightleftharpoons}} C' \tag{10}$$

$$C + A \underset{k_{-3}}{\overset{k_3}{\rightleftharpoons}} C'' \tag{11}$$

For simplification, the charged and uncharged colloidal particles are approximated by C. Due to the interaction of the double layers of the colloids, the concentration of ions in the double layer increases. In addition, there is evidence that ions within the double layer have diffusion coefficients lower than that in the bulk[57]. Both of these effects lead to the increase of the density of the colloidal particles until it surpasses a certain critical value. As a result, these particles auto-catalyze their own growth and the formation of

new colloidal particles[58]:

$$C + p'A + q'B \overset{k_4}{\rightleftharpoons} 2C \tag{12}$$

where p' and q' are integers. Coupling the kinetics of this autocatalytic growth model to diffusion leads to equations that give rise to the possibility of the growth of macroscopic structures even in the absence of external gradients[50, 59]. The entire set of reaction-diffusion processes can be represented by:

$$\frac{\partial C}{\partial t} = D_c \frac{\partial^2 C}{\partial x^2} + k_1 A^p B^q + k_4 A^{p'} B^{q'} C \tag{13}$$

$$\frac{\partial A}{\partial t} = D_a \frac{\partial^2 A}{\partial x^2} - pk_1 A^p B^q - p'k_4 A^{p'} B^{q'} C - k_3 CA + k_{-3} C \tag{14}$$

$$\frac{\partial B}{\partial t} = D_b \frac{\partial^2 B}{\partial x^2} - qk_1 A^p B^q - q'k_4 A^{p'} B^{q'} C - k_2 CB + k_{-2} C \tag{15}$$

The analysis of the reaction-diffusion equations postulates that imposing an external gradient might alter the shape of the spatial structure, but it is not the main reason for the formation of that structure. These predictions were confirmed by experiments performed on lead iodide (PbI_2)[60]. The colloidal formation mechanism could also prove successfully the secondary structures of precipitating bands, and the revert spacing in some systems such as ferrous ferricyanide ($Fe_3[Fe(CN)_6]_2$)[24], silver iodide (AgI)[23], and cadmium sulfide (CdS)[61].

As most of the systems in Liesegang phenomena exhibit spatially static patterns, in the sense that they are locked in space once they are formed, Ross and co-workers[24, 60, 62] considered Liesegang structures as a physical example of Turing-type patterns[63]. The latter are stationary periodic concentration structures originating in the sole coupling of reaction and diffusion processes without the interference of convection[38]. The word "stationary" in Turing's work does not necessarily require the obtained pattern to be stationary in time, but rather in space. Experiments indicate

11

evidences for developing time-dependent[24] and time-independent[64, 65] Turing structures. Besides, for a pattern to qualify as a Turing pattern, the system must have a spatially uniform steady state that is stable to any spatially homogeneous infinitesimal perturbation, but allows certain spatially nonuniform perturbations of particular symmetry to grow rather than decay. Therefore, the formation of a Turing pattern is a symmetry-breaking phenomenon.

In 1952, Alan Turing[63] suggested a possible connection between patterns in biological systems and patterns that could form spontaneously in chemical reaction-diffusion systems. He established the theoretical possibility that chemical systems with an autocatalytic step (or feedback–retroaction loop) in their reaction mechanism[66], having appropriate nonlinear kinetics, and containing activator and inhibitor species diffusing with different mobilities, might give rise to spontaneous pattern formation of the type encountered in living organisms. Examples of such Turing patterns include the formation of spots or stripes on animal coat (zebras, giraffes, tigers, seashells, tropical fish [11, 35]), the division and differentiation of spherically symmetric fertilized egg into many different kinds of cells present in an adult organism, the classification of right and left-handed organisms with bilateral or left-right symmetry, the arrangement of leaves on the stems of plants [63], etc. . . .

Turing's main goal was not to describe morphogenesis quantitatively, but rather to discover a clear plausible mechanism that could teach scientists how to think about pattern formation and complex phenomena. Despite the profound effect Turing's theory had, and the huge theoretical work it stimulated, the experimental confirmation of this phenomena didn't appear until the year 1990, when De Kepper and colleagues in Bordeaux reported the first evidence of a Turing structure in the well-known chlorite-iodide-malonic acid (CIMA) reaction[64, 67, 68]. A rich variety of the stationary spatial structures – hexagonal arrays of spots, labyrinthine arrangements of stripes, and mixed states – were observed[68] (Fig. 5). These patterns possess an intrinsic wavelength that

12
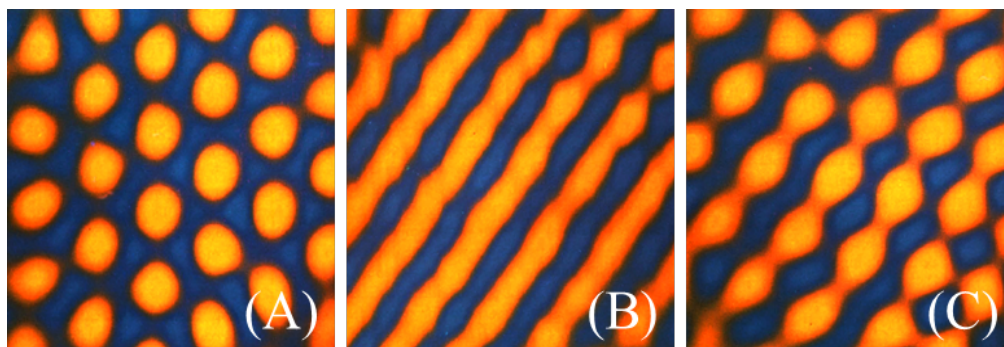
Figure 5: Turing structures obtained in the CIMA reaction[68]: (A) Hexagons (B) Stripes (C) Mixed state.

depends only on the diffusion coefficients, kinetic constants, and concentration of some control species in the reaction, and not on the geometry of the system. Later on, this work was extended and verified using different reactor configurations[69, 70, 71].

The difficulty in satisfying all the criteria required for pattern formation is the reason why it took chemists nearly four decades to produce Turing patterns. The development of Turing patterns requires that the two species (inhibitor and activator) diffuse at different rates, with the inhibitor being faster than the activator. Since small molecules in aqueous solution have approximately similar diffusion coefficients, reaction-diffusion systems didn't generate Turing patterns. In the CIMA reaction however, the effective diffusion of iodide, the activator, could be retarded by adding starch indicator which forms an immobilized complex with I^- and I_2 present. On the other hand, attempts to generate Turing patterns in the Belousov-Zhabotinsky (BZ)[72, 73] reaction were unsuccessful because no complexing agent was available to interact with the bromous acid, which serves as the activator in this case. By running the BZ reaction in AOT microemulsion[74], the diffusion of polar species is slowed down, allowing the inhibitor, Br_2, to diffuse significantly faster than the bromous acid, thus satisfying Turing criterion for pattern formation.

d. Spinodal Decomposition

Another important mean-field theory that has gained a particular interest in re-cent years is the spinodal decomposition scenario adapted to precipitation pattern formation[75, 76]. It is a powerful postnucleation model that is shown to be suited to describe both: the regular[21] and the inverse banding[22, 23] in Liesegang-type precipitation patterns, and to reproduce many experimentally observed spacing laws such as the Matalon-Packter law[48, 77], without using artificial thresholds for nucleation and growth. In the discussion of the mechanism of spinodal decomposition for the formation of Liesegang patterns, the interpreters of the theory restricted themselves to the intermediate compound theories. They assume that due to the reaction of the outer electrolyte (A) and the inner electrolyte (B), an intermediate compound (C) is formed. For a broad class of reactions, this compound has a constant density (c_0) behind the diffusion front of the outer electrolyte[48], and it can move only by diffusion due to the presence of the gel. As time progresses, small clusters of the intermediate particles (C) nucleate and aggregate behind the front. This mechanism is known as nucleation and growth described in the previous section. However, if the characteristic time scale for nucleation is much larger than the time needed by the front to put out the local concentration c_0, the system reaches the unstable region, and phase separation or Liesegang band formation takes place on a short time scale. This band acts as a sink for the particles and, in the vicinity of the band, the local concentration of the particles decreases and the front is no longer in the unstable state of the phase space. When the front moves far enough, the depleting effect of the band diminishes. Thus the concentration of the particles grows again and the process repeats, leading to the formation of Liesegang patterns. In short, the new feature of this scenario is the assumption that the state of the front is quasi periodically driven into the unstable states domain.

The dynamics of the propagating front ($A + B \rightarrow C$) and the production of C in the reaction diffusion process have been solved[78]. The new aspect of the spinodal decomposition theory is therefore to describe the dynamics of their phase separation,

which can be approximated by the non-linear, so called Cahn–Hilliard (CH) equation[79, 80]:

$$\frac{\partial \varphi}{\partial t} = -\lambda \Delta (\varepsilon \varphi - \gamma \varphi^3 + \sigma \Delta \varphi) + kab, \tag{16}$$

where Δ is the 2D Laplacian operator, and φ is the shifted and rescaled concentration defined as:

$$\varphi = (2c - c_h - c_l)/(c_h - c_l), \tag{17}$$

where c_l and c_h being the low- and high-density phases of C. σ and λ are the rescaled surface tension and kinetic constant characterizing the dynamics of C respectively, while ε and γ are positive constants that define the boundaries between the stable, metastable, and unstable regions. The reaction term (kab) provides the source for the precipitation of C, which takes the form of a diffusing front whose position, width, and shape are fully characterized[78].

C. Scaling Laws of Periodic Precipitation

The spatiotemporal dynamics of the precipitation patterns obtained in Liesegang phenomena proved to obey several scaling laws irrespective of the geometry of the system and the chosen salt pairs. Four main empirical laws have been defined: the spacing law[81], the Matalon-Packter law[77], the time law[82], and the width law[83].

1. Spacing law

The spacing law was first described by Jablczynski in 1923[81], when he realized that for a certain periodic precipitating system, the ratio of the spatial positions of successive precipitation bands (x_n and x_{n+1}) measured form the gel surface, form a geometrical series as follows:

$$x_{n+1} = rx_n. \tag{18}$$

15

Here r is constant for large values of n, and it is known as the "spacing coefficient" usually expressed as: $r = 1 + p$, where p ranges between 0.05 and 0.4[48]. In general, the spacing between consecutive bands tends to increase as the distance from the interface between the gel and the solution increases[48]. This is known as the normal or the direct spacing. On the other hand, there are some Liesegang systems that exhibit revert spacing, whereby the distance between bands decreases upon moving away from the interface. Silver iodide (AgI)[23], Ferrous Ferricyanide $Fe_3[Fe(CN)_6]_2$[24], and lead chromate $(PbCrO_4)$[22], are all examples of precipitating systems displaying this feature.

2. Matalon-Packter law

A better description of the spacing law was made possible by Matalon and Packter[77]. They noted that the spacing coefficient $r = 1 + p$ is not a universal quantity, but depends mainly on the initial concentrations a_0 and b_0 of the outer and inner electrolytes respectively:

$$p = F(b_0) + \frac{G(b_0)}{a_0},$$

(19)

where F and G are decreasing functions of b_0. For different systems, they found that $F(b_0) \sim b_0^{-\gamma}$ with γ ranging as $0.2 \leq \gamma \leq 2.7$, and the function $G(b_0)$ decreases generally with b_0 but it is less known.

3. Time law

The time law given by Morse and Pierce[82] relates the position of the nth band (x_n) to the time required for its formation (t_n):

$$x_n = \alpha t_n^{\frac{1}{2}} + \beta,$$

(20)

where α and β are constants, and the ratio x_n^2/t approaches a constant value as n increases. The comparison between this relation and the diffusion coefficient definition directly reflects the diffusion-controlled nature of the obtained phenomena.

4. Width law

The width law[83] for Liesegang patterns describes how the thickness (w_n) of the precipitating zone varies with its position (x_n). Experiments show that the width increases with n and obeys the following linear relation[84, 85]:

$$w_n = \varepsilon x_n, \tag{21}$$

where ε is a constant. Moreover, it has been confirmed experimentally and theoretically that the ratio of the widths of two consecutive bands is constant $w_{n+1} = q\, w_n$.

D. Cadmium Sulfide System

After Liesegang observed the well-defined visible bands in silver dichromate system, a number of investigations were carried out on different weakly soluble salts, and various spatial patterns were reported. These include bands, fractals, spirals, etc. ... For systems that exhibit parallel Liesegang bands, two different trends might be observed: the direct spacing where the distance between two consecutive bands increases as the bands get further away from the interface, and the revert spacing where the distance decreases.

In the cadmium sulfide system, a 'Direct' type of periodic precipitation has been observed by Daus and Tower[86] upon mixing sodium sulfide of 0.4 to 1N in agar gel and using 0.8 to 2N of cadmium chloride as an outer electrolyte. Later on, Kant *et al.* (1970) studied Liesegang rings of cadmium sulfide in three gel media: gelatin, agar agar, and starch[87]. A similar 'Direct' spatial pattern of cadmium sulfide in agar agar was

obtained, whereas for the gelatin and starch media, they detected both 'Direct' and 'Revert' type of rings, depending whether the cadmium ions are allowed to diffuse into the gel containing sulfide or vice versa. In 1985, Ramasamy and his coworkers[88] reported a new observation made in cadmium sulfide salt that produces revert followed by direct system in the same tube under certain specific pH ranges. That is, the distance between successive bands goes on decreasing (revert type), reaches a minimum, and then increases with the increasing order of the ring (direct type). Although Kanniah *et al.* have reported similar observations in the case of silver iodide system in 1981[23], they did not observe such conversion for a semiconducting substance like cadmium sulfide. The experimental conditions of the pattern transformation from revert to direct were explained on the basis of autocatalytic reaction coupled to diffusion[24].

E. Aims of the Present Work

In the present work, we report for the first time the formation of a new precipitation pattern observed in the cadmium sulfide/hydroxide system, which displays a transition from parallel rings to spots with square/hexagonal symmetry. The transition threshold, the prevalence of spots versus rings, the wavelength of the selected pattern, the size of the resulting spots, and the percentage of their coverage are shown to be controllable by adjusting the concentrations of the inner and outer electrolytes, temperature, gel thickness, capping agent addition, ionic strength variation, and direct electric field application. The aims can be summarized as follows:

1. Study the spatiotemporal evolution of the new square/hexagonal precipitation pattern obtained in the cadmium sulfide/hydroxide precipitation system in two dimensions.

2. Explore the effects of different parameters on the morphology and the dynamics of the obtained pattern.

3. Carry out computational study using the spinodal decomposition scenario to investigate theoretically the dynamics of the obtained pattern, and demonstrate that this model corresponds mathematically to the well-known Cahn-Hilliard equation for phase separation. The resulting evolution equations are solved numerically using the Finite Element Method (FEM).

4. Study the Turing patterns obtained in three dimensions due to the stacking of layers of the two dimensional patterns and include 3D simulation.

CHAPTER II

TWO-DIMENSIONAL PATTERNS

A. Introduction

The similarity between precipitation structures in reaction-diffusion systems and naturally obtained patterns have motivated scientists to mimic nature and learn from its ability to reproduce chemically generated patterns programmed in space and time to perform desired tasks[32, 89]. For instance, these patterns are expected to have wide applications in bottom-up fabrications[2, 89], thereby competing with the traditional top-down methods, and opening possibilities for new technological processes[90]. However, the major obstacle to successful implementation of reaction-diffusion phenomena in modern technologies has been the lack of control over their progress. The idea of controlling spatiotemporal patterns in reaction-diffusion systems has therefore become one of the most challenging problems in materials science. This paves the way for better understanding the underlying dynamics, which in turn is a key element to display any desired pattern by imposing a relatively weak external perturbation.

Several studies have been made on different systems in an attempt to control pattern formation. It is well known that the variation of some conditions and experimental parameters, under which Liesegang precipitation patterns are formed, can to some extent control the characteristics of the pattern as well as its dynamical properties. For example, the appropriate choice of the concentrations of the reagents and the temperature has a direct influence on the morphological features of the resulting pattern[20, 77, 91]. Moreover, the nature of the gel used and its concentration[20, 92], the dimensions of the system, and the process followed can also have an impact on the obtained structures. For instance, wet stamping method has been used recently to fabricate various precipitation

structures of micro- and nanoarchitectures which could be technologically useful[2, 93]. Further studies have also shown that the formation of patterns and the motion of the propagating fronts could be altered by the application of an electric field[94, 95, 96]. Thus, the above methods of control play a crucial role in developing an effective and powerful scope for architecting the desired pattern, depending on the experimental conditions used.

Similar to other rhythmic precipitates, the macroscopic evolution and the characteristics of the obtained spots in the cadmium sulfide/hydroxide system can be altered by a proper control of the experimental conditions; these include the concentrations of the inner and outer electrolytes, temperature, concentration of the gel, use of a capping agent, variation of ionic strength, and application of a static electric field. The effect of each parameter on the dynamical properties and the characteristics of the resulting spots will be discussed in this chapter. SEM images exhibiting the transition from bands to spots and their morphological features are also presented.

B. Experimental Procedure

A sample of cadmium chloride monohydrate $CdCl_2.H_2O$ (Mallinckrodt) is weighed to the nearest 0.0001 g using an analytical balance and dissolved in double distilled water to obtain the required concentration. After salt dissolution, 5% per volume of powdered gelatin (Difco) is added to the solution. The mixture is then heated with continuous stirring for a few minutes until the entire solid gel material dissolves. The resulting homogenous hot solution is then immediately transferred into a circular Plexiglass reactor (diameter = 15 cm) and is covered with a transparent Plexiglas cover (diameter = 12 cm) equipped with spacers in order to have a homogeneous gel thickness of 0.7 mm. The cover is connected to a small cylindrical reservoir (diameter = 3 cm) in the center for the outer solution addition. The gel is left in the reactor for 24 hours at room temperature to rest and polymerize. After that, the gel is neatly removed from the bottom of the pouring
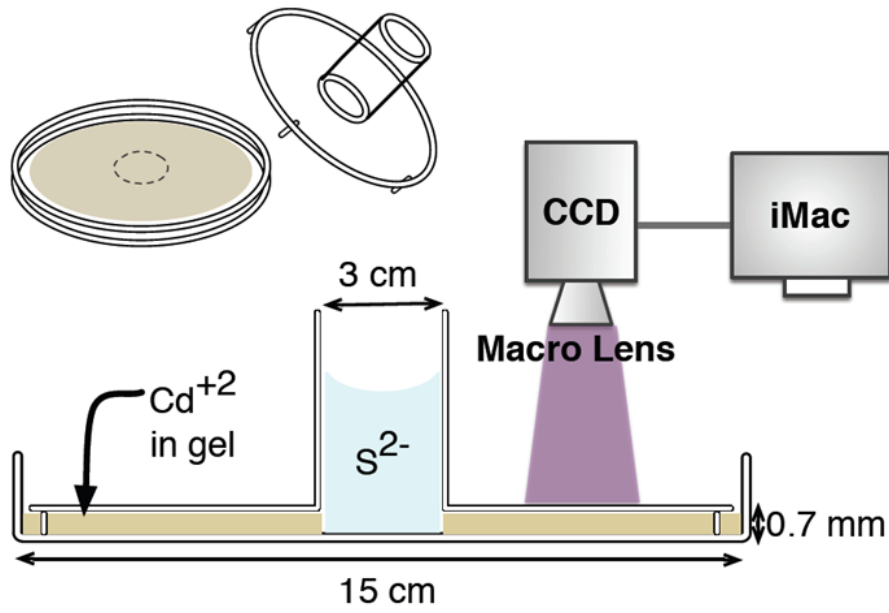
Figure 6: A sketch of the experimental setup. The gelled Cd^{2+} is sandwiched between the dish bottom and its cover and the outer electrolyte S^{2-} is added to the central reservoir. Photographs are taken using a Canon digital camera interfaced with a computer.

cylindrical reservoir and the outer electrolyte, sodium chloride nonahydrate $Na_2S.9H_2O$ (Alfa Aesar), is gently added. The plate is then left in an air thermostat chamber at 22.0 $\pm$ 0.1 °C. The diffusion of the sulfide ions through the cadmium-doped gel, as well as the formation of the precipitates are monitored over a period of two days. The patterns and their evolution are captured by a mounted CCD digital camera equipped with a Macro lens and controlled by a computer as shown in Figure 6.

C. Pattern Evolution

The spatiotemporal evolution of the system is initiated directly after the sulfide solution is diffused into the cadmium-doped gel. The dissolution process of sodium sulfide in water, described in (R_1), releases hydroxide ions (OH^-). Since the diffusion coefficient of the hydroxide ions is about four times greater than that of the hydrogen sulfide ions (HS^-), a white precipitate is formed at the liquid-gel interface first, indicating a spontaneous reaction between the diffusing hydroxide ions and the cadmium ions (Cd^{2+})
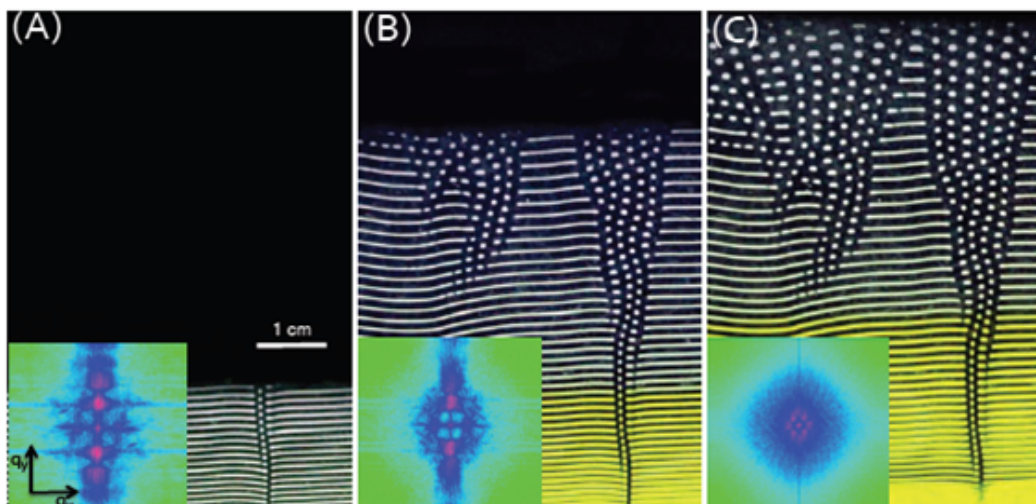
Figure 7: Transition from Rings to Spots. (A) t = 6 hrs; (B) t = 18 hrs; (C) t = 26 hrs. The inset figures are the 2D power spectra of the displayed patterns. The purple color indicates highest modes expressed in the pattern. Transition from stripes (A) to hexagonal pattern (C) is reflected in the power spectrum where the aligned wavenumbers along q_y in (A) are changed into 6 wavenumbers in (C) with a hexagonal symmetry.

existing in the pores of the gel (R_2). For a given set of initial outer and inner concentrations, the precipitation of $Cd(OH)_2$ exhibits concentric rings (Fig. 7A) at early times of evolution. As time progresses, white spots start appearing as defects among the rings in several locations as shown in Figure 7A. They start multiplying and propagating in the direction of the diffusion front (Fig. 7B). Eventually, the whole domain of the reactor is invaded with such an unexpected pattern as shown in Figure 7C. The investigation of the time evolution of the power spectra of the patterns in Figure 7 (insets) reveals the transition from bands to spots possessing a mixture of square and hexagonal symmetry.

It is noticeable that in the resulting pattern the distance between consecutive spots seems to increase as the distance from the center of the reactor increases towards its boundaries. Moreover, the spatial evolution of the white solid is followed by a yellow back-front resulting from the formation of yellow cadmium sulfide CdS due to the anionic exchange between OH^- and S^{2-} (R_3). The latter is due to the higher thermodynamic stability of the sulfide, where the solubility product constant of CdS $\left(K_{sp} = 10^{-28}\right)$ is much lower than that of the precipitating $Cd(OH)_2$ $\left(K_{sp} = 10^{-14}\right)$. Therefore, the more soluble $Cd(OH)_2$ is converted into CdS during the reaction[97]. All underlying chemical

23

reactions are summarized as follows:

$$Na_2S(s) \overset{H_2O}{\Rightarrow} 2Na^+(aq) + HS^-(aq) + OH^-(aq) \qquad (R_1)$$

$$Cd^{2+}(gel) + 2OH^-(aq) \rightarrow Cd(OH)_2(s) \qquad\qquad (R_2)$$

$$Cd(OH)_2(s) + S^{2-}(aq) \rightarrow CdS(s) + 2OH^-(aq) \qquad (R_3)$$
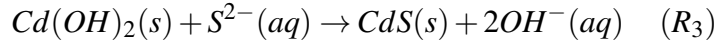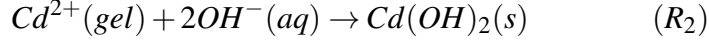
The ion exchange process is shown to be diffusion-limited, where the yellow front travels linearly proportional to the square root of time $\left(d = t^{1/2}\right)$ when the reaction-diffusion is performed in 1-D test tube. According to Gálfi and Rácz[78], for a simple bimolecular system $(A + B \rightarrow C)$ in which the transport of the reagents is dominated by diffusion and the reaction kinetics is of second order, the dependence of the distance travelled by the pulse on time exhibits a diffusion-like profile of the form $d \sim t^\beta$, where $\beta = 1/2$. In an attempt to detect whether the white and the yellow fronts for the propagating $Cd(OH)_2$ and CdS follow this diffusion profile in 2-D, a log-log fit of the distance travelled by each pulse versus time is plotted for a plate with 80 mM inner concentration and 400 mM outer concentration. The exponent of the diffusion profile β, extracted as the slope of the log-log fit is determined to be $\approx 1/3$ for both, the white and yellow pulses, as shown in Figure 8. This indicates that the precipitation of $Cd(OH)_2$ and CdS in 2-D is sub-diffusive. The reason why the exponent β is slightly different than $1/2$ as compared to 1-D could be attributed to the anomalous diffusion resulting from the gel porosity, thus allowing the diffusion to take place with spatial defects that could lower the value of β[98].

24
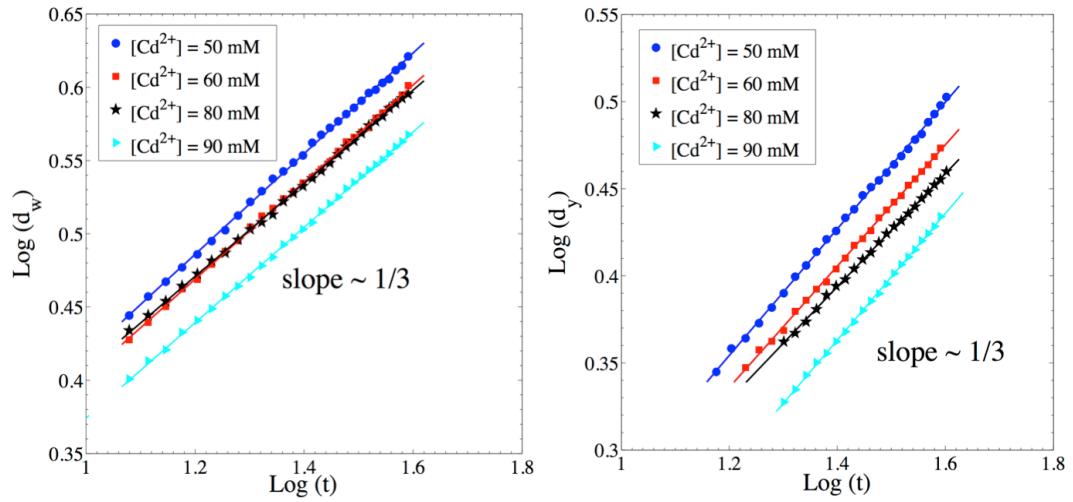
Figure 8: Log-log plots of the white front displacement (d_w) and the yellow front displacement (d_y) as a function of time (t). Left plot represents the white front and the right plot represents the yellow front. Initial conditions: outer, $[S^{2-}]_0 = 400$ mM. A range of different initial inner concentrations in 5% per volume of gelatin gel are tested: $[Cd^{2+}]_0 = 50, 60, 80$ and 90 mM.

D. Effect of Inner and Outer Concentration

To detect the effect of the concentrations of the inner and outer electrolytes on the pattern morphology, five sets of different outer concentrations (varying between 200 mM and 400 mM) are prepared, each containing 14 reactors at different inner concentrations (varying between 10 mM and 140 mM), using the same experimental procedure described above. The emerging patterns are then grouped in the phase diagram shown in Figure 9. At low cadmium concentration (less than 20 mM), only a continuous precipitating white front of $Cd(OH)_2$ is obtained without rings or spots. A diffusing yellow back-front indicating the formation of CdS then follows. This regime is denoted by 'C'. When the inner concentration is increased from 10 mM to 20 mM for all outer concentrations in the aforementioned range, clearly separated thin rings of a white/yellow precipitate are observed. This regime is denoted by 'R'. Upon increasing the concentration of cadmium from 30 mM to 60 mM, numerous well-resolved spots with square/hexagonal symmetry emerge just after the formation of a few rings. This region is labeled 'S'. When the inner concentration increases beyond 60 mM, the structure of the phase diagram gets more complex, resulting in a mixture of predominating rings and some spots (denoted
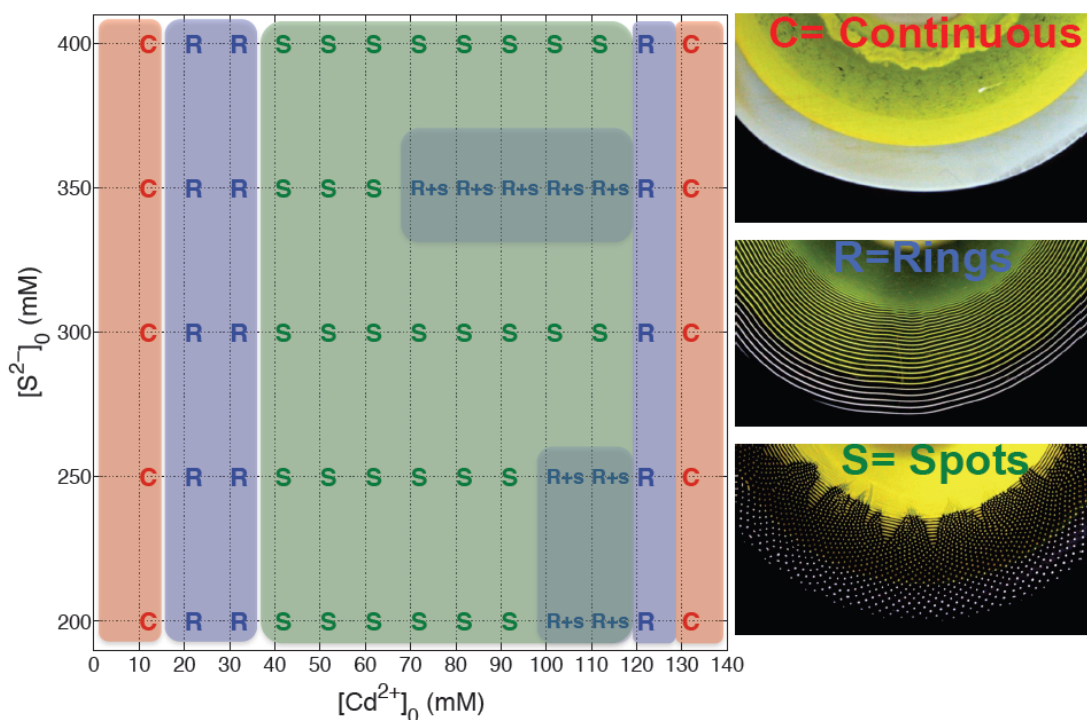
Figure 9: Phase diagram representing the different morphologies obtained upon varying the inner and outer concentrations. **C** = continuous precipitation band; **R** = precipitation rings; **S** = spots. The **R+s** (lowercase s) on the phase diagram indicates occurrence of rings with some spots.

as 'R+s') for outer concentrations ranging between 200 mM and 250 mM, and around 350 mM. For inner concentration between 120 mM and 130 mM, we get back to the 'R' regime but with thicker and fewer rings than what is obtained on the left-hand side of the phase diagram. For concentrations higher than 130 mM, we go back to the continuous precipitation zone 'C'.

The effect of inner and outer concentrations is further investigated. If we move horizontally across the phase diagram at a fixed outer concentration $[S^{2-}]_0 = 400$ mM, as shown in Figure 10, starting at an inner concentration $[Cd^{2+}]_0 = 30$ mM, well-resolved thin rings are obtained (Fig. 10A). By increasing the inner concentration from 30 mM to 60 mM, a transition from thin rings to spots is clearly exhibited in Figure 10B, and the resulting pattern after 48 hours is clearly dominated by spots with a square/hexagonal symmetry. Further increase in the inner concentration to 90 mM (Fig. 10C) and to 110 mM (Fig. 10D) results in the formation of larger and closer spots until they all merge
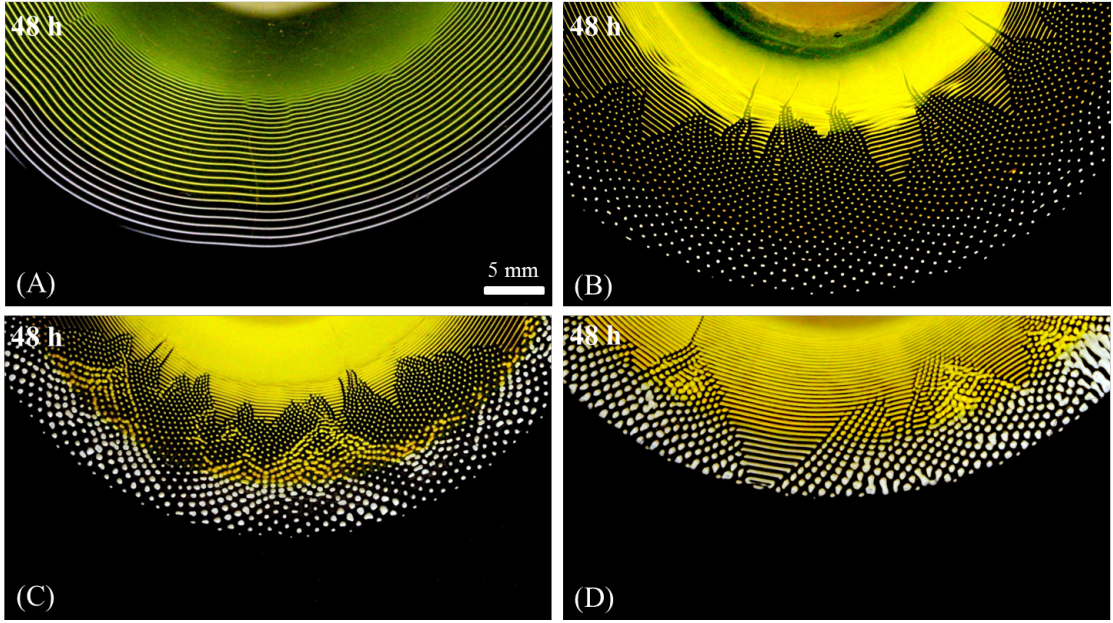
Figure 10: The evolution of precipitation patterns within 48 hours at constant outer concentration $[S^{2-}]_0 = 400$ mM and various inner concentrations $[Cd^{2+}]_0$: (A) = 30 mM; (B) = 60 mM; (C) = 90 mM; (D) = 110 mM; Gelatin = 5%; Temp = 22 °C.

together at a concentration beyond 130 mM to form a continuous band as shown in the phase diagram.

In analogy to Liesegang rings, the obtained spots are labeled by their number (n) along a special line of symmetry chosen to pass through them and starting at the first spot appearing in the system. To quantify, the size of a spot is given in terms of the measured area (A) it occupies. The plot of A versus n represented in Figure 11 shows that the size of the spots changes almost linearly along the diffusion flux away from the interface, with larger sizes obtained at higher concentrations. In the case of Figure 10B, the spot size ranges from 0.1 mm^2 to 0.32 mm^2, whereas in the case of Figure 10C, the spot size ranges from 0.45 mm^2 to 1.44 mm^2, and from 0.91 mm^2 to 2.6 mm^2 in the case of Figure 10D. Therefore, the spots are shown to increase in size with the increase of the inner concentration.

On the other hand, moving vertically in the phase diagram, the effect of varying the outer concentration does not noticeably affect the spot size, but it directly influences the spacing between spots and the distance they cover. Figure 12 shows that the increase
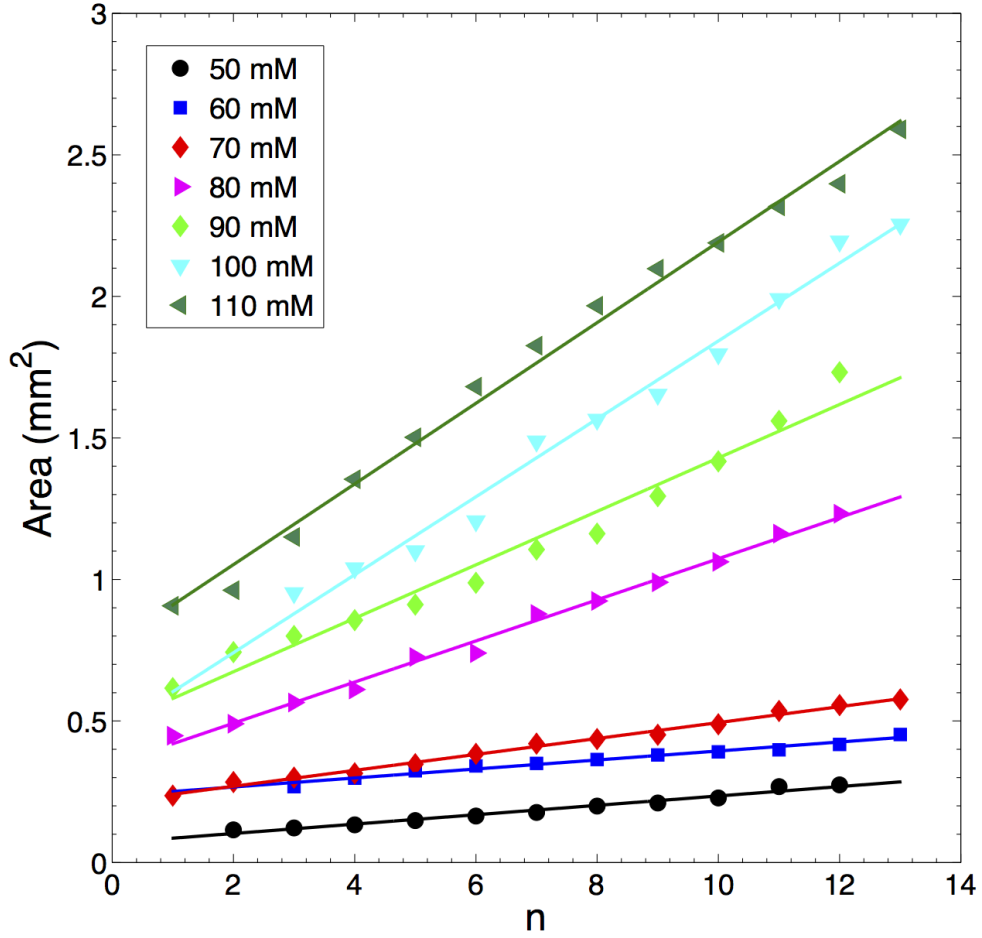
Figure 11: Plot displaying the area (A) occupied by each spot versus the spot number (n). The concentration of the outer electrolyte $[S^{2-}]_0$ is fixed at 400 mM while the concentration of the inner electrolyte $[Cd^{2+}]_0$ varies from 50 mM to 110 mM. The temperature is maintained constant at 22 °C and the concentration of gelatin used is 5% per volume.

in the outer concentration at a fixed inner concentration ($[Cd^{2+}]_0 = 60$ mM) results in a faster reaction-diffusion process, thus allowing the precipitation and formation of closer spots that cover larger distances.

In order to shed more light on the control of the spots, the spacing between consecutive spots is measured for two sets of plates: *Set (I)* is prepared at constant outer concentration $[S^{2-}]_0 = 250$ mM. with different inner concentrations $[Cd^{2+}]_0$ ranging between 40 mM and 80 mM. Set (II) is prepared at constant inner concentration ($[Cd^{2+}]_0 = 60$ mM) with different outer concentrations $[S^{2-}]_0$ ranging between 200 mM and 350 mM. The spacing in a given pattern with spots is defined as $\lambda_n = x_{n+1} - x_n$ where x_n and
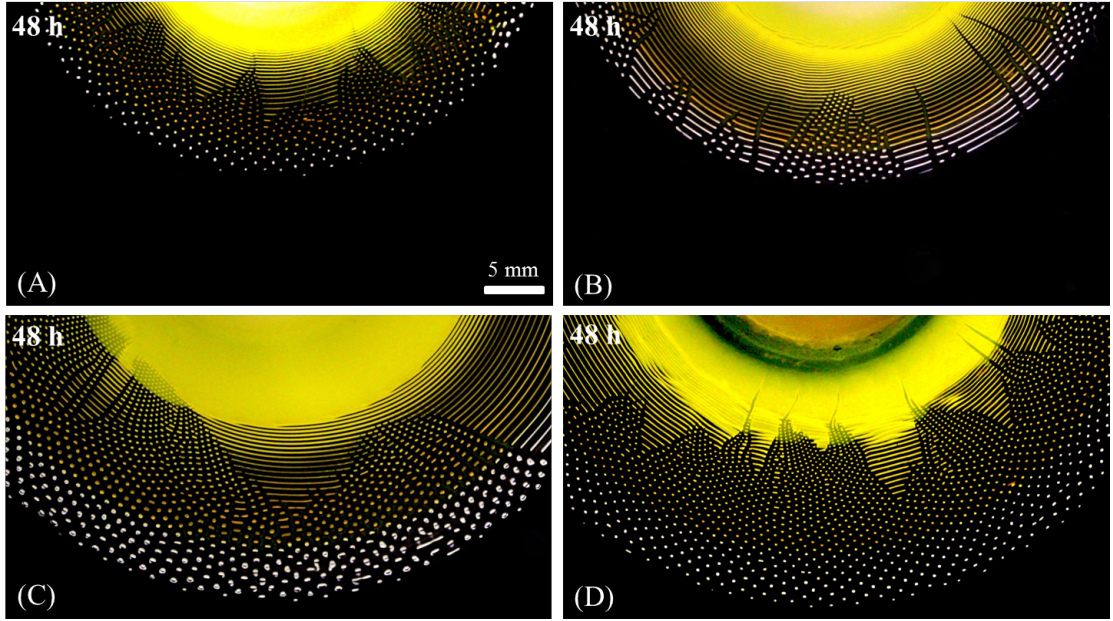
Figure 12: The evolution of precipitation patterns within 48 hours at constant inner concentration $[Cd^{2+}]_0 = 60$ mM and various outer concentrations $[S^{2-}]_0$: (A) = 200 mM; (B) = 250 mM; (C) = 350 mM; (D) = 400 mM; Gelatin = 5%; Temp = 22 °C.

x_{n+1} are the locations of spot n and the following one, $n+1$. Consequently, for *Set (I)*, the obtained five curves in Figure 13A for λ_n versus n exhibit a linear relationship with a positive slope that increases with a decrease of the inner concentration. As for *Set (II)*, a linear direct spacing law is also obtained as shown in Figure 13B, with a positive slope increasing with a decrease in the outer concentration. Moreover, a spacing law for spots can be verified by computing the ratio $r = \frac{x_{n+1}}{x_n}$, where r is the spacing coefficient expressed as $1 + p$, with p ranging between 0.09 and 0.16 for *Set (I)* and between 0.13 and 0.08 for *Set (II)*.

This observation is similar to the direct spacing law encountered in Liesegang banding systems[21, 77], whereby the rate of diffusion increases with the increase of the outer electrolyte concentration[96], thus resulting in spots forming at closer distances than those with a lower outer concentration. On the other hand, the increase in the spot size with the increase in the inner concentration results in the formation of closer and bigger spots until they merge, which leads to smaller values of p. On that account, the initial concentrations of reactants provide suitable spatial control parameters for the spots. By

29
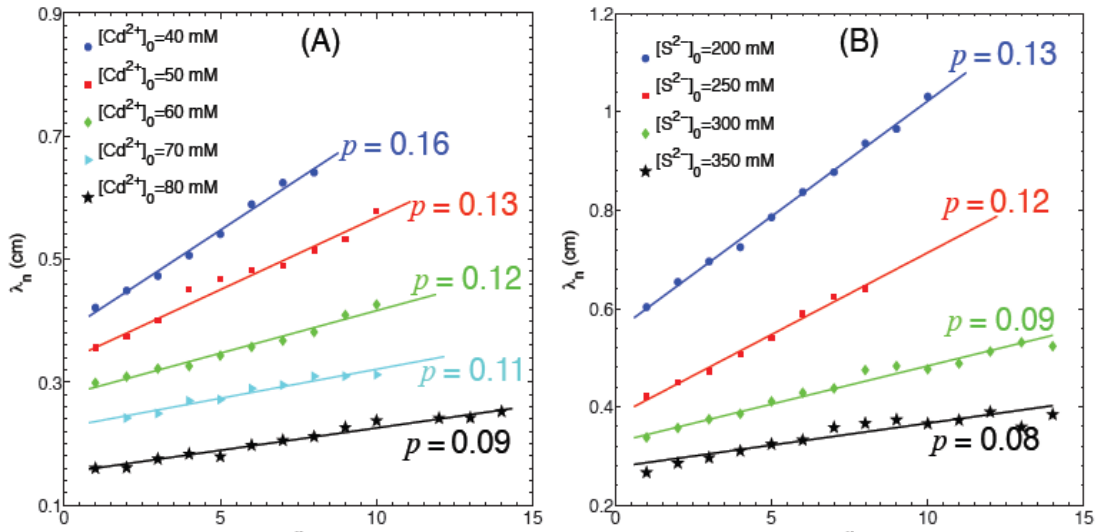
Figure 13: Plots of the spacing between two consecutive spots λ_n versus the spot number (n). (A) represents *Set (I)* with fixed outer concentration $[S^{2-}]_0 = 250$ mM and different inner concentrations. (B) represents *Set (II)* with fixed inner concentration $[Cd^{2+}]_0 = 60$ mM and different outer concentrations. The coefficient p for each case is also shown.

the same token, a time law[82] is also observed, whereby the ratio of x_n^2/t_n, t_n being the time elapsed until the formation of the nth band, is found to lead to a constant value at large n for all initial inner and outer concentrations (Fig. 14).

E. Effect of Temperature

Temperature is one of the main parameters that influence the kinetics and the evolution of the patterns. In the case of chemical reactions, it is well-known that rates can eventually change upon varying the temperature – and in most cases, the higher the temperature is, the faster the reaction. In reaction-diffusion systems, however, the temperature variation can greatly alter the precipitate solubility and the diffusion velocity of the invading electrolyte.

To check the effect of temperature on the formation of spots, a preparation method similar to the ones described in previous parts is followed. Three plates are prepared, each containing 80 mM cadmium chloride and 400 mM sodium sulfide. The first
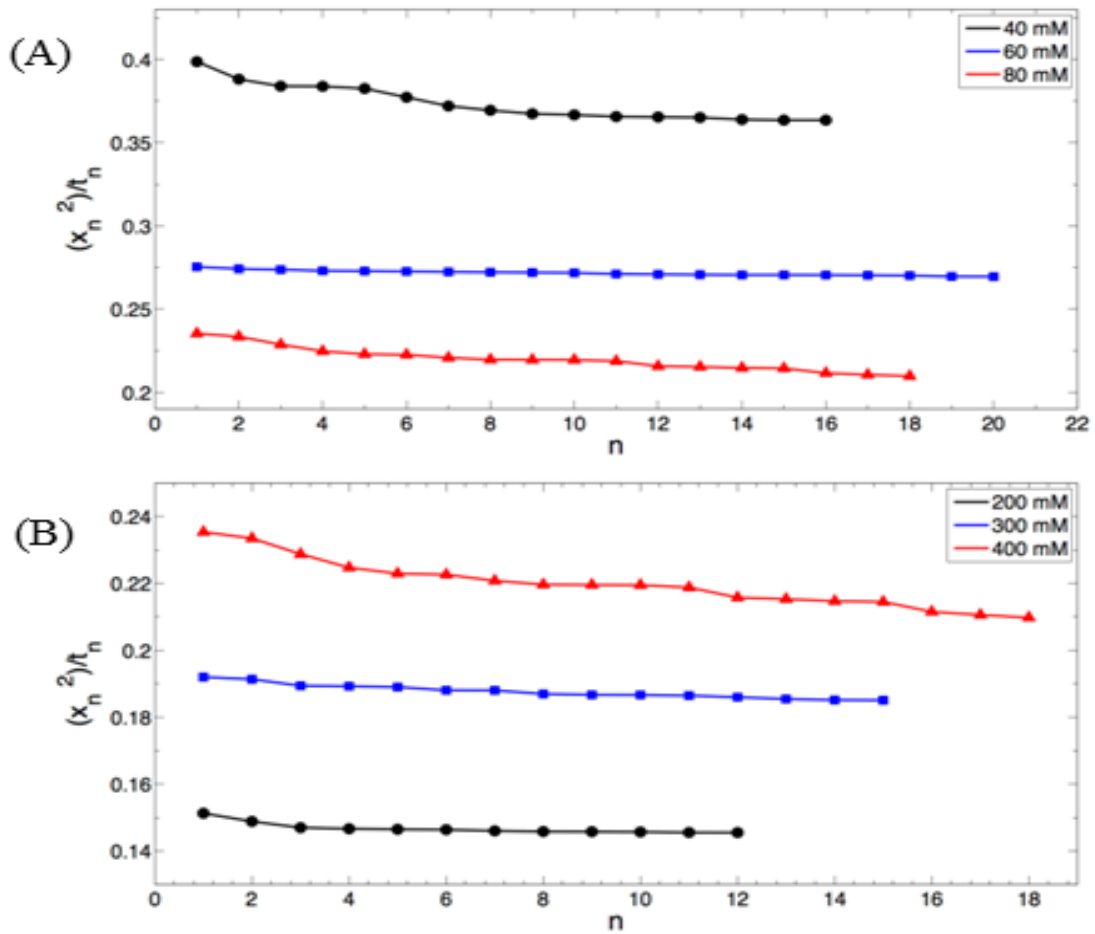
Figure 14: Plot displaying the ratio $\left(x_n^2\right)/t_n$ vs. n for different inner concentrations (A) and outer concentrations (B). At high values of n, the ratio approaches a constant value.

plate is placed in a thermostat where the temperature is maintained at 22.0 ± 0.1 °C, while the other two are placed in a refrigerator at a temperature of 2.0 and 10.0 ± 0.1 °C, respectively. The experiment is also performed at higher temperatures, but it is difficult to monitor the evolution due to the deformation of the gel. The obtained patterns are represented in Figure 15, which clearly shows that after 24 and 48 hours, the transition from bands to spots occurs at a lower rate when the reaction is performed at lower temperatures (2.0 and 10.0 °C) compared to that at a higher temperature (22.0 °C).

In order to gain more quantitative insight into this progression, the front distances traveled by the white and yellow bands for a certain period of time, as well as the distances of the first and the last spots from the interface, are measured after 24 and 48 hours for the three plates. Results show that as the temperature increases, both the precipitation reaction

31
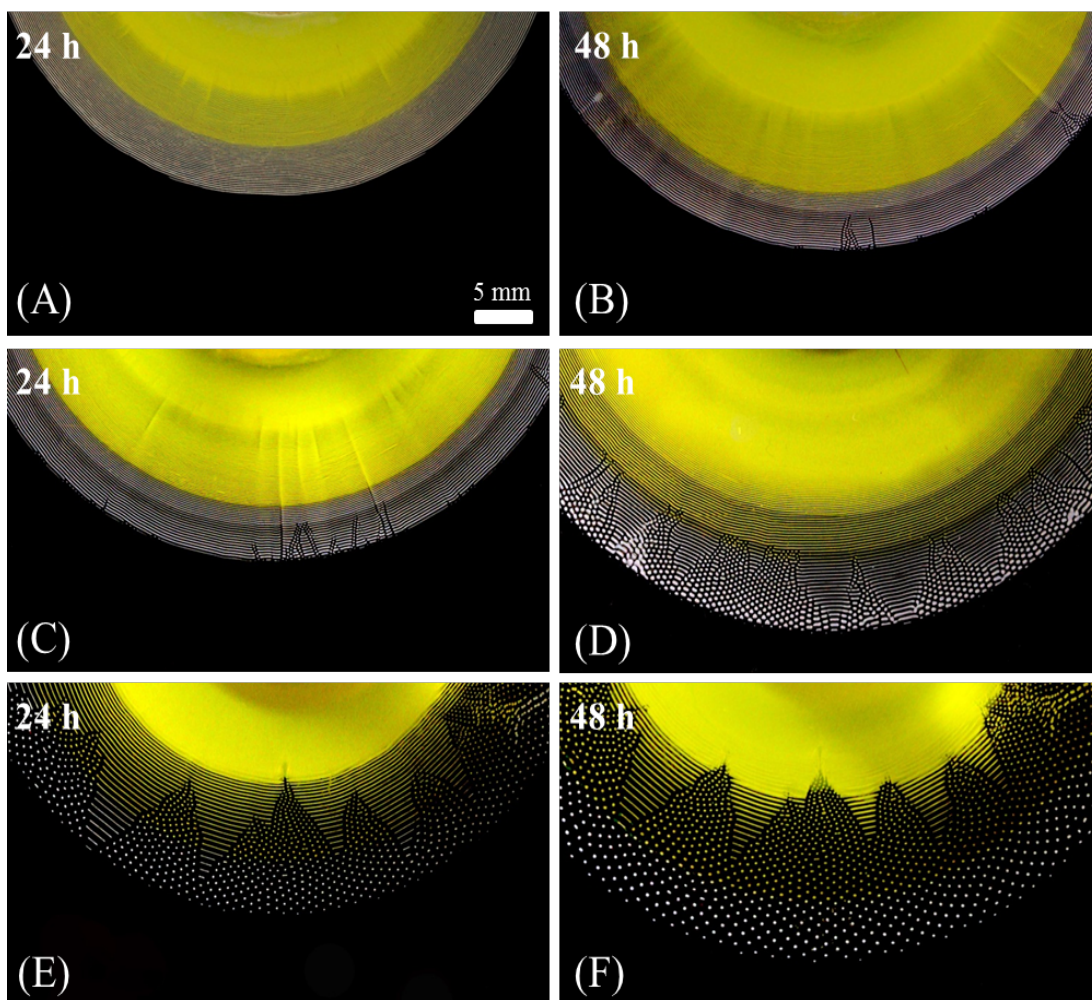
Figure 15: The evolution of precipitation patterns at different temperatures: After 24 hours of reaction-diffusion: (A) at 2 °C; (C) at 10 °C; (E) at 22 °C. After 48 hours of reaction-diffusion: (B) at 2 °C; (D) at 10 °C; (F) at 22 °C. Initial conditions: Inner $[Cd^{2+}]_0 = 80$ mM; Outer $[S^{2-}]_0 = 400$ mM; Gelatin = 5%.

giving the white $Cd(OH)_2$ and the ion exchange process producing the yellow CdS, are faster when the reaction-diffusion takes place at a higher temperature. Moreover, after 24 hours, the first spot appears at a distance of 0.8 cm from the interface for the case of 22 °C, while it appears at 1.5 cm for the case of 10 °C. In the case of 2 °C, there is only formation of rings and no transition to spots is noticed. Similarly, the last spot formed after 48 hours is farther away from the interface at 22 °C (2.5 cm) as opposed to that at 10 °C (2.0 cm) and 2 °C (1.7 cm). On the other hand, we intend to measure the whole area covered by the formed precipitate (bands and spots) and that covered solely by the spots for each plate after 48 hours using Photoshop software. The ratio of spots area to the total precipitation area is then calculated. The obtained results are displayed in Figure 16, which clearly reveals that the percentage of spots coverage increases with the increase in the temperature due to the higher transition rate. All these results show that the diffusion process at a higher temperature proceeds faster, thus allowing the precipitation process to cover larger distances and resulting in more spots whose formation starts at an earlier time.

F. Effect of Gel Concentration

Liesegang experiments are usually performed in gel media in order to prevent convection and sedimentation which would destroy the resulting patterns. Gels, moreover, provide a suitable medium for the diffusion of electrolytes and create a stable regime of concentration gradients. However, the nature of the gel used and its concentration can greatly affect the morphology of the precipitating pattern and can even suppress pattern formation in some cases[20].

In an attempt to detect the effect of varying the gel thickness on the obtained spots in the cadmium sulfide/hydroxide system, three plates, each containing 80 mM of cadmium chloride, are prepared at ambient temperature. A certain mass of gelatin is then

Figure 16: Histogram representing the percentage of the area covered by the spots with respect to the total area covered by the precipitate as the temperature varies between 2 °C and 22 °C and after 48 hours of reaction-diffusion. Initial conditions: Inner $[Cd^{2+}]_0 = 80$ mM; Outer $[S^{2-}]_0 = 400$ mM; Gelatin = 5%.

added into each plate in such a way to obtain the following gel concentrations: 3%, 5%, and 7% per volume. After complete gelation, the same solution of sodium sulfide (400 mM) is added to the three plates. The obtained results are displayed in Figure 17.

In order to compare the resulting patterns, the ratio of the area covered by the spots is measured with respect to the total area covered by the precipitate after 48 hours. Figure 18 shows that the thick spots obtained when the concentration of gelatin is 3% occupy about 35% of the total precipitation area. This percentage increases to 70% when the concentration of gelatin reaches 5% per volume. At higher gel concentration (7%), the formation of bands is predominant and the percentage of spots coverage decreases to reach 24%.

Moreover, the spacing between two consecutive spots (λ_n) is measured in each
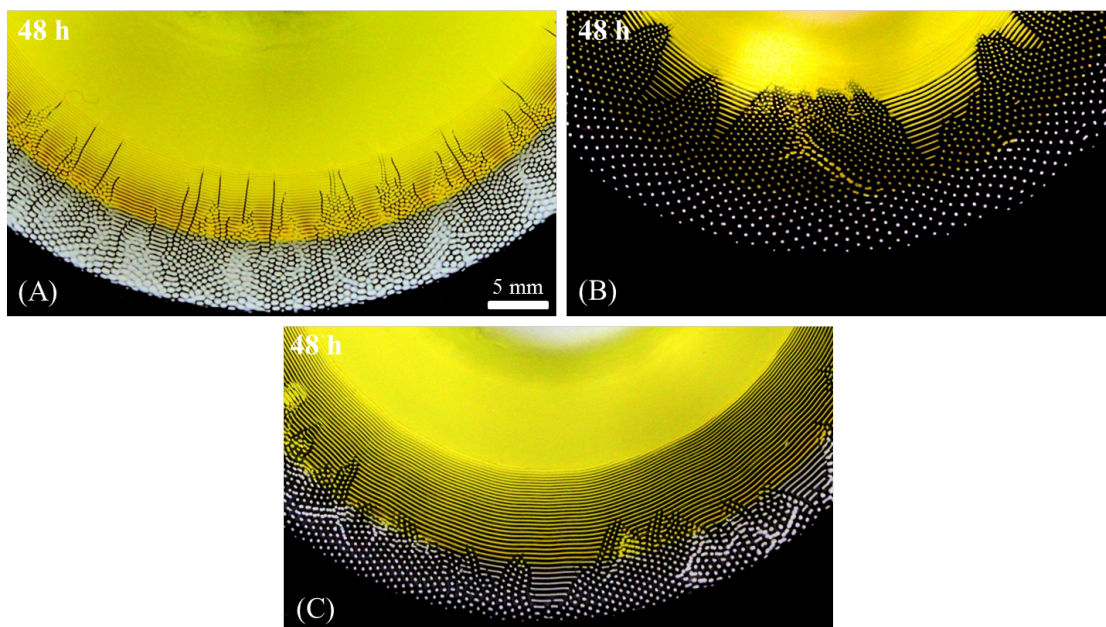
Figure 17: The evolution of precipitation patterns at 48 hours using different gel concentrations: (A) = 3%; (B) = 5%; (C) = 7%. Initial conditions: Inner $[Cd^{2+}]_0 = 80$ mM; Outer $[S^{2-}]_0 = 400$ mM; Temp = 22 °C.

plate. Figure 19 depicts a plot of λ_n versus the spot number (n) for the three different gel concentrations used. All three curves show an increasing trend, which is typical for a system showing direct spacing, and the higher gel concentration curves lie above the lower concentration ones. These observations agree with the results already mentioned in the literature about Liesegang bands[22]. According to Schacht *et al.*, increasing gelatin concentration leads to a higher number of pores of smaller size due to an increase in the nucleation rate[99]. Moreover, the diffusion coefficient of the diffusing ions in the gel medium is reduced upon increasing the gel concentration[96]. Hence, the rate of diffusion of the sulfide/hydroxide ions is decreased, contributing to an increase in the spacing between the spots.

G. Effect of Capping

Capping agents have physical or chemical affinity to the surface of nanoparticles and another unreactive part that extends towards the environment to impede the agglom-
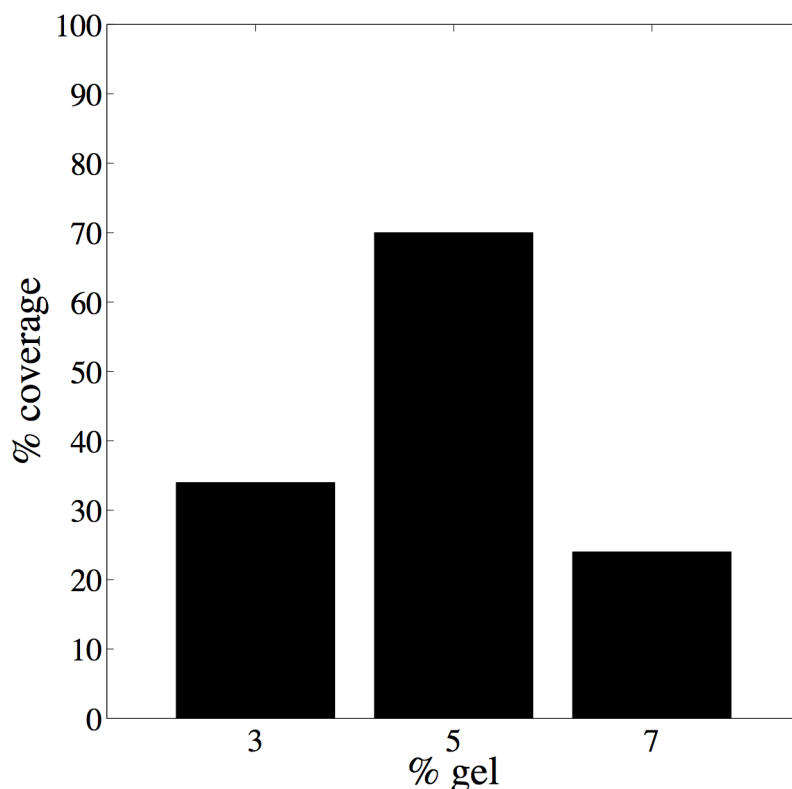
Figure 18: Histogram representing the percentage of the area covered by the spots with respect to the total area covered by the precipitate as the concentration of gelatin gel varies between 3% and 7%. Initial conditions: Inner $[Cd^{2+}]_0 = 80$ mM; Outer $[S^{2-}]_0 = 400$ mM; Temp = 22 °C.

eration of nanoparticles and control their growth[100]. In particular, $\beta-$mercaptoethanol ($HO - CH_2 - CH_2 - SH$) is used as a stabilizing agent to control the size of monodispersed CdS nanoparticles[101]. To investigate the sensitivity of the pattern formation to the addition of the capping agent, $\beta-$mercaptoethanol ($\beta-$ME), five solutions of cadmium chloride with a concentration of 80 mM are prepared in 5% per volume gelatin gel. After heating the mixture, different concentrations (2, 4, 6, 8, and 10 mM) of $\beta-$ME (Acros) are added to each solution and then homogenized. When the mixture gels in the reactor, sodium sulfide solution (400 mM) prepared in doubly distilled water and containing $\beta-$ME is introduced to the reservoir of each plate. It is important to note that the concentration of $\beta-$ME inside the gel and above is kept the same to prevent the diffusion of the capping agent. The obtained results are compared to a control plate that has the same concentrations of the inner and outer electrolytes (80 and 400 mM respectively), but
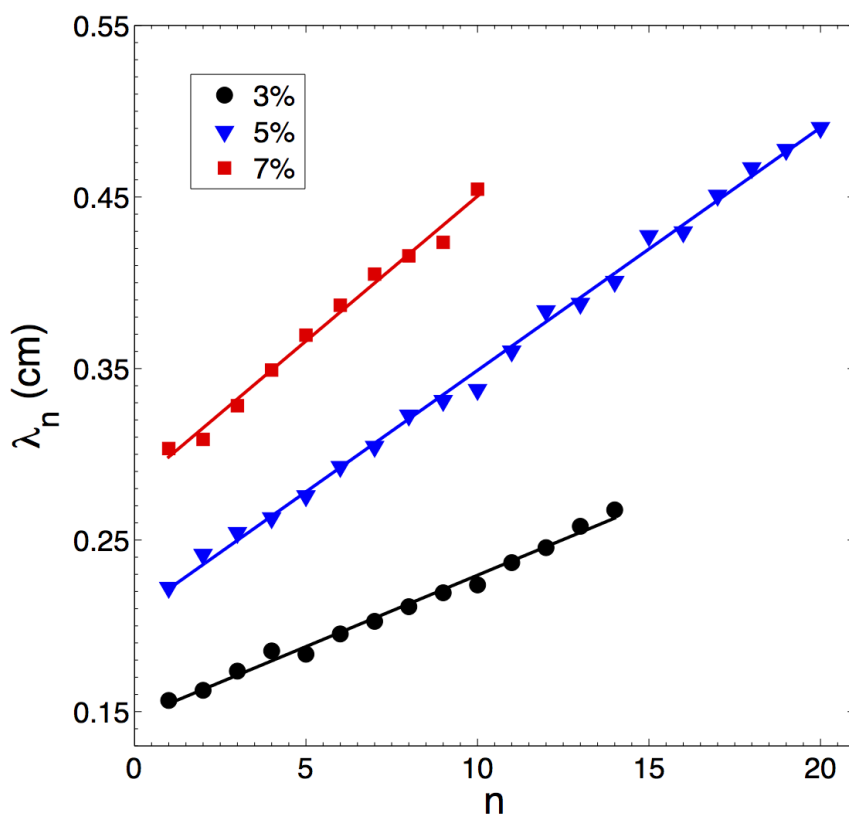
Figure 19: Plot of the spacing between two consecutive spots (λ_n) versus the spot number (n) for the different gel concentrations used: 3%; 5%; and 7%. Initial conditions: Inner $[Cd^{2+}]_0 = 80$ mM; Outer $[S^{2-}]_0 = 400$ mM; Temp = 22 °C.

free of $\beta-$ME.

Results show that the presence of ME favors the formation of bands over the formation of spots, and this observation becomes more pronounced as the concentration of the ME is increased (Fig. 20). Quantitatively, the precipitation area covered only by the spots is measured with respect to the total area covered by the whole precipitate after 48 hours. Results in Figure 21 show that the spots formation is gradually suppressed upon increasing the concentration of ME.
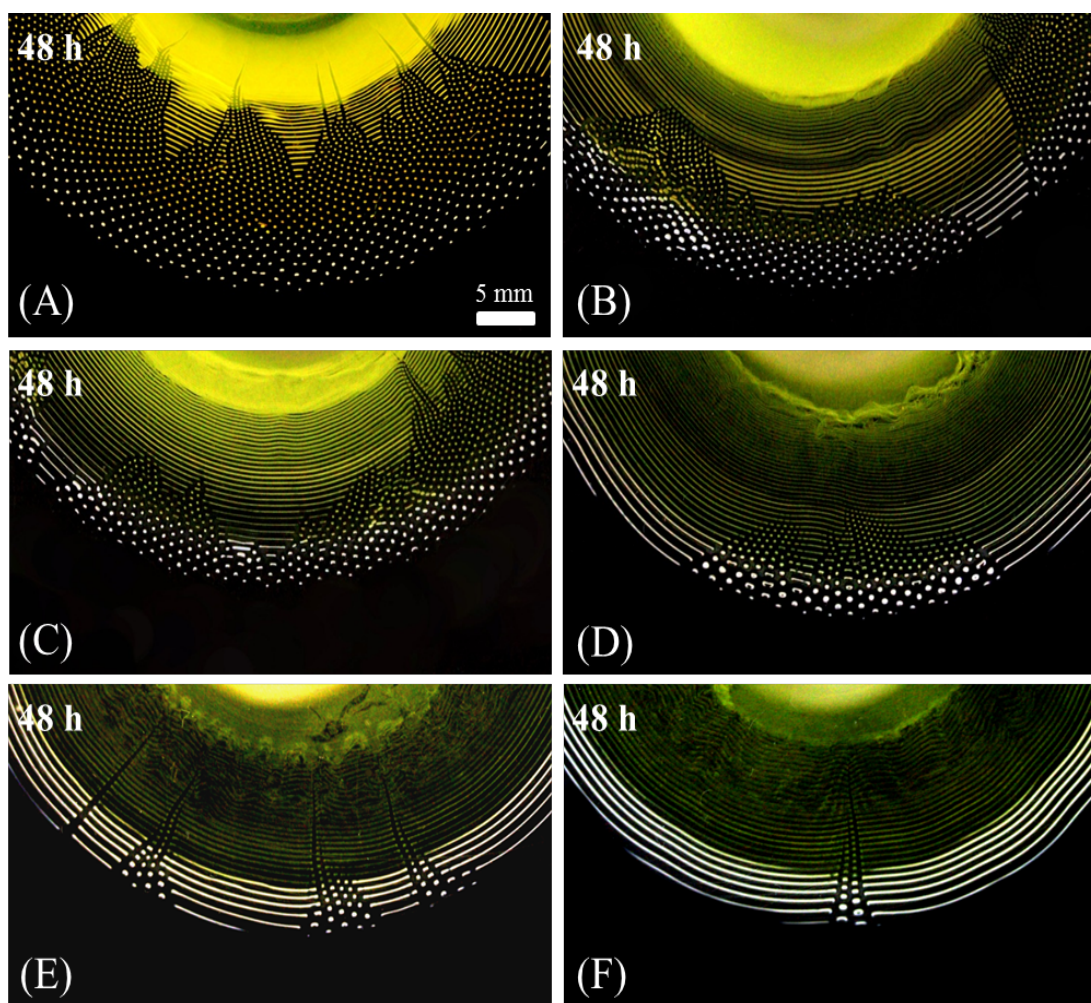
Figure 20: The evolution of precipitation patterns at 48 hours for different $\beta-$ME concentrations: (A) = 0 mM; (B) = 2 mM; (C) = 4 mM; (D) = 6 mM; (E) = 8 mM; (F) = 10 mM. Initial conditions: Inner $[Cd^{2+}]_0 = 80$ mM; Outer $[S^{2-}]_0 = 400$ mM; Gelatin= 5%; Temp = 22 °C
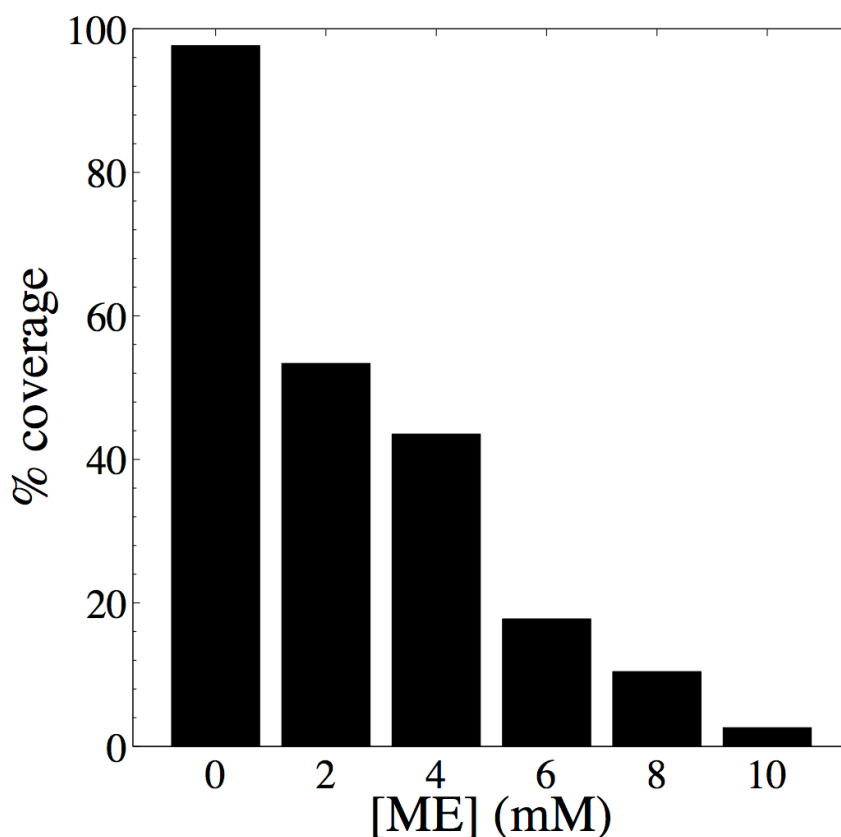
Figure 21: Plot representing the percentage of the area covered by the spots with respect to the total area covered by the precipitate as the concentration of $\beta-$ME varies between 0 mM and 10 mM. Initial conditions: Inner $[Cd^{2+}]_0 = 80$ mM; Outer $[S^{2-}]_0 = 400$ mM; Gelatin = 5%; Temp = 22 °C.

H. Effect of Ionic Strength

To find out the effect of varying the ionic strength of the inner electrolyte on the pattern morphology, the spatiotemporal evolution of the reaction at different concentrations of sodium chloride is monitored. Four solutions of cadmium chloride with a concentration of 80 mM are prepared in 5% per volume gelatin. When the mixtures are heated, different concentrations (50, 100, and 200 mM) of sodium chloride (Merck), are added to each solution and then homogenized. After complete gelation, sodium sulfide solution (400 mM) is poured to the reservoir of each plate. A control dish (0 mM NaCl, 80 mM Cd^{2+}, and 400 mM S^{2-}) is used to compare the change in the pattern. The obtained results are represented in Figure 22.

The ionic strength of the solution can be calculated using the following relation:
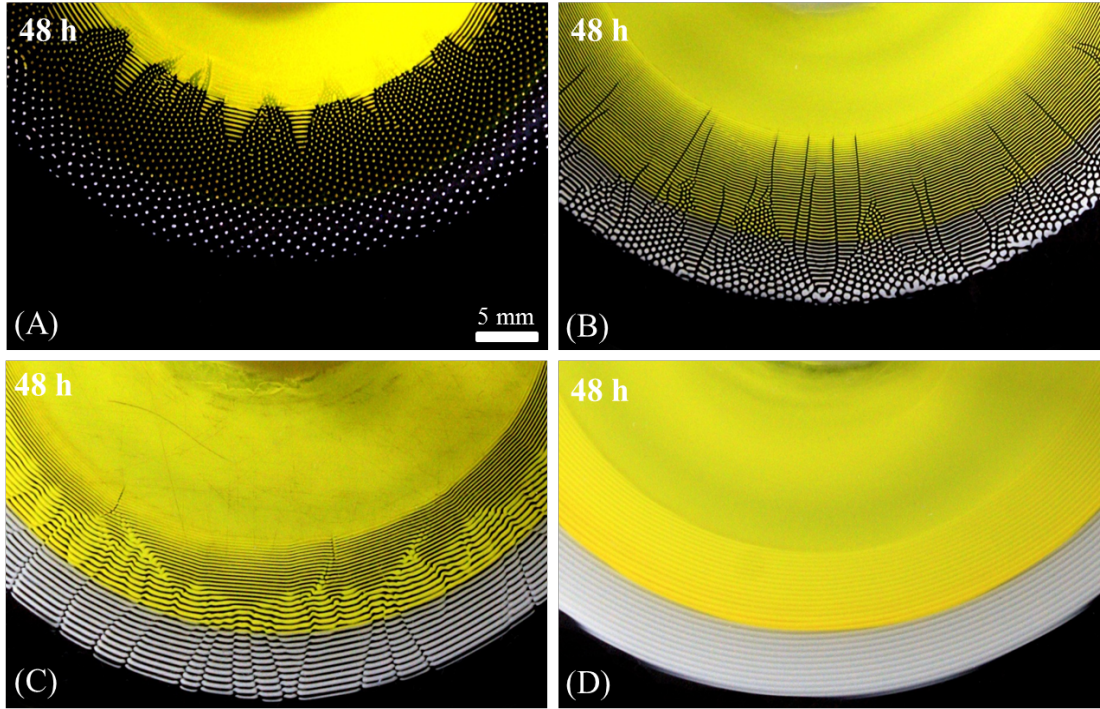
Figure 22: The evolution of precipitation patterns within 48 hours after NaCl addition: (A) = 0 mM; (B) = 50 mM; (C) = 100 mM; (D) = 200 mM. Initial conditions: Inner $[Cd^{2+}]_0 = 80$ mM; Outer $[S^{2-}]_0 = 400$ mM; Gelatin = 5%; Temp = 22 °C.

$I = \frac{1}{2}\sum C_i(Z_i)^2$ where I is the ionic strength (M), C_i is the concentration of the present ions (M), and Z_i is the charge of the ion. For the control plate, it is found that $I = 0.24$ M. Upon adding NaCl, the value of I increases to reach $0.29, 0.34,$ and 0.44 M when the concentration of NaCl used is 50, 100 and 200 mM respectively. As confirmed by Figure 23, the increase in the ionic strength of the inner electrolyte due to NaCl addition suppresses the formation of spots and results in the formation of thick rings.

I. Effect of Electric Field

The effect of applying a static electric field across the reaction-diffusion medium is another parameter of particular interest. When an electric field is applied, the spatial distribution of the precipitation pattern and the motion of the reaction zone are altered. This influence on the properties of the pattern occurs because ionic species are involved in the system of diffusion and chemical reactions. The coupling between reaction, diffusion,
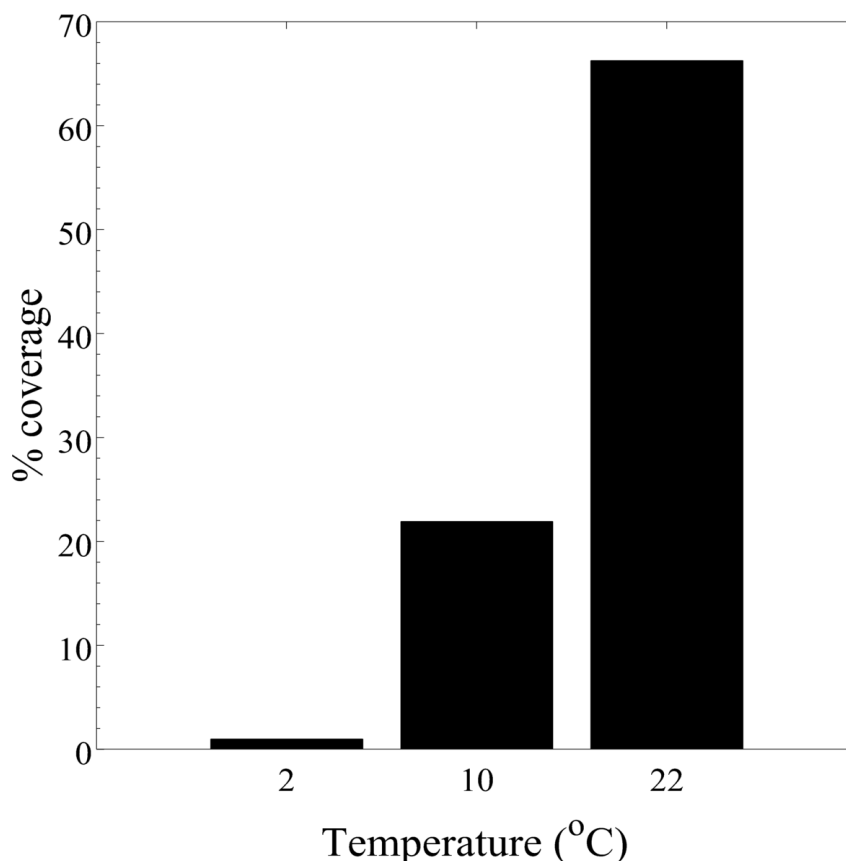
Figure 23: Histogram representing the percentage of the area covered by the spots with respect to the total area covered by the precipitate as the concentration of NaCl varies between 0 mM and 200 mM. Initial conditions: Inner $[Cd^{2+}]_0 = 80$ mM; Outer $[S^{2-}]_0 = 400$ mM; Gelatin = 5%; Temp = 22 °C.

and applied electric field in chemical systems has been closely examined in many studies of different Liesegang systems which exhibit band formation[102, 103, 104]. It has been established that the band spacing depends on both the intensity and direction of the applied field[94]. For instance, applying a positive electric field among the $Co(OH)_2$ system is shown to accelerate the front propagation and causes an increase in the band spacing, and the latter increases with the increase of the field strength[104]. On the other hand, Das *et al.*[105] demonstrate that the precipitation of the yellow HgI_2 is retarded in the presence of a reversed electric field, which is opposite to that of the diffusion front (negative field), and that the velocity of propagation decreases as the field strength increases.

In order to study the effect of applying a static electric field on the formation of spots in the cadmium sulfide/hydroxide system, two dishes are prepared under the normal conditions: 80 mM inner concentration dissolved in 5% per volume of gelatin gel and 400

mM outer concentration. The first plate is used as a control plate on which no electric field is applied. For the second plate, on which the electric field is to be applied, a circular-shaped tungsten wire (ALDRICH, 356972-18.9G) of 0.5 mm cross-sectional diameter is placed in the peripheral cavity of the Petri-dish cover. A straight wire electrode of the same material is placed vertically in the cylindrical tube to be filled later with sodium sulfide. In the case of a direct positive field, the outer circular electrode is connected to negative pole (cathode) of a power supply, and the inner straight electrode to the positive pole (anode). The opposite connections (outer electrode to the positive pole and the inner electrode to the negative pole) are set when a negative field is applied. The potential differences applied across the reaction medium are as follows: 0.5 V, 1.0 V, 1.5 V, and 2.0 V, but higher voltages were difficult to apply because the gel is deformed.

Results (Figs. 24 and 25) reveal that, upon applying a positive field of 0.5 V among the plate for 48 hours, the spots formation is slightly suppressed. Upon applying 1.0 V and 1.5 V for 48 hours, the formation of spots completely disappears, and the precipitation results in the formation of very thin rings and continuous bands respectively. 2.0 V marks a turning point, since the spot formation reappears but in a less prominent manner than when no electric field is applied. On the other hand, after a negative field is applied for 48 hours, the formation of spots is enhanced for the cases of 0.5 V and 1.0 V. Similarly, after 1.5 V is applied for 24 hours, more spots are formed as compared to the plate on which no electric field is applied. Note here that the plates are compared after 24 hours because the gel is deformed after 48 hours of electric field application. Again, 2.0 V marks a turning point since the formation of spots disappears completely. The percentage of the area covered by the spots with respect to the total area covered by the precipitate is measured for each plate after 48 hours in both, the positive and the negative field application. The obtained results are displayed in Figure 26 and 27
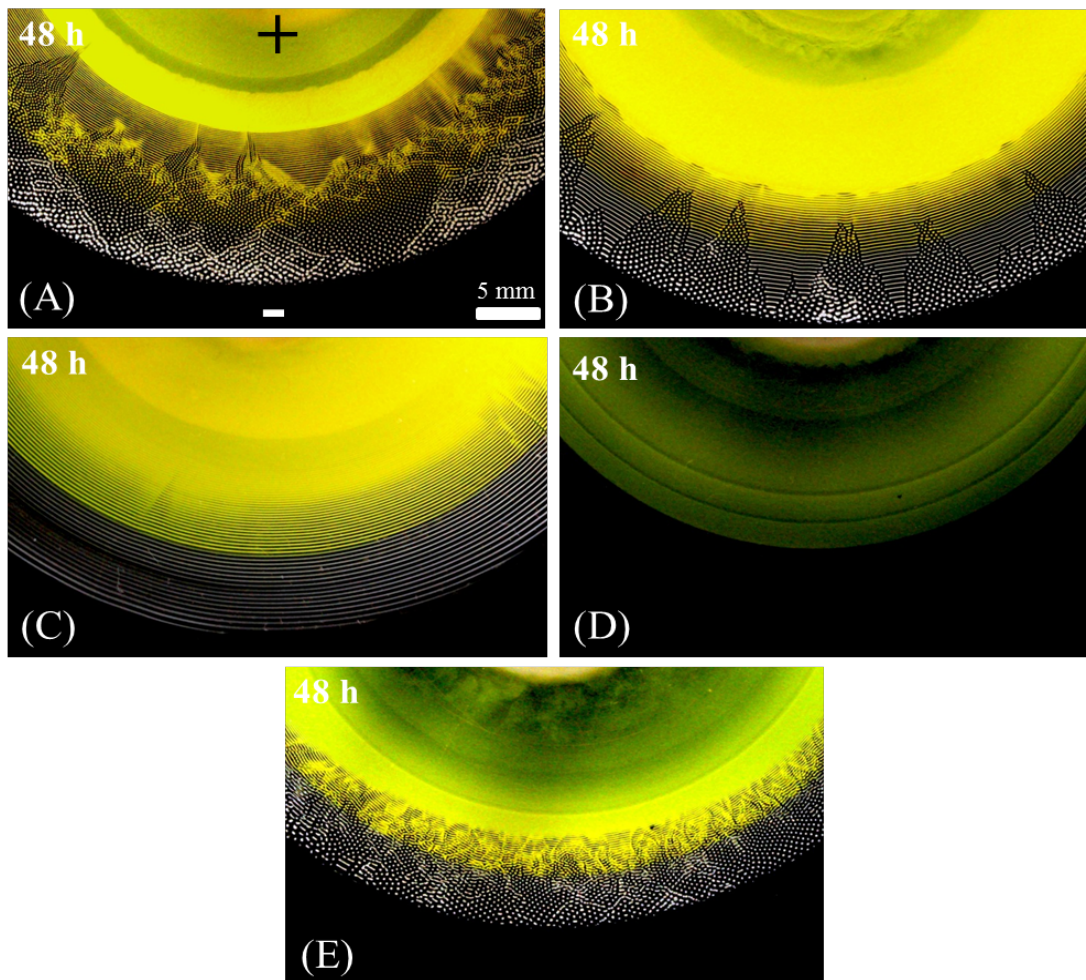
Figure 24: The evolution of precipitation patterns within 48 upon applying positive electric field: (A) = 0 V; (B) = 0.5 V; (C) = 1.0 V; (D) = 1.5 V; (E) = 2.0 V . Initial conditions: Inner $[Cd^{2+}]_0 = 80$ mM; Outer $[S^{2-}]_0 = 400$ mM; Gelatin = 5%; Temp = 22 °C.

J. Microscopic Approach

In order to inspect more the actual structure of the new precipitation pattern obtained, we employ Scanning Electron Microscopy (MIRA TESCAN) technique which allows us to examine the size and the shape of the precipitating bands and spots. To prepare the sample, a portion of the gel containing the precipitation pattern is cut cautiously from inside the reactor and placed on a glass slide. The sample is then dried using freeze-drying machine to form a dried-up thin film of the gel with the bands and spots trapped inside. The film is then placed on a carbon tape and coated with a few nanometers of platinum to be observed under SEM with SE and Inbeam detectors. Figures 28, 29, and

43
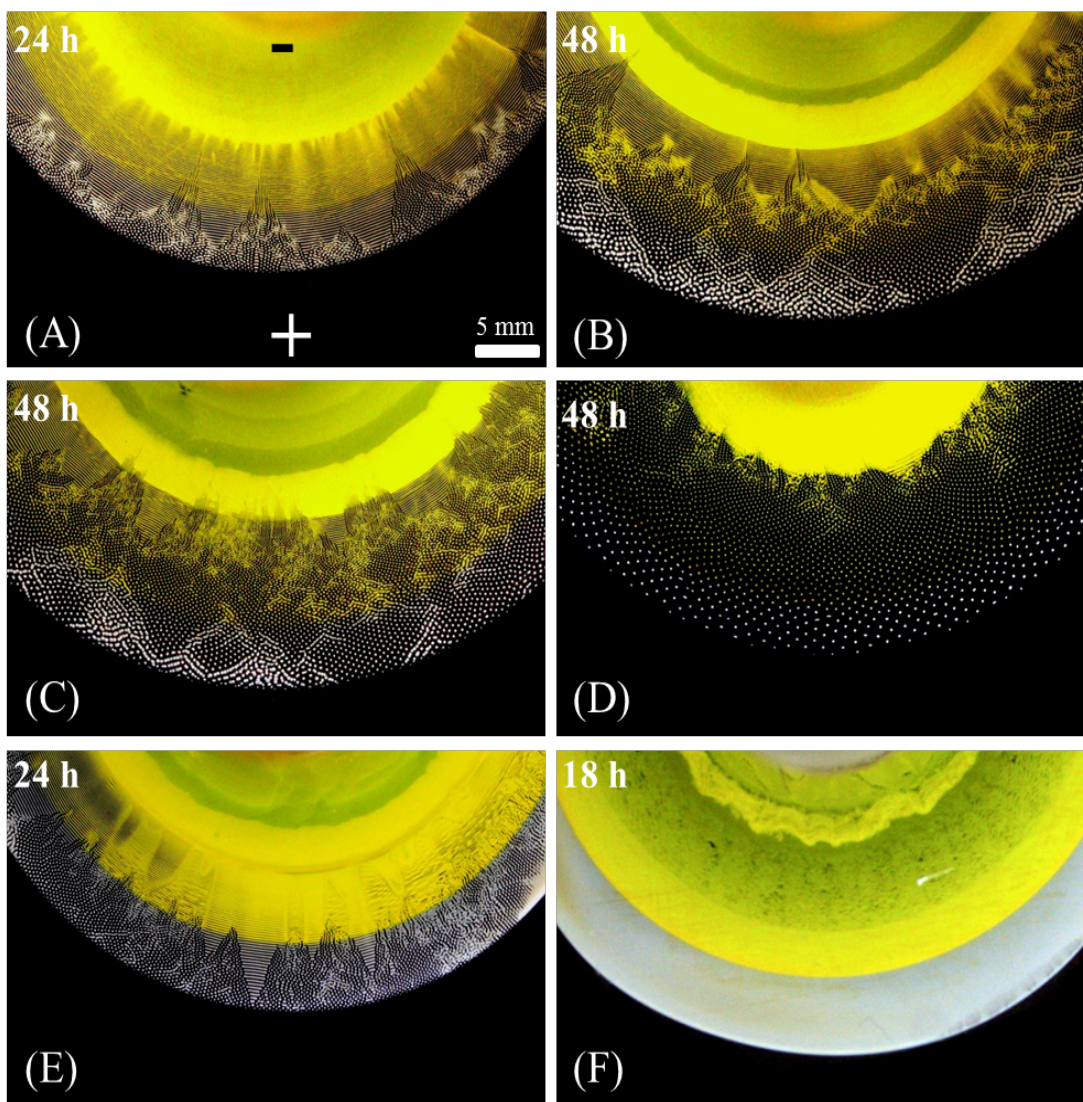
Figure 25: The evolution of precipitation patterns upon applying negative electric field: (A) = 0 V after 24 hours; (B) = 0 V after 48 hours; (C) = 0.5 V after 48 hours; (D) = 1.0 V after 48 hours; (E) = 1.5 V after 24 hours; (F) = 2.0 V after 18 hours. Initial conditions: Inner $[Cd^{2+}]_0 = 80$ mM; Outer $[S^{2-}]_0 = 400$ mM; Gelatin = 5%; Temp = 22 °C.
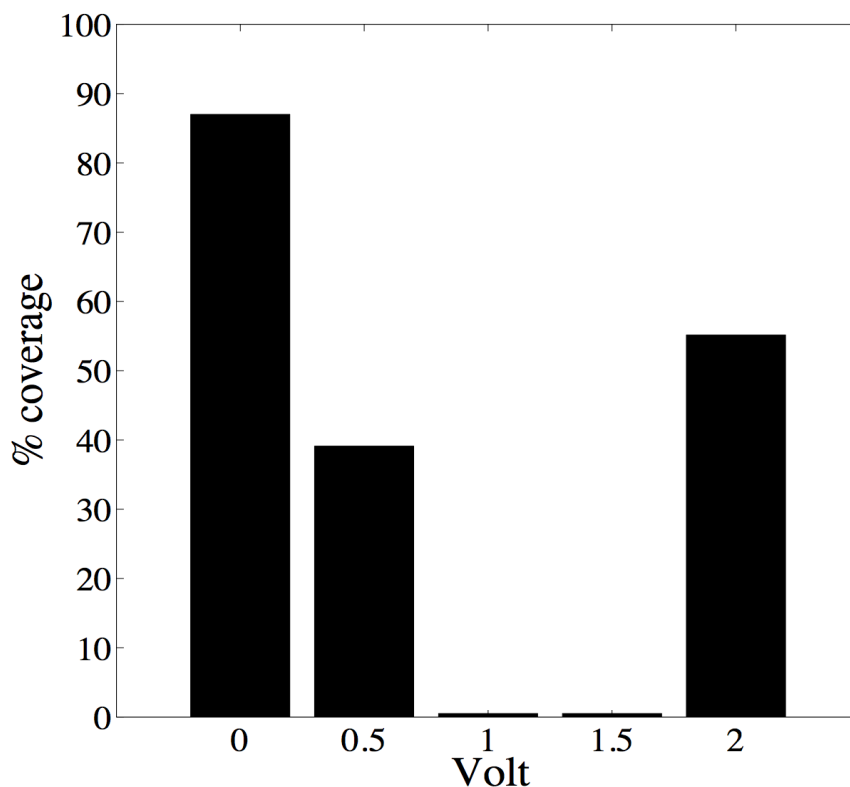
Figure 26: Histogram representing the percentage of the area covered by the spots with respect to the total area covered by the precipitate as the applied positive electric field varies between 0.0 V mM and 2.0 V. Initial conditions: Inner $[Cd^{2+}]_0 = 80$ mM; Outer $[S^{2-}]_0 = 400$ mM; Gelatin = 5%; Temp = 22 °C.

30 represent a panel of the captured images that display various attractive morphological structures of the bands and spots.

The obtained micrographs clearly show the morphology of the precipitation pattern. The spots have spherical or oval shapes with an average diameter of 120 μm. They are thick and compact solids sticking out of the thin film of gel and exhibiting a porous structure. On a higher magnification, the inside structure of the pores appears to be formed of agglomerated spherules of 0.4 μm in diameter. On the other hand, the precipitation bands are also protruding structures of about 55 μm thickness and clearly shaped walls that are 100 μm in height. On a closer view, the bands show small aggregated spheres of 0.4 μm. Between the spots an area of thinner and nearly transparent structure is seen which corresponds to the depletion zone in the gel medium.
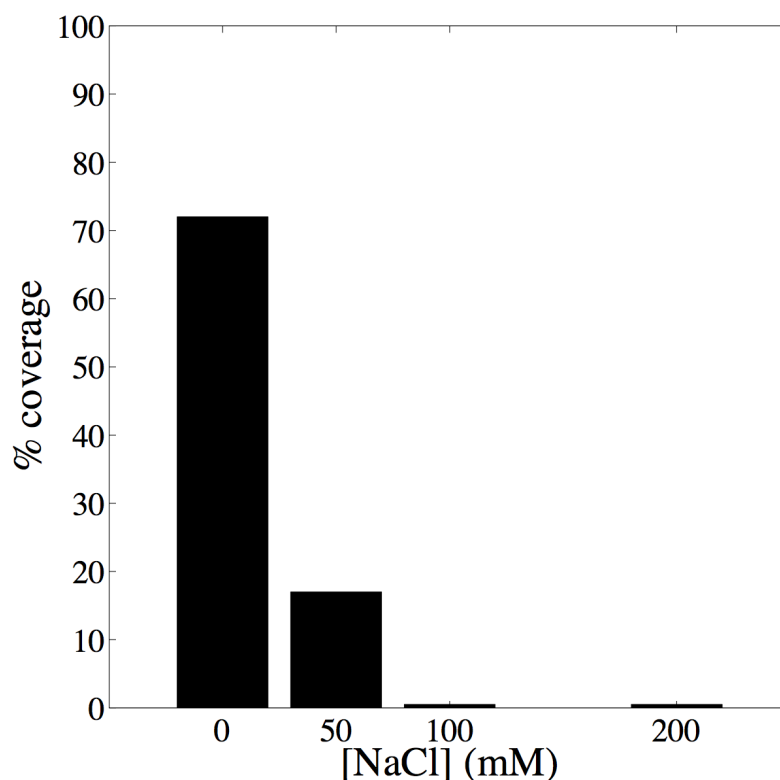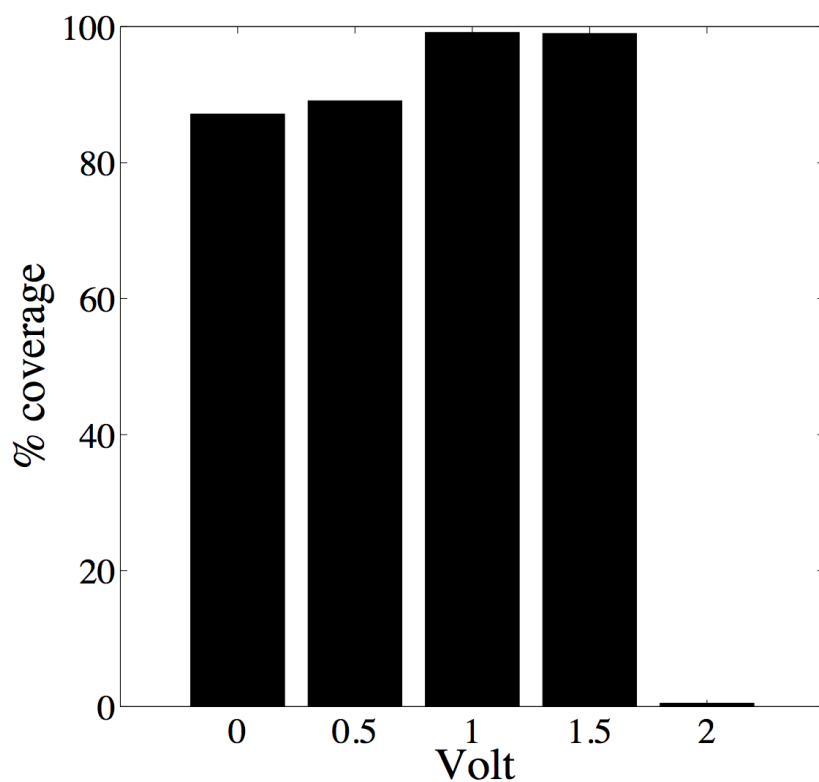
Figure 27: Histogram representing the percentage of the area covered by the spots with respect to the total area covered by the precipitate as the applied negative electric field varies between 0.0 V and 2.0 V. Initial conditions: Inner $[Cd^{2+}]_0 = 80$ mM; Outer $[S^{2-}]_0 = 400$ mM; Gelatin = 5%; Temp = 22 °C.
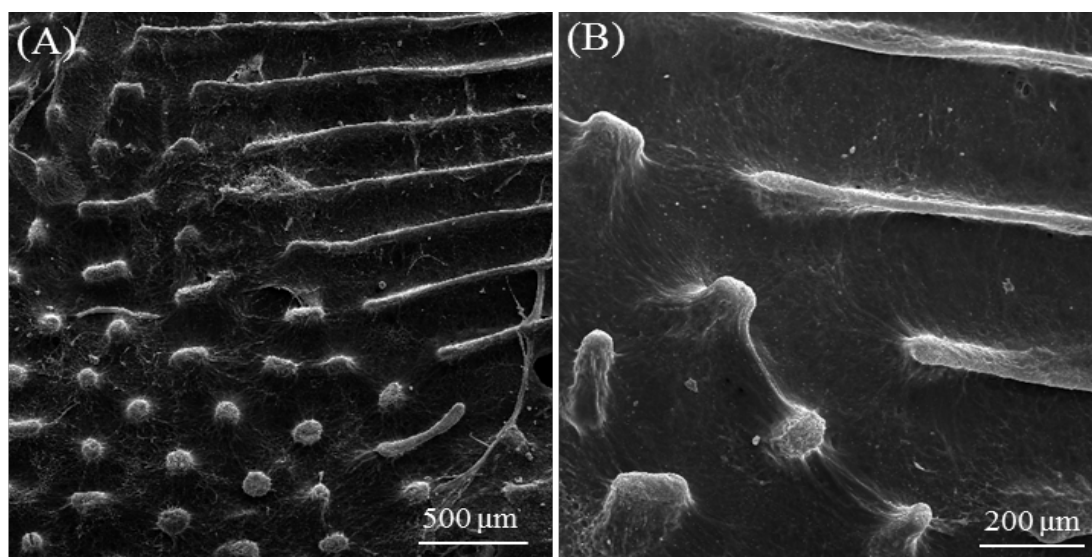
Figure 28: (A) SEM image representing the transition from bands to spots. Initial conditions: inner, $[Cd^{2+}]_0 = 80$ mM in 5% per volume gelatin gel, outer, $[S^{2-}]_0 = 400$ mM. (B) A magnified image displaying the protruding structure of the bands and spots.
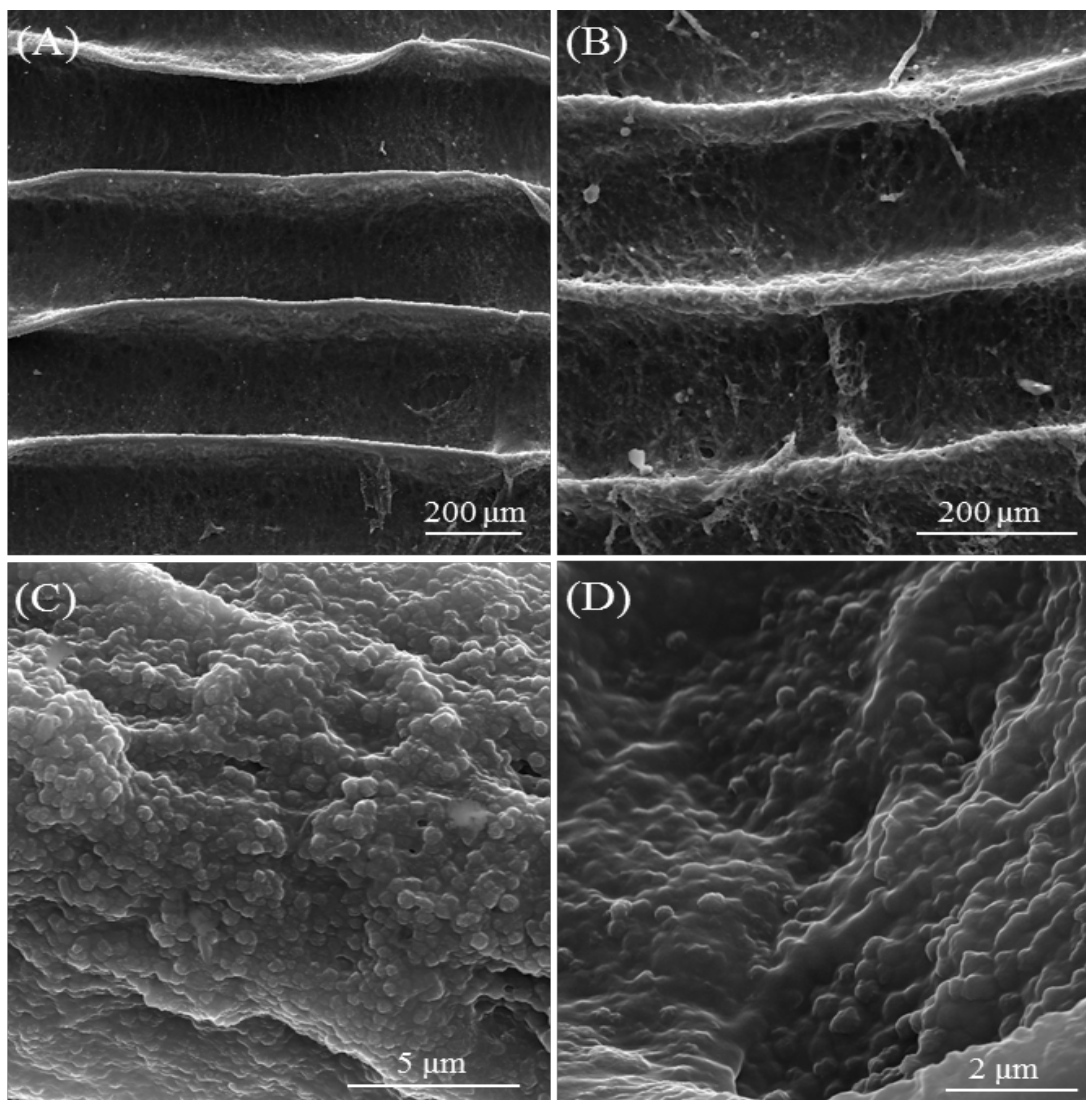
Figure 29: Panel showing several SEM micrographs captured for various regions of the precipitation bands. Initial conditions: inner, $[Cd^{2+}]_0 = 80$ mM in 5% per volume gelatin gel, outer, $[S^{2-}]_0 = 400$ mM. (A) and (B) display the height and the width of the band calculated to be 100 μm and 55 μm respectively. (C) and (D) represent a magnified image for the band consisting of small agglomerated spheres with a diameter of 0.4 μm.
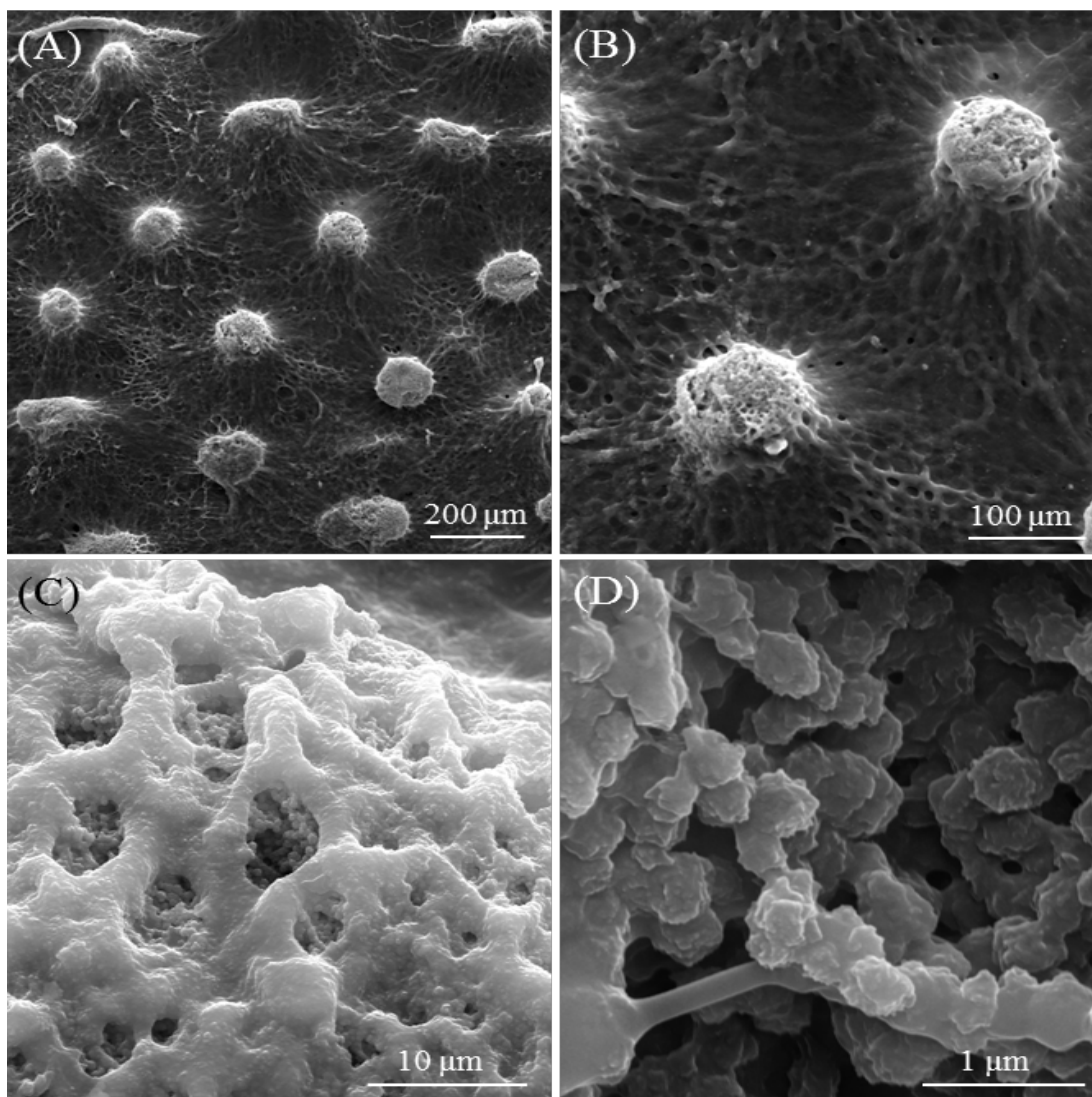
Figure 30: SEM micrographs of the dried gel containing the spots pattern. Initial conditions: inner, $[Cd^{2+}]_0 = 80$ mM in 5% per volume gelatin gel, outer, $[S^{2-}]_0 = 400$ mM. (A) represents the hexagonal symmetry of the precipitating spots and the empty surrounding corresponding to the depletion zone. (B) and (C) show a closer and outer view of the spots with a diameter of 120 μm. (D) displays a higher magnification for the spot consisting of small aggregated spherules with a diameter of 0.4 μm.

CHAPTER III

THEORETICAL STUDY

A. Introduction

Spinodal decomposition scenario is an important mean-field theory that was first described in 1999 by Antal, Droz, Magnin and Rácz[75, 76] in an attempt to model the formation of Liesegang patterns. It is a standard model for phase transition and it has several applications to phase transition in binary mixtures[106], alloys[107], liquid crystals[108], vapor condensation[109], and formation of sand ripples[110]. In reaction-diffusion systems, this model has also proved its power by describing regular patterns and, furthermore, by explaining how those patterns can be influenced by the concentration of the outer and inner electrolytes[76], and by an external electric field[94].

In this chapter, a scenario analogous to spinodal decomposition using the Cahn-Hilliard (CH) equation is shown to reproduce the transition from bands to spots obtained in the cadmium sulfide/hydroxide precipitation system. We try to alter the initial conditions and other space parameters to investigate the threshold beyond which such a transition is suppressed. We also carry out a linear stability analysis to detect the stable and unstable modes of the system.

B. Spinodal Decomposition Scenario

According to the spinodal decomposition model, the two electrolytes A and B react to produce a constant density of colloidal particles C, denoted by c_0[48], which might subsequently undergo a phase separation[111, 112]. The value of c_0 can be determined from the initial concentration of A and B, a_0 and b_0, and their diffusion coefficients D_a

and D_b assumed to be equal $(D_a = D_b = D)$[78]:

$$c_0 \approx 0.85 K a_0 \sqrt{D/D_f}, \tag{22}$$

where $K = (1 + b_0/a_0)(2\sqrt{\pi})^{-1} \exp(-D_f/D)$ with the diffusion constant D_f derived from the following equation:

$$\text{erf}\left(\sqrt{D_f/2D}\right) = (a_0 - b_0)/(a_0 + b_0). $$

The properties of the front and the production of C are known[78]. Namely, the front moves diffusively with its position given by:

$$x_f(t) = \sqrt{2D_f t}, \tag{23}$$

and the production of C is restricted to a slowly widening narrow interval whose width in three dimensions shows the following behavior: $w_f(t) \sim t^{\frac{1}{6}} k$ around x_f, k being the reaction rate of the $A + B \rightarrow C$ process. The rate of production $(S(x,t) = kab)$ of C can be approximated by a Gaussian:

$$S(x,t) = \frac{S_0}{t^{2/3}} \exp\left[-\frac{\left[x - x_f(t)^2\right]}{2w_f^2(t)}\right], \tag{24}$$

where S_0 represents the amplitude of the source, and it is a function of the initial conditions and proportional to the reaction rate k[76].

Having a description of the production of C, it is time to move to the dynamics of their phase separation. Since the emerging pattern is macroscopic, the phase separation can be described by the CH equation[79, 80], which is considered the simplest hydrodynamical equation that respects the conservation of C. However, the CH equation requires the knowledge of the free-energy density functional $F[c]$ of the system. In a ho-

mogeneous equilibrium state, $F[c]$ should have two minima corresponding to the low (c_l) concentrations of C (no precipitate) and high (c_h) concentrations of C (precipitate). As a convenient form with minimal number of parameters, one can take F in the Ginzburg-Landau form[75] which is symmetric about $\bar{c} = (c_h + c_l)/2$:

$$F[c] = -\frac{1}{2}\varepsilon(c-\bar{c})^2 + \frac{1}{4}\gamma(c-\bar{c})^4 + \frac{1}{2}\sigma_0(\nabla c)^2, \tag{25}$$

where ε, γ, and σ_0 are phenomenological parameters, and the minima of $F[c]$ are fixed at c_h and c_l by setting $\sqrt{\varepsilon/\gamma} = (c_h + c_l)/2 \approx c_h/2$, due to the fact that $c_h \gg c_l$, i.e. the gaps between the precipitation zones have very low steady-state concentration of C. This function can be rewritten in terms of a shifted and rescaled concentration field $\varphi = (2c - c_h - c_l)/(c_h - c_l)$ over the spatial domain Ω :

$$F[\varphi] = \int_\Omega \left(-\frac{1}{2}\varepsilon\varphi^2 + \frac{1}{4}\gamma\varphi^4 + \frac{1}{2}\sigma(\nabla\varphi)^2 \right) d\Omega. \tag{26}$$

Here σ is the rescaled surface tension, while ε and γ are the positive constants that define the boundary between the stable and metastable regions $\left(\varphi = \pm\sqrt{\varepsilon/\gamma}\right)$ and the spinodal line between the metastable and unstable regions $\left(\varphi = \pm\sqrt{\varepsilon/3\gamma}\right)$.

By including the source term, the CH equation takes the following form:

$$\frac{\partial c}{\partial t} = -\lambda_0 \Delta(\delta F/\delta c) + kab, \tag{27}$$

where λ_0 is a kinetic coefficient.

In principle, the CH equation should contain two noise terms. The first is the thermal noise and the other is a noise in the source term (S). Both of these terms are neglected here. The reason for omitting the first is the low effective temperature of the phase separation, whereas the second is dropped because the properties of the $A + B \rightarrow C$ type reaction fronts have been shown to be mean-field like above dimension two[113], which is considered as an indication that the noise in the source term (S) can be neglected.

Figure 31 represents a schematic diagram of the free energy curve F plotted as a function of the rescaled concentration φ at temperature T_2. c_l and c_h correspond to the free energy minima, that is where the second derivative of the free energy $F[\varphi]$ with respect to composition is positive $[\frac{\partial^2 F}{\partial^2 c} > 0]$. By joining these two minimal points by a common tangent, the region of phase separation, known as the miscibility gap, is defined. For any homogeneous solution brought into the miscibility gap, the phase separated system is energetically favorable. The locus of c_l and c_h as the temperature varies is known as the coexistence or the binodal curve. Within the binodal is a region called the spinodal, which is characterized by a negative curvature on the free energy curve $[\frac{\partial^2 F}{\partial^2 c} < 0]$, and it lies within the inflection points of the curve $[\frac{\partial^2 F}{\partial^2 c} = 0]$ that are called the spinodes (pointed by S_1 and S_2 on figure 31). The binodal and spinodal lines meet at a critical point defined by the condition $\frac{\partial^3 F}{\partial^3 c} = 0$, and the corresponding temperature is called the critical temperature T_c.

As the concentration of the produced C particles increases, the system crosses the binodal curve to the metastable region, which has a higher free energy than the phase separated state. Although the mixed state is no longer thermodynamically favored, there is an energy barrier that must be overcome to achieve phase separation. Therefore, large fluctuations in composition (nuclei) are necessary to overcome the energy barrier separating the local free energy minimum of the mixed state from the global minimum associated with the phase-separated state. In periodic precipitation, this process is described by nucleation and growth mechanism, in which nucleation occurs when the local concentration of C reaches some threshold value c^*. Importantly, there is a characteristic rate associated with nucleation. If this rate of nucleation is very small compared to the rate at which C particles are produced, a very fast transition, often called a quench, moves the system directly from the single stable regime to the spinodal region before forming any nuclei, and the initially dispersed C particles in the solution tend to decompose into C-rich (i.e., the precipitation zone) and C-deficient regions (i.e., the empty regions between successive precipitating zones); a process known as the spinodal decomposition. A homogeneous

52
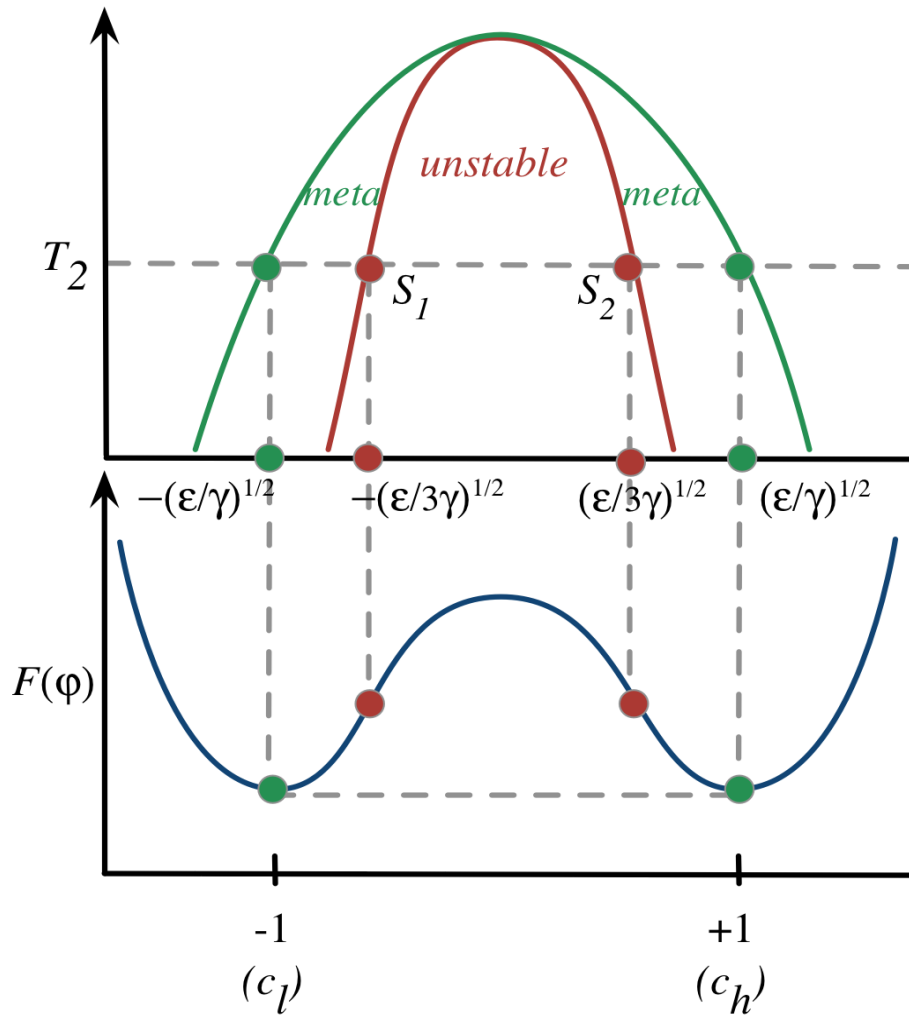
Figure 31: (a) Theoretical phase diagram for the spinodal decomposition model. (b) The free energy F as a function of the rescaled concentration field φ. The green line indicates the binodal curve separating the stable and the metastable states, with the green binodal points corresponding to the boundaries of the miscibility gap. The red curve defines the spinodal line that separates the metastable and the linearly unstable regions, and the red points S_1 and S_2 represent the spinodes.

solution within the spinodal region is unstable against infinitesimal linear perturbations, and any small local change in composition is amplified. Moreover, within the spinodal line there is no thermodynamic barrier for the reaction to proceed, and the phase separation is driven solely by diffusion. The separation process therefore starts with microscopic fluctuations in the chemical composition, and it proceeds with a net reduction in the free energy.

It is worth to mention here that in spinodal decomposition, material flows from regions of low concentration to regions of high concentration, a process known as uphill diffusion. This is the inverse of the regular situation, in which materials diffuses from regions of high concentration to regions of low concentration to avoid concentration gradients and reach uniform spatial distributions. This is because the main quantity that has to be uniform at equilibrium is the chemical potential (μ), not the concentration. The material will therefore diffuse according to the chemical potential gradient, from regions of high chemical potential to regions of low chemical potential. The chemical potential, however, is defined as the partial derivative of the Gibbs' free energy F with respect to the concentration of the species: $\mu = \frac{\partial F}{\partial c}$. So if the second derivative of free energy with respect to concentration is positive $\left(\frac{\partial^2 F}{\partial^2 c} > 0 \right)$, then chemical potential gradient has the same sign as the concentration gradient, and the material flows from region of high concentration to region of low concentration-downhill diffusion. Nevertheless, inside the spinodal region, $\frac{\partial^2 F}{\partial^2 c} < 0$, this means that low concentration regions have high chemical potential and the diffusion is reversed-uphill diffusion (Fig. 32).

C. Theoretical Modeling

The transition from bands to spots in the cadmium sulfide/hydroxide precipitation system is explained on the basis of this aforementioned spinodal decomposition scenario. First, the reaction front emerges due to the inhomogeneous initial distribution of
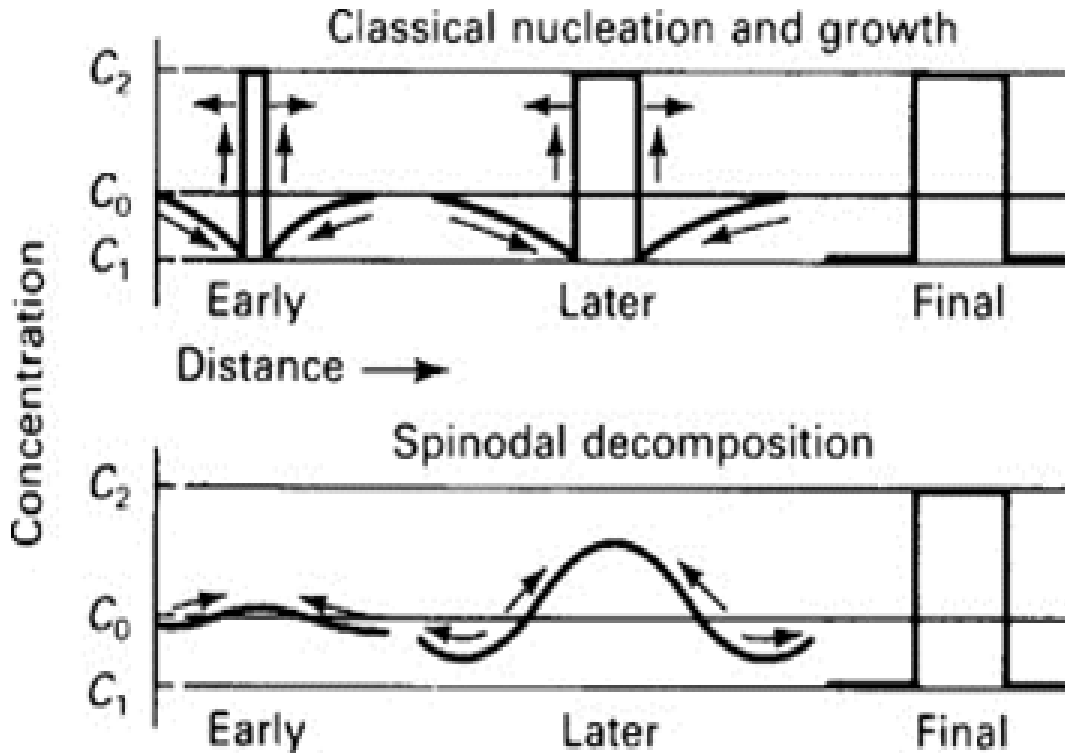
Figure 32: Schematic concentration profiles illustrating the different development of phase decomposition by nucleation and growth and by spinodal decomposition. The arrows indicate the direction of diffusion. During nucleation and growth, there is a sharp interface between the nucleating phase and the parent phase; the precipitate at all stages of its existence has the required equilibrium composition; the diffusion is always down a concentration gradient. In contrast, during spinodal decomposition, an initially homogeneous solution develops fluctuation of chemical composition when it reaches the spinodal region, these fluctuations are at first small in amplitude but grow with time until there are identifiable precipitates of equilibrium composition; the diffusion is up against a concentration gradient.

the electrolytes A and B. The concentration of the outer electrolyte $[a(x < 0, t = 0) = a_0]$ is considered to be much larger than that of the inner electrolyte $[b(x > 0, t = 0) = b_0$ with $a_0 \gg b_0]$ at a fixed point $x = 0$. Assuming an irreversible mean-field reaction, the electrolytes A and B yield the reaction product C $(A + B \rightarrow C)$. Since the process takes place in a gel, no convection is present, and thereby it can be modeled as a simple reaction-

diffusion process:

$$\frac{\partial a}{\partial t} = D_a \Delta_a - kab, \tag{28}$$

$$\frac{\partial b}{\partial t} = D_b \Delta_b - kab, \tag{29}$$

where a and b denote the concentrations of the inner cadmium and outer hydroxide ions respectively, D_a and D_b are their respective diffusion coefficients, Δ is the 2D Laplacian operator, and k is the precipitation reaction rate constant. We also assume that the reaction of cadmium ions with the hydroxide ions (R_2) is bimolecular. We do not attempt in this model to incorporate the yellow back-front due to ion exchange in (R_3) as it can be simply described as a diffusion-controlled process, independent of the precipitation reaction.

To simplify things further, unitless time and concentration variables are defined:

$$a = \alpha A; \ \ b = \beta B;$$

$$\tag{30}$$

$$t = \tau T; \ \ x = \xi L.$$

where α and β are the rescaled concentrations; and τ and ξ are the rescaled time and distance respectively.

After substituting equations (30) into (28) and (29), and multiplying through by T/A and T/B for equations (28) and (29) respectively, the following dimensionless equations are obtained:

$$\frac{\partial \alpha}{\partial \tau} = \Delta_\alpha - k\alpha\beta, \tag{31}$$

$$\frac{\partial \beta}{\partial \tau} = D\Delta_\beta - k\alpha\beta, \tag{32}$$

56

where $1/D_a = T/L^2$; $1/B = kT$; $D = D_b/D_a$, A is assumed to be equal to B, and k is taken to be equal to 1 with appropriate choice of time and length scales.

Similarly, the CH equation is solved for the dimensionless variables:

$$\bar{c} = \frac{c_h + c_l}{2}; \quad \hat{\mathbf{c}} = \frac{c_h - c_l}{2} \approx \frac{c_h}{2}; \tag{33}$$

$$\varphi = (2c - c_h - c_l)/(c_h - c_l) = \frac{c - \bar{c}}{\hat{\mathbf{c}}} \approx \frac{c}{\hat{\mathbf{c}}} - 1; \tag{34}$$

$$t = \tau T; \quad x = \xi L; \tag{35}$$

along with the dimensionless free energy:

$$F[\varphi] = \int_{\Omega} F[\varphi] = \left(-\frac{1}{2}\varepsilon\varphi^2 + \frac{1}{4}\gamma\varphi^4 + \frac{1}{2}\sigma(\nabla\varphi)^2 \right) d\Omega. \tag{36}$$

The following simple CH equation of dimensionless form is obtained:

$$\frac{\partial\varphi}{\partial\tau} = -\lambda\Delta(\varepsilon\varphi - \gamma\varphi^3 + \sigma\Delta\varphi) + k\alpha\beta, \tag{37}$$

where the parameters λ and σ are the rescaled kinetic coefficient and surface tension, respectively[76] $[\lambda = \lambda_0 T/L^2$ and $\sigma = \sigma_0/L^2]$. The ratio σ/λ defines a characteristic time scale of the growth of unstable modes in precipitation. In general, comparing this time scale with the time it takes for the front to pass through a certain region determines whether slow nucleation-and-growth (metastable region) or fast spinodal decomposition (unstable region) dominates the pattern formation[114], especially in the presence of internal fluctuations.

Equations (31, 32, and 37) are solved numerically using a vertex-based finite volume method on unstructured meshes, whereby the spatial discretization is carried out using the control volume finite element method (CVFEM). The resulting nonlinear differential equations are successfully integrated using a fast and robust scheme based on operator splitting and a line search Jacobian-free Newton-Krylov method[115]. The struc-
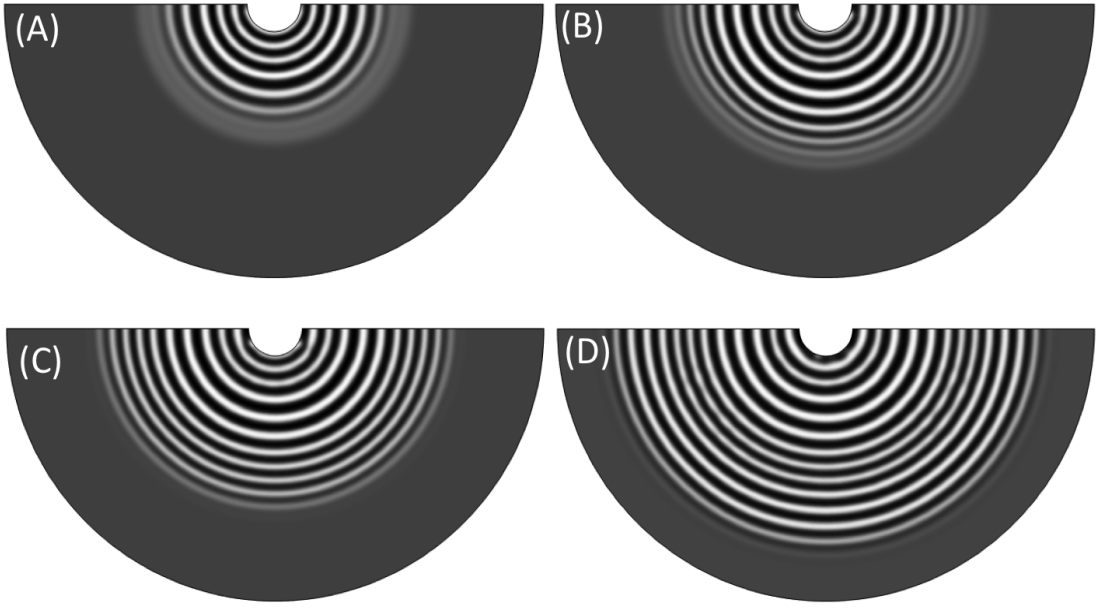
Figure 33: Time evolution of the field φ exhibiting rings formation. (A) t = 1000 (B) t = 1500; (C) t = 2500; (D) t = 3000. Parameters are $k = 1$, $D_a = 1$, $D_b = 1$, $\sigma = 3$, $\lambda = 0.1$, $\varepsilon = 1$, $\gamma = 0.15$. Initial conditions: $a_0 = 200$, $b_0 = 0.5$, $\varphi_0 = -1$ perturbed with 1% random noise. No-flux boundary conditions are applied at the external boundaries. The radius of the large circle is taken to be 8 times greater than that of the small circle. Number of elements is 11456.

tureless mesh, which is generated by the open source software *Triangle*[116], is suitable to reproduce the complex geometry of our circular reactor (Fig. 6). The initial conditions for a, b and φ are chosen such that $a_0 = a(t = 0) \gg b_0 = b(t = 0)$ and $\varphi_0 = \varphi(t = 0) = -1$, where a_0 is maintained at the inner circular boundary, and no-flux boundary conditions along the outer circular boundary are applied. In Figure 33, for a given set of parameters, the numerical solution reveals the formation of Liesegang rings only throughout the whole evolution.

When the initial conditions are altered, the simulation results depict the formation of Liesegang rings at the early stages of evolution (Fig. 34A) in the wake of a well-localized front that moves diffusively forward. The transition to spots takes place after the formation of a few rings (Fig. 34B) until the whole domain is filled with spots that coarsen with time in agreement with the experiment (compare Fig. 34C-D with Fig. 7).
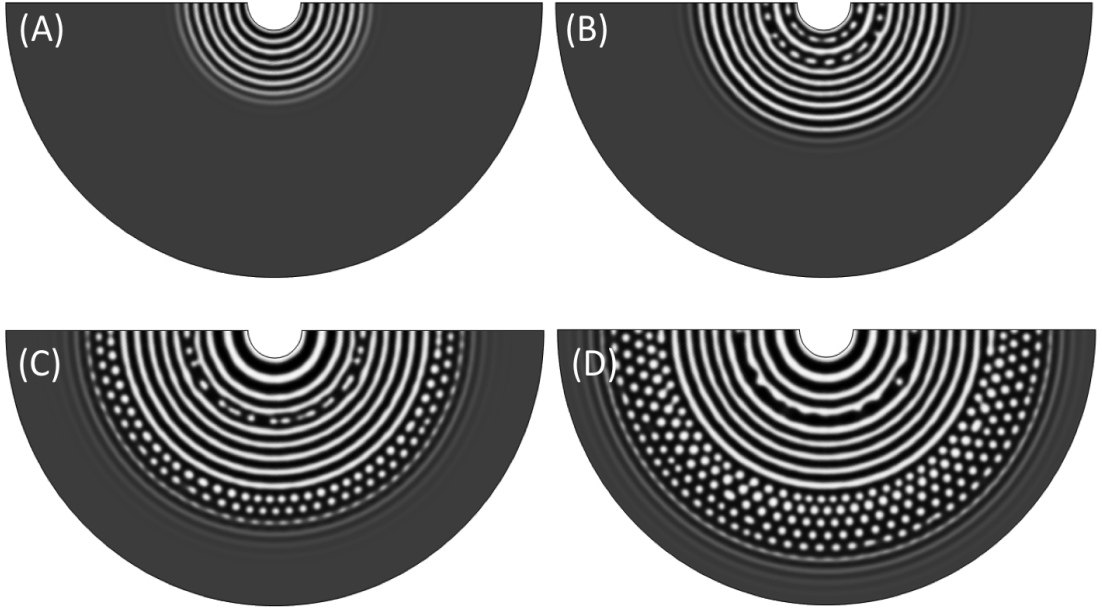
Figure 34: Time evolution of the field φ exhibiting transition from rings to spots. (A) t = 10; (B) t = 20; (C) t = 33; (D) t = 37. Parameters are $k = 1$, $D_a = 1$, $D_b = 1$, $\sigma = 1.5$, $\lambda = 0.15$, $\varepsilon = 1$, $\gamma = 0.15$. Initial conditions: $a_0 = 100$, $b_0 = 0.5$, $\varphi_0 = -1$ perturbed with 1% random noise. No-flux boundary conditions are applied at the external boundaries. The radius of the large circle is taken to be 8 times greater than that of the small circle. Number of elements is 11456.

D. Linear Stability Analysis

In order to study the stability conditions of the CH equation against a small perturbation, the following perturbation equation is used:

$$\varphi = \varphi_0 + \varphi', \tag{38}$$

where φ' is the perturbation term. By substituting this equation into (37), and linearizing it around φ_0 (i.e. neglecting the nonlinear terms), the following linearized CH equation with perturbation terms is obtained:

$$\frac{\partial \varphi'}{\partial \tau} = -\lambda \Delta (\varepsilon \varphi' + \sigma \Delta \varphi'). \tag{39}$$

The system is considered to be symmetric (all variations in θ direction are neglected), and all effects are occurring in the radial direction (r). Considering φ as a sum

59

of the Fourier modes:

$$\varphi = \sum_q \varphi_q e^{iq.r + \omega t}, \qquad (40)$$

where φ_q is the Fourier coefficient at $t = 0$, the following amplification factor $\omega(q)$ is obtained (Fig. 35):

$$\omega = q^2 \sigma \lambda \left[\frac{\varepsilon}{\sigma} - q^2 \right]. \qquad (41)$$

This shows immediately that for $\omega = 0$ and $\varepsilon > 0$, the system is linearly stable, whereas a band of Fourier modes are unstable for $\omega > 0$ and $\varepsilon > 0$, because in this case $-\sqrt{\frac{\varepsilon \lambda^2}{\sigma}} < q < \sqrt{\frac{\varepsilon \lambda^2}{\sigma}}$, and the temporal part of equation (40) grows exponentially. When $q > \sqrt{\frac{\varepsilon \lambda^2}{\sigma}}$ and $q < -\sqrt{\frac{\varepsilon \lambda^2}{\sigma}}$, $\omega < 0$ which means that the system is stable. Moreover, the most unstable mode is for $q_{C-H} = \sqrt{\frac{\varepsilon}{2\sigma}}$.
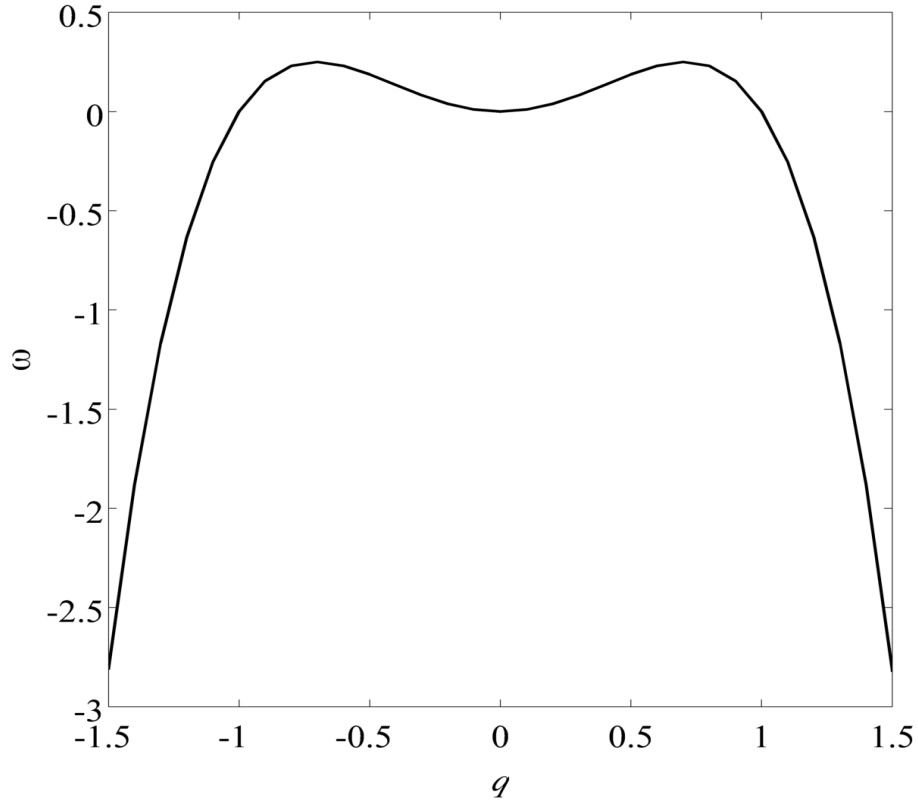
Figure 35: Dispersion relation between ω and q with σ, λ, and ε are taken to be equal to 1.

This wave number of maximum amplification factor will dominate during the first stage of the dynamics and this explains the reason why the homogeneous domains

appear at length scales close to $L = \lambda_{C-H}/2 = \pi/q_{C-H}$, half the wave length associated with the instability. For longer times, interfaces separating each domain interact through Ostwald ripening, causing L to change slowly towards higher values.

E. Numerical Results

The parameter space is then explored in order to locate a possible threshold beyond which the transition from bands to spots is suppressed. It is noticeable that if the estimated φ_0 generated by the reaction front is in the unstable region but close to the spinodal line, only rings are obtained. On the other hand, the deeper the system penetrates into the unstable region away from the spinodal line, the faster the transition to spots occurs. In the case of Figure 34, the threshold value is obtained for $\varepsilon = 1$ and $\gamma \approx 0.15$. This could be attributed to strong nonlinear coupling and interactions between unstable modes that can be expressed as patterns that are more complex than regular bands. Moreover, we investigate the effect of varying different parameters on the morphology of the theoretical pattern obtained. The simulation results confirm the transition from bands to spots when the concentration field φ_0 lies in the unstable regime for a fixed a_0 and b_0 (Fig. 36). As the inner concentration b_0 is increased, the concentration field φ_0[76] increases too. This corresponds to moving horizontally on the phase diagram at a given outer concentration (Fig. 37). For high values of b_0, the obtained spots start to coarsen and then merge to form thicker bands as confirmed experimentally by the phase diagram represented in Figure 9.

Furthermore, we study the effect of varying the rescaled surface tension σ and the kinetic constant λ. The numerical solutions are represented in Figure 38 and 39, which reveals that the increase in σ or the decrease in λ results in a total suppression of spots.
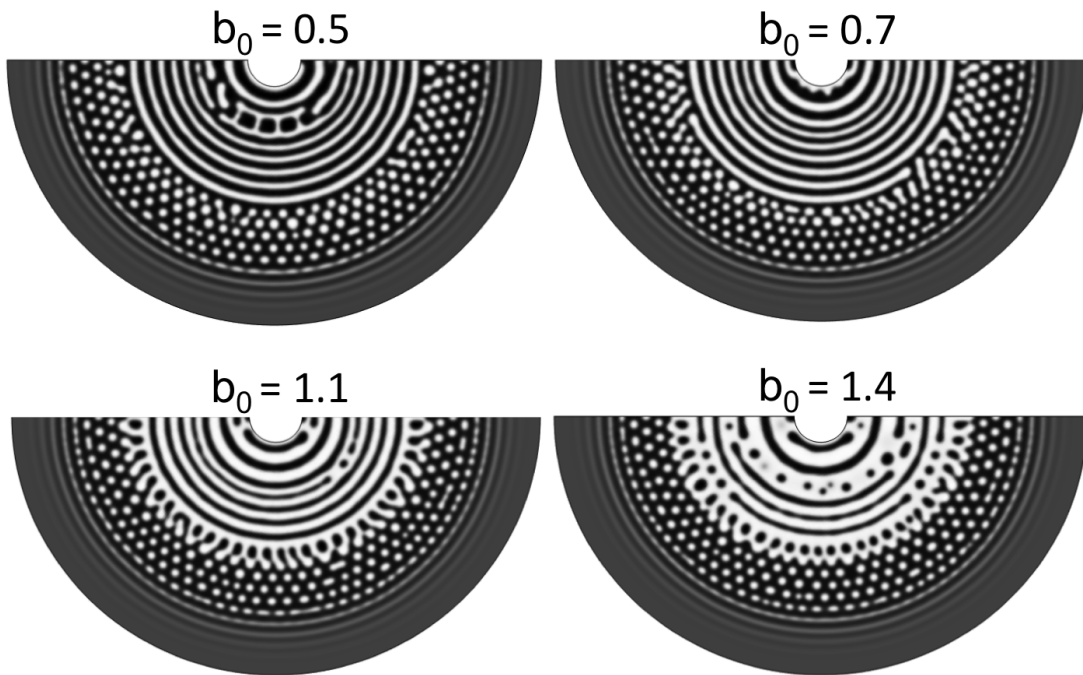
Figure 36: Time evolution of the field φ exhibiting transition from rings to spots at different b_0. Parameters are $k = 1$, $D_a = 1$, $D_b = 1$, $\sigma = 1.5$, $\lambda = 0.15$, $\varepsilon = 1$, $\gamma = 0.15$. Initial conditions: $a_0 = 70$, $\varphi_0 = -1$ perturbed with 1% random noise. No-flux boundary conditions are applied at the external boundaries. The radius of the large circle is taken to be 8 times greater than that of the small circle. Number of elements is 11456. As the concentration of b_0 increases, the obtained spots start to merge to form thicker bands as confirmed by the phase diagram.
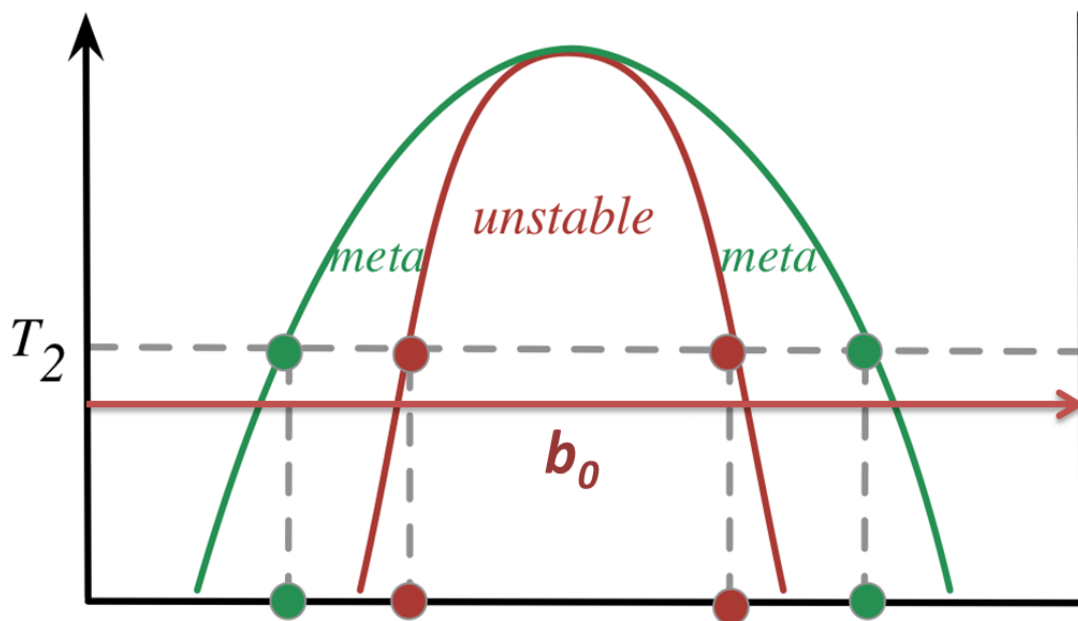
Figure 37: Phase diagram for spinodal decomposition representing the direction of the concentration field φ_0 as the initial concentration of the inner electrolyte b_0 is increased.
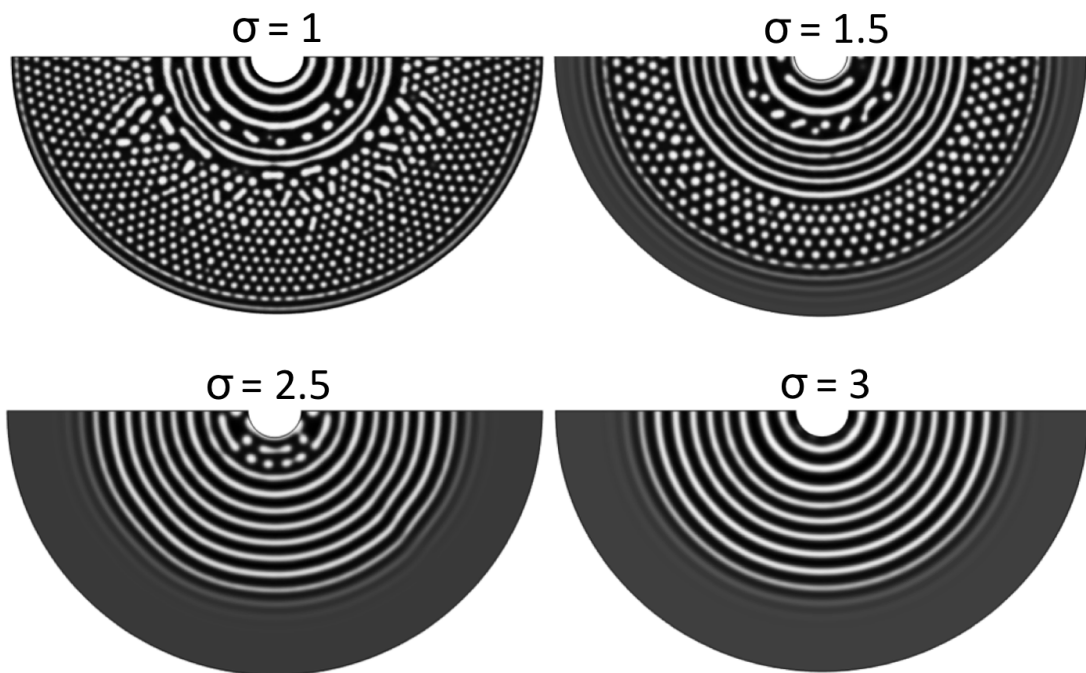
Figure 38: Time evolution of the field φ exhibiting transition from rings to spots at different σ. Parameters are $k = 1$, $D_a = 1$, $D_b = 1$, $\lambda = 0.15$, $\varepsilon = 1$, $\gamma = 0.15$. Initial conditions: $a_0 = 60$, $b_0 = 0.3$, $\varphi_0 = -1$ perturbed with 1% random noise. No-flux boundary conditions are applied at the external boundaries. The radius of the large circle is taken to be 8 times greater than that of the small circle. Number of elements is 11456.
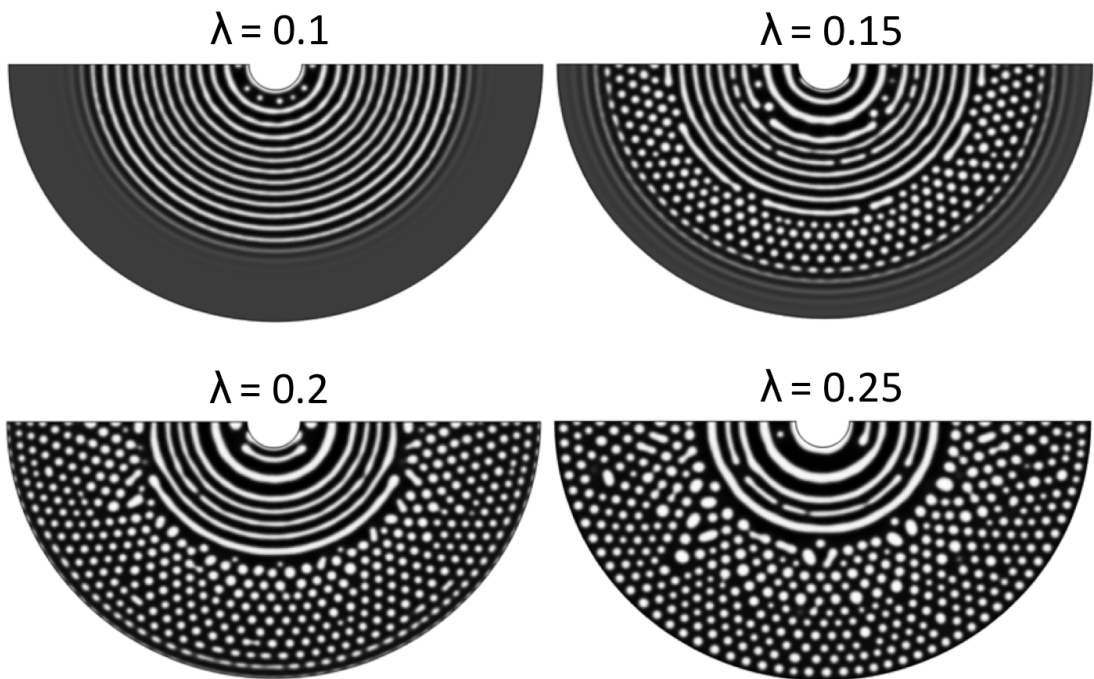
Figure 39: Time evolution of the field φ exhibiting transition from rings to spots at different λ. Parameters are $k = 1$, $D_a = 1$, $D_b = 1$, $\sigma = 1.5$, $\varepsilon = 1$, $\gamma = 0.15$. Initial conditions: $a_0 = 80$ $b_0 = 0.3$, $\varphi_0 = -1$ perturbed with 1% random noise. No-flux boundary conditions are applied at the external boundaries. The radius of the large circle is taken to be 8 times greater than that of the small circle. Number of elements is 11456.

F. Discussion

As mentioned before, the simulation results reveal that the transition from bands to spots takes place only when the front brings the system into the unstable region, whereas if the front is in the unstable region but close to the spinodal line, only rings are obtained. A theoretical phase diagram representing the numerical patterns obtained upon moving along a line at T_2 is represented in Figure 40. The trend of the resulting theoretical patterns, 'C', 'R', 'S', 'R', and 'C', is in very good agreement with the trend observed along a horizontal line on the experimental phase diagram displayed in Figure 9, with the exception of the 'R+s' region, which might require the inclusion of fluctuations in the diffusion coefficients of the species to imitate the static disorder in the gel[117]. Based on these results, the suppression of spots and the formation of more rings obtained upon varying some experimental parameters and their effect on the density of the formed colloids will be discussed.
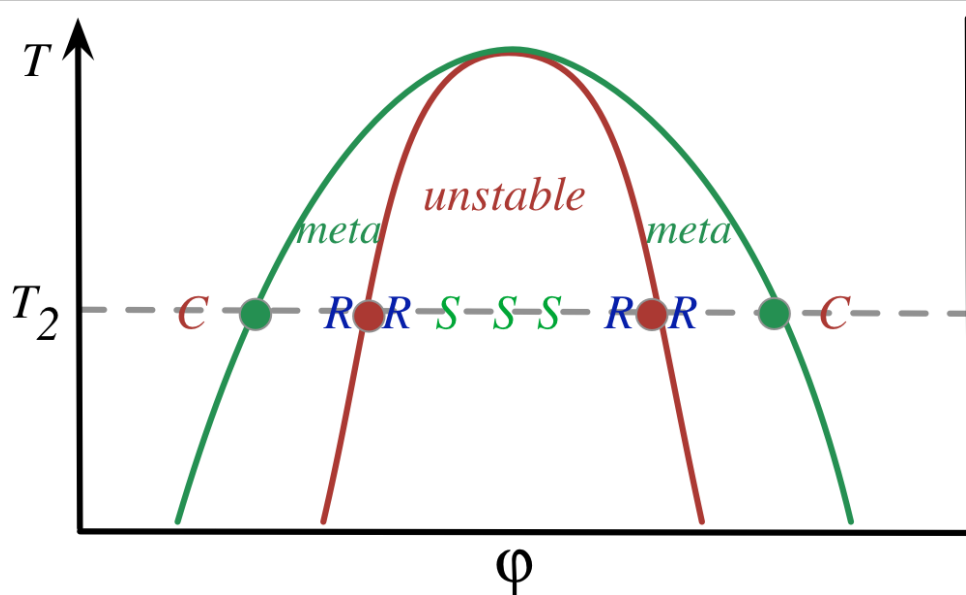
Figure 40: Theoretical phase diagram for spinodal decomposition representing the numerical patterns obtained after simulation. (C) = continuous precipitation band; (R) = precipitation rings; (S) = spots.

1. Effect of Inner and Outer Concentration

The phase diagram represented in Figure 9 shows that the initial concentrations of the inner and outer electrolytes provide a suitable spatial control for the morphology of the obtained pattern. Theoretically, it is assumed that at low inner and outer concentrations, the diffusion of the sulfide/hydroxide ions produces a low density of colloids. This allows the system to stay near the spinodal line where clearly separated thin rings, in agreement with the theoretical results, are formed (Fig. 10A). As the concentration of the electrolytes increases, a higher density of colloids is generated, which corresponds to an increase in the concentration field φ_0[76]. The system therefore crosses the metastable region and moves directly to the unstable state where the transition from rings to spots takes place (Fig. 10B). This corresponds to the state 'S' on the theoretical phase diagram (Fig. 40). A further increase in the concentration of the electrolytes results in the formation of thick rings with few spots in some cases (Fig. 9). The prevalence of rings versus spots in this case could be attributed to the high density of colloids produced upon increasing the inner and outer concentrations, which moves the front again around the metastable state where the formation of spots is less favored and the theoretical 'R' state dominates.

2. Effect of Gel Concentration

In order to detect the effect of gel on the size of the CdS colloids, a study was conducted by Mokalled *et al.* [118], which compares the absorption spectra of the front regions for two tubes having the same cadmium and sulfide concentrations, but one with 5% gelatin (tube 1), and the other with 1% agar (tube 2). The calculations of the size of the particles show that those in tube 1 are smaller than those in tube 2, which demonstrates that gelatin itself might play the role of a capping agent, thus preventing the agglomeration of CdS particles. Moreover, many publications have highlighted the use of gelatin to control the nucleation process and the size of the nanoparticles, because it is characterized

by a wide variety of functional groups that act as binding sites to Cd^{2+} ions, which in turn controls the growth of the CdS particles[119, 120].

In Figure 17, it is clear that upon increasing the gel concentration from 5% to 7%, the formation of rings predominates and the percentage of spots coverage decreases. This could be attributed to the limited growth of colloids resulting from high concentration of gelatin, which keeps the system around the spinodal line rather than going deep to the unstable region where spots are normally obtained.

3. *Effect of Capping*

Capping agents are generally added to protect the surface of the nanoparticles. This is due to the fact that favorable interactions between the capping agents and the solvents provide the energy barrier to overcome the Van der Waals attractions between the nanoparticles[121]. In particular, $\beta-$ME stabilizes the colloidal suspension of CdS produced in the bulk of the gel against aggregation or coagulation to maintain nanoparticles[101]. The capping occurs through the mercapto group, which covalently binds to the surface of the cadmium ions[122]. In an attempt to check the effect of ME on the front propagation and the growth of particles in CdS system, a recent study was conducted by Mokalled *et al.*[118]. Results show that the presence of the capping agent $\beta-$ME results in a faster front propagation because ME tends to compete against gelatin and bind to Cd ions, thus freeing the Cd-gelatin binding sites. Moreover, the absorbance spectra obtained for the front regions show that the size of the CdS nanoparticles in the presence of ME is smaller. This clearly reveals the role of ME in reducing the agglomeration and thus controlling the size of the particles. Therefore, the addition of ME to the cadmium sulfide/hydroxide system contributes to the formation of smaller CdS clusters, and the increase in the concentration of ME results in more capping and less agglomeration. Hence, a lower density of colloids is formed and the system goes near the spinodal line where rings are more

favored. This assumption is based on the comparison between the theoretical pattern 'R' resulting at low density of colloids (Fig. 40), and the thin rings obtained experimentally at low colloid concentration (Fig. 9), which matches the appearance of thin rings with a gradual suppression in spots when the concentration of ME gets higher (Fig. 20).

4. *Effect of Ionic Strength*

The suppression of spots formation upon increasing the ionic strength is explained again on the basis of colloidal growth. In 2010, a study was conducted by Mullaugh *et al.*[123] to detect the effect of the ionic strength on the diameter of CdS nanoparticles measured by Dynamic Light Scattering (DLS). Results show that, at high ionic strength, CdS nanoparticles tend to aggregate as the concentration of the salt becomes higher due to the diminishing electrostatic repulsion between the nanoparticles. Therefore, aggregates of the nanoparticles diffuse more slowly in the solution than individual nanoparticles; as such, the hydrodynamic diameter determined by DLS reflects the size of the aggregate rather than the primary size of the nanoparticle. A similar study was also done in 2010 by Tai *et al.*[124] which presents similar results of CdS nanoparticles agglomeration at increased NaCl concentrations based on XRD and photoluminescence spectra analysis. This shows that the formation of thick rings at high ionic strength (Fig. 22 C and D) could be attributed to the fact that the presence of a strong electrolyte such as NaCl allows the aggregation of the CdS nanoparticles, thus bringing the front again near the spinodal line due to the high concentration of colloids, and therefore the formation of spots is suppressed. This result is confirmed by the similar thick rings formed experimentally at high inner and outer concentration of electrolytes (Fig. 9) and the dominance of the state 'R' theoretically at high density of colloids (Fig. 40).

Based on these results, we can conclude that the formation of spots taking place deep inside the unstable region requires a critical density of colloids, beyond and above

which no transition to spots takes place. Therefore, any factor that would influence the concentration of colloids such as the increase in the gel concentration, the addition of ME or the variation of the ionic strength will have a direct effect on the morphology of the obtained pattern.

CHAPTER IV

THREE-DIMENSIONAL PATTERNS

A. Introduction

The idea that reaction diffusion phenomena are essential to the functioning of biological processes[125, 126] and living organisms[127, 128] appears to be quite intuitive. Astonishingly, however, a clear-cut evidence that links reaction diffusion to living systems and natural patterns is relatively fresh, and dates back only to the 1940's, when the British mathematician, Alan Turing, proposed a mechanism for morphogenesis in biological systems based on chemical reactions coupled to diffusion[63]. At that time, nobody had an idea which fundamental evolution equations to use in order to describe morphogenesis, and it was expected that any suggested mathematical model would be very complicated due to the known complexity of cells and their interaction with one another. In his famous paper, entitled "The Chemical Basis of Morphogenesis", Turing suggested that while diffusion alone tends to create uniform spatial distribution, it could lead to the formation of cellular structures and nonuniform spatially extended patterns when coupled to chemical reactions with nonlinear chemical kinetics. Turing's 1952 paper was his only published venture into chemistry, and it was not provided with any quantitative details, yet it suggested the idea that morphogenesis could have a simple origin, and it had a profound effect on the way scientists thought about pattern formation and complex phenomena.

Due to the difficulty in satisfying all the requirements for their formation, the first clear-cut experimental observation of Turing patterns occurred nearly 40 years after their theoretical prediction, when De Kepper and co-workers realized stationary periodic concentration structures in a variant of chlorite-iodide reaction in a gel reactor[64]. These Turing structures are characterized by an intrinsic wavelength (λ), which depends

70

only on the kinetic and the diffusion constants. Depending on how this λ compares to the other dimensions (the distance between the critical Turing planes Δ, the length L, and the height h), two-dimensional[64, 129] (hexagonal arrays of dots and parallel stripe patterns) or three-dimensional patterns[130, 131] (lamella, hexagonal prisms and body centered cubic arrays) can develop. However, most of the previous investigations were restricted to two-dimensions, and only a few research groups were interested in Turing structures in three dimensions[130, 132]. This is because the numerical simulations of three-dimensional structures in reaction diffusion systems were technically demanding and time consuming, and many researchers thought that two-dimensional patterns could be sufficient to understand the general properties of these dissipative structures.

In the present work, three-dimensional Turing-like patterns are obtained when the diffusion of sulfide/hydroxide ions into the cadmium-doped gel is performed in a 3D reactor. The effect of the inner and outer electrolyte concentrations on the morphology of the obtained pattern is investigated, and the results are compared to the patterns obtained in 2D.

B. Experimental Procedure

To attain the exact concentration of cadmium (II) solution, varying amounts of cadmium chloride monohydrate $CdCl_2.H_2O$ (Mallinckrodt) corresponding to concentrations that range from 40 mM to 120 mM are dissolved in a 50.0 ml beaker containing 25.0 ml of double distilled water. 1.2500 g of gelatin powder (Difco) are then added to each salt mixture to make a 5% gelatin solution. After thorough mixing and heating at 80 °C, homogeneous clear solutions are obtained. The mixtures in the beakers are then covered with parafilm papers and allowed to stand for 24 hours at room temperature. After complete gelation, sodium sulfide nonahydrate $Na_2S.9H_2O$ (Alfa Aesar) of concentration ranging from 200 mM to 400 mM is taken over the surface of five sets of gel. The beakers

are then covered with parafilm and left in a thermostatic chamber at 22.0 ± 0.1 °C. The diffusion of the sulfide/hydroxide ions to the cadmium-doped gel and the pattern formation are monitored over a period of 24 hours. The beaker is attached to a clamp stand and photographs are taken from the bottom side of the beaker using a CCD camera (Fig. 41). The obtained pictures show a bottom view of the newly formed layer of precipitate.

C. Results and Discussion

At the moment the sulfide solution is introduced to the cadmium-doped gel, a white precipitate is formed at the liquid-solid interface, indicating a spontaneous reaction between the diffusing hydroxide ions OH^- and the cadmium ions Cd^{2+} embedded in the gel. When the control parameters are switched into a regime where patterns arise, chaotic pseudo-stationary spatial patterns in the form of cracks start to emerge spontaneously from the uniform white gel surface. Within a few hours, these cracks grow slowly and evolve with time until the system settles down to a nearly stationary state of Turing-like patterns. The obtained results are represented in Figure 42. It is noticeable that pattern formation starts to grow on the white surface of the precipitated $Cd(OH)_2$, however, its evolution ends up on a yellow background. This results from the anionic exchange process between OH^- and S^{2-} to form the yellow CdS as explained previously.

The transition from the uniform state to Turing-like patterns is studied using the concentrations of the inner and outer electrolytes as a control parameter. A phase diagram delineating the various patterns obtained is presented in Figure 43, and the resulting morphologies are displayed in Figure 44. At low cadmium concentration (40 mM), stationary labyrinthine structure (Fig. 45) appears initially at the grain boundaries, and then gradually spreads out to cover the whole domain. This common type of Turing patterns is observed at different wavelengths for any outer concentration in the used range. When the inner concentration is increased from 40 mM to 60 mM, the system exhibits two new
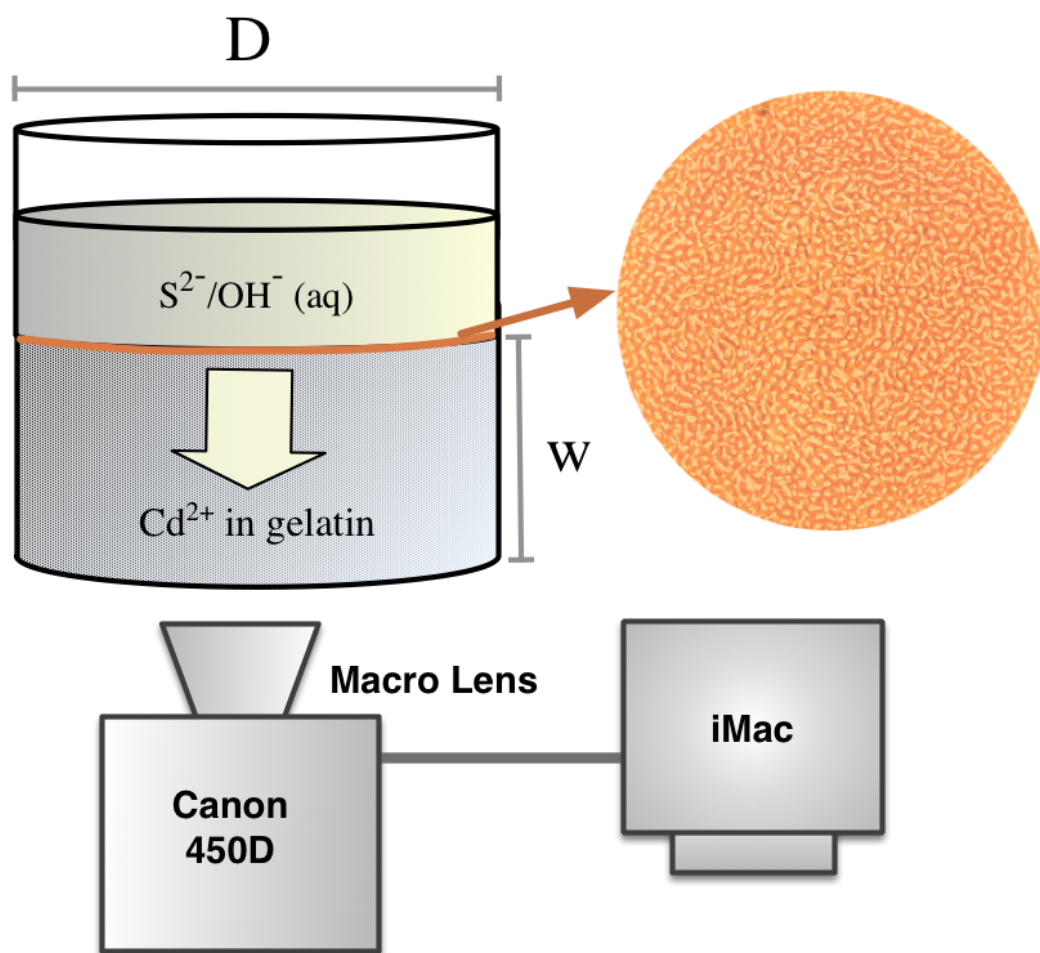
72

Figure 41: Schematic representation of the experimental setup under which the snapshots of the reaction are captured using a computer-controlled CCD and transferred to the computer for display. The outer sulfide is added to gelatin gel containing the cadmium ions. The screen on the right display a bottom view of the patterns as appearing in the white/yellow front parallel to the gel interface. The diameter of the reactor is $D = 4.0$ cm and the width of the gel $d = 3.0$ cm.
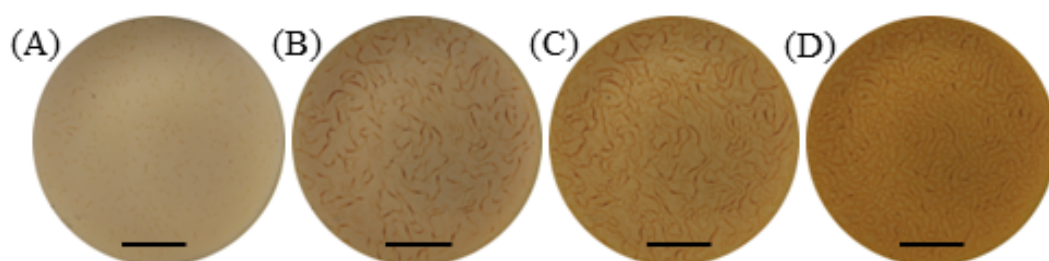

Figure 42: The evolution of Turing structures in cadmium sulfide/hydroxide system with time in three dimensions (bottom view). Initial conditions: Gelatin = 5%; Inner $[Cd^{2+}]_0 = 40$ mM; outer $[S^{2-}]_0 = 300$ mM; Temp = 22 °C. (A) t = 5 hrs; (B) t = 12 hrs; (C) t = 16 hrs; (D) t = 21 hrs. The scale bar represents 1 cm.

morphologies depending on the concentration of the outer electrolyte being used. At low outer concentration (200 M), we observe stationary island-like pattern (Fig. 46) that appears just like smudged points whose boundaries are not well defined and characterized by some randomness. At higher outer concentrations (250-350 mM) however, a mixed state of stripes and spots (Fig. 47) is obtained. Further increase in the cadmium concentration (80 mM) results in the formation of spatially distributed small spots with more or less defined shapes (Fig. 48) that gradually emerge and occupy homogeneously the initially unstructured area when the outer concentration is between 300 and 350 mM, whereas at lower sulfide concentrations (200-250 mM), the stationary island-like pattern is resumed. This latter appears to be a common pattern in most cases when the concentration of the doped cations reaches 120 mM. The obtained patterns are maintained for days without much change except for a very slow motion of the grain boundaries separating different domains, and therefore they are described as stationary Turing-like patterns. Beyond the critical values of the control parameters no pattern would emerge.
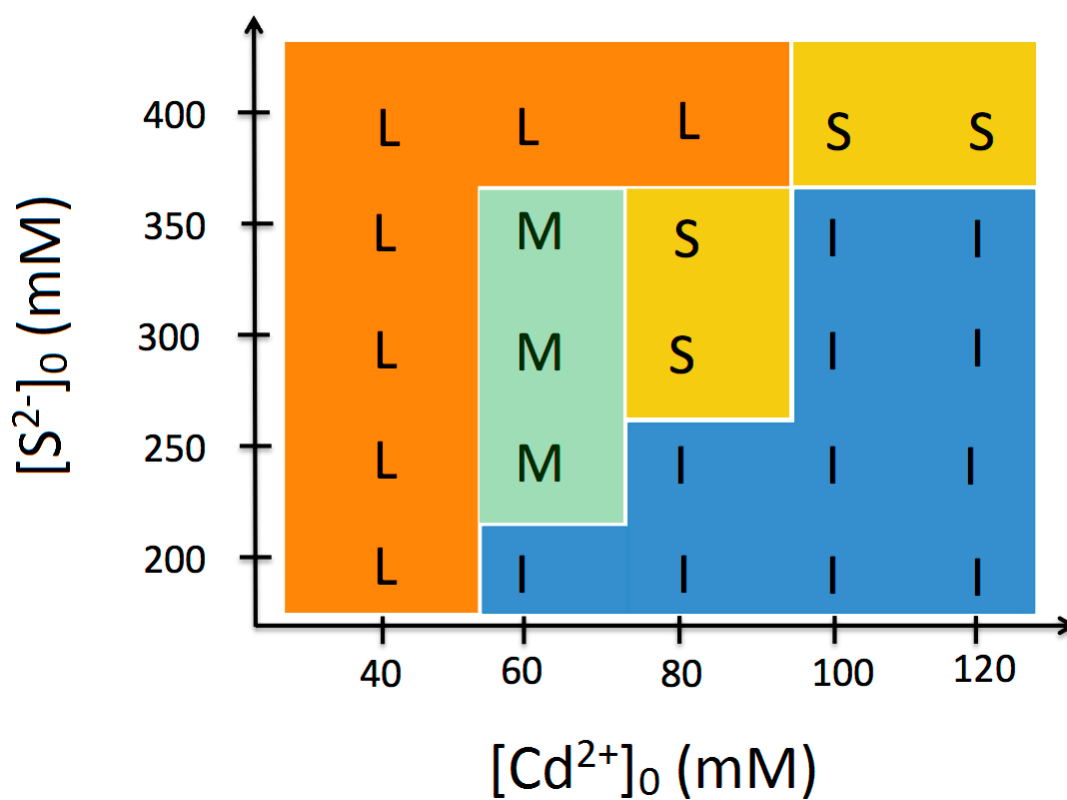
Figure 43: Phase diagram as a function of the inner $[Cd^{2+}]_0$ and the outer $[S^{2-}]_0$ showing the most probable type of self-organized patterns appearing in 3D reactor at every pair of inner/outer concentrations. **(L)** denotes labyrinth, **(M)** mixed state, **(S)** spots, **(I)** island.
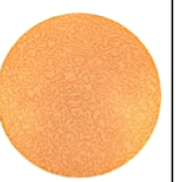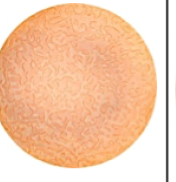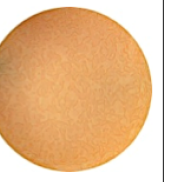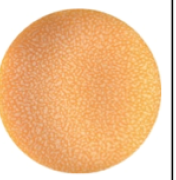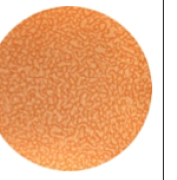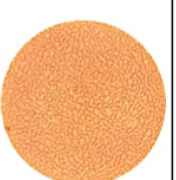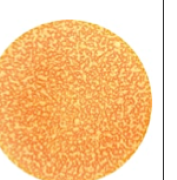
Figure 44: Different morphologies of Turing-like patterns obtained in a 3D reactor upon varying the inner and outer concentrations.

Figure 45: Labyrinthine pattern obtained at 40 mM $[Cd^{2+}]_0$ and 200 mM $[S^{2-}]_0$. Gelatin = 5%; Temp = 22 °C.

Figure 46: Stationary island-like pattern obtained at 60 mM $[Cd^{2+}]_0$ and 200 mM $[S^{2-}]_0$. Gelatin = 5%; Temp = 22 $^\circ$C.

Figure 47: Mixed state of stripes and spots obtained at 60 mM $[Cd^{2+}]_0$ and 350 mM $[S^{2-}]_0$. Gelatin = 5%; Temp = 22 °C.

Figure 48: Spot-like pattern obtained at 80 mM $[Cd^{2+}]_0$ and 300 mM $[S^{2-}]_0$. Gelatin = 5%; Temp = 22 $^\circ$C.

D. Relation between 2D and 3D Patterns

The formation of Turing-like patterns in a 3D reactor results from the stacking of layers of the 2D patterns along the third dimension. This gives rise to the complex patterns obtained due to one more degree of freedom. In order to show the correlation between the rings and spots formed in the 2D circular reactor and the 3D structures resulting in the beaker, a vertical sectional view of the pattern inside the beaker is captured. To do so, a glass slide is used to cut the gel perpendicularly to the precipitation front layer. A picture is then taken for the lateral cut to show the relation between the two dimensions. The obtained results are gathered in Figure 49. The sectional view of the Labyrinthine pattern (A) shows parallel tied bands similar to the periodic rings obtained in 2D, whereas the sectional view of the spot-like pattern (B) depicts the transition from parallel lines to spots with square/hexagonal symmetry.
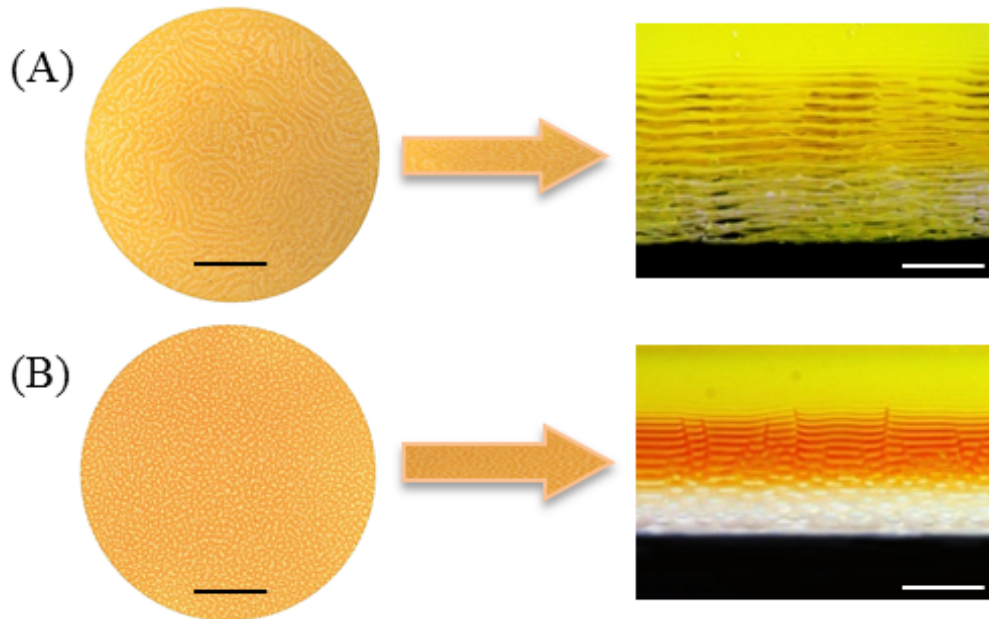
Figure 49: Sectional view of the different precipitation patterns obtained in a 3D reactor upon varying the inner and outer concentrations. (A) displays the sectional view of a labyrinthine pattern obtained when $[Cd^{2+}]_0 = 40$ mM and $[S^{2-}]_0 = 250$ mM; (B) displays the sectional view of the spot-like pattern obtained when $[Cd^{2+}]_0 = 80$ mM and $[S^{2-}]_0 = 300$ mM. The scale bar represents 1.0 cm.

Moreover, we intend to investigate theoretically the evolution of the Turing-like patterns in 3D. A numerical simulation using the CH equation is carried out. The obtained
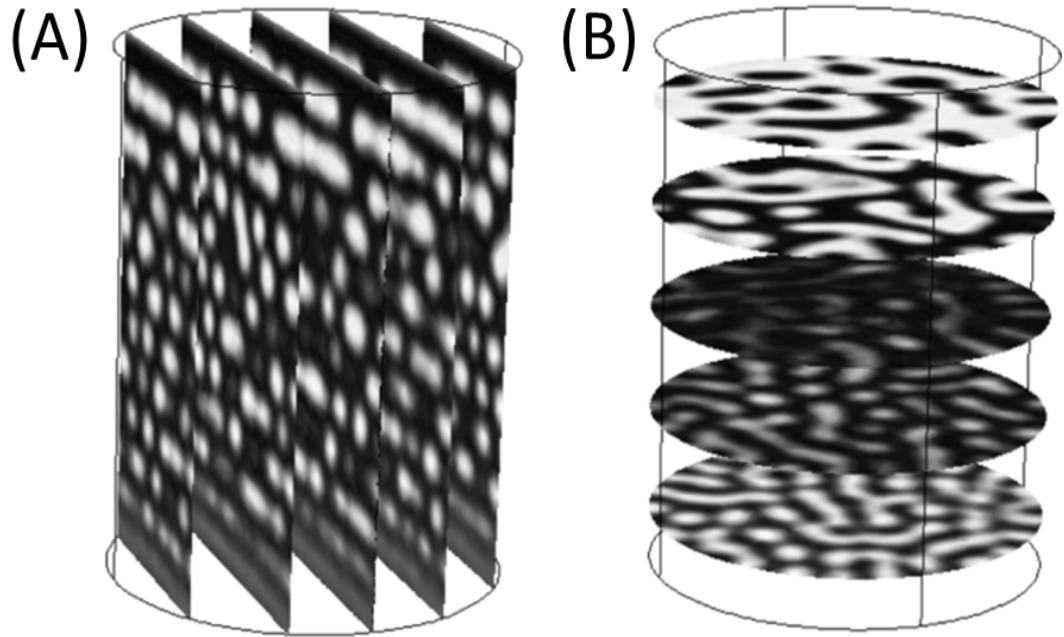
Figure 50: Three dimensional simulation representing the evolution of Turing-like patterns. (A) shows a lateral view for the resulting pattern whereas (B) displays a transversal view corresponding to the different stages obtained before reaching the stationary structure. The parameters used: $k = 1$, $D_a = 1$, $D_b = 1$, $\sigma = 0.15$, $\lambda = 1$, $\varepsilon = 1$, $\gamma = 0.15$. Initial conditions: $a_0 = 60$, $b_0 = 0.3$.

results are displayed in Figure 50, which represents transversal and lateral views at five different positions among the obtained pattern. The lateral layers (A) correspond to the lateral cuts as shown in Figure 49, while the transversal layers (B) correspond to the bottom view of the stationary precipitation front at different times during evolution (Fig. 42). The obtained model appears to match the experimental results, where the transversal layers show a mixed state of stripes and spots, and the lateral layers exhibit spots with hexagonal symmetry.

CHAPTER V

CONCLUSION

In this work, we carry out reaction-diffusion experiments that result in the formation of a new precipitation pattern in the cadmium sulfide/hydroxide system. The process takes place in gelatin gel media using the co-precipitates cadmium chloride and sodium sulfide. The first solution is placed in the gel medium and serves as the inner electrolyte and the second forms the outer electrolyte. The macroscopic evolution of the system consists of a leading white front reflecting the formation of cadmium hydroxide $Cd(OH)_2$ precipitate followed by the yellow back front designating the transformation to the cadmium sulfide CdS due to the ionic exchange process.

First, the system is studied in a two dimensional setup, which produces a transition from parallel rings to spots with square/hexagonal symmetry. A phase diagram delineating the onset of the transition and the regions of various patterns obtained upon varying the initial concentrations of the inner and outer electrolytes is presented. The inner cadmium concentration imposes a significant effect on both, the obtained morphology and the size of the resulting spots. As the concentration of cadmium increases, the system exhibits a transition from thin rings to spots whose size increases gradually with a decreasing wavelength until they all merge together to form a continuous band. On the other hand, the effect of varying the outer sulfide concentration shows no direct influence on the spot size, but it rather alters the distance covered by the spots and the spacing between them. As the concentration of the outer increases, the reaction-diffusion process proceeds faster, thus resulting in more spots whose formation occurs at closer distance. SEM images displaying the morphology and the size of the obtained bands and spots are also presented.

Second, the effect of varying other initial reaction conditions is investigated;

83

these include the variation of the temperature, gel thickness, capping agent addition, ionic strength, and electric field application. Results show that the wavelength of the resulting spots tends to increase as the concentration of the gel is increased. Moreover, the diffusion process at higher temperatures appears to proceed faster, thus allowing the precipitation and the diffusion of the white/yellow fronts to cover larger distances, and resulting in more spots whose formation starts at an earlier time. On the other hand, prevalence of rings versus spots is obtained upon increasing both, the concentration of the capping agent (β-ME) and the ionic strength of the inner electrolyte. The suppression of spots is also noticed upon applying a positive static electric field (0-1.5 V) along the reaction-diffusion system, whereas when a negative electric field is applied, the formation of spots is enhanced.

Third, the system is studied in a three-dimensional reactor, in which an interesting collection of self-organized patterns that are similar to Turing patterns are observed. The nucleated patterns represented by a bottom view of the reaction medium include: labyrinthine structure, island-like pattern, a mixed state of stripes and spots, and spatially distributed spots. A phase diagram representing these different structures obtained upon varying the concentration of the inner and outer electrolytes is also provided.

Finally, we carry out a theoretical study based on spinodal decomposition model to investigate the spatiotemporal dynamics of the obtained patterns in two and three dimensions. The gist of this theory is based on a phase separation scenario of colloidal particles that are first produced by the reaction. Under suitable conditions, these colloidal particles could subsequently phase separate into regions of low concentration (no precipitate) and high concentration (precipitate) leading to precipitation patterns. Such dynamics is described by the nonlinear Cahn-Hilliard equation which is shown to capture the experimental results.

BIBLIOGRAPHY

[1] P. Ball. *The Self-Made Tapestry: Pattern Formation in Nature*. Oxford University Press, USA, 2001.

[2] B. A. Grzybowski, K. J. M. Bishop, C. J. Campbell, M. Fialkowski, and S. K. Smoukov. Micro- and nanotechnology via reaction-diffusion. *Soft Matter*, 1(2): 114–128, 2005.

[3] R. J. Field and M. Burger. *Oscillations and Traveling Waves in Chemical Systems*. Wiley New York, 1985.

[4] P. Gray and S. K. Scott. *Chemical Oscillations and Instabilities: Non-linear Chemical Kinetics*. Oxford University Press on Demand, 1994.

[5] I. R. Epstein and J. A. Pojman. *An Introduction to Nonlinear Chemical Dynamics: Oscillations, Waves, Patterns, and Chaos*. Oxford University Press, USA, 1998.

[6] M. C. Cross and P. C. Hohenberg. Pattern formation outside of equilibrium. *Reviews of Modern Physics*, 65(3):851, 1993.

[7] P. E. Cladis and P. Palffy-Muhoray. *Spatio-temporal Patterns in Nonequilibrium Complex Systems*. Addison-Wesley, 1995.

[8] A. Koch and H. Meinhardt. Biological pattern formation: From basic mechanisms to complex structures. *Reviews of Modern Physics*, 66(4):1481, 1994.

[9] A. Goldbeter. *Biochemical Oscillations and Cellular Rhythms: The Molecular Bases Of Periodic and Chaotic Behaviour*. Cambridge University Press, 1997.

[10] M. Farkas. *Dynamical Models in Biology*. Academic Press, 2001.

[11] J. Murray. *Mathematical Biology*. Springer, 2002.

[12] P. J. Ortoleva. *Geochemical Self-Organization*. Oxford University Press, USA, 1994.

[13] J. H. Kruhl and L.-O. Rentfel. *Fractals and Dynamic Systems in Geoscience*. Springer-Verlag, 1994.

[14] A. Boudreau. The evolution of texture and layering in layered intrusions. *International Geology Review*, 53(3-4):330–353, 2010.

[15] R. J. Donnelly, R. Herman, and I. Prigogine. *Non-Equilibrium Thermodynamics, Variational Techniques, and Stability*. Univ. of Chicago Press, 1966.

[16] R. E. Liesegang. Ueber einige eigenschaften von gallerten. *Naturwissenschaftliche Wochenschrift*, 11:353–362, 1896.

[17] R. E. Liesegang. *Chemical Reactions in Gels*. Liesegang, Dusseldorf, 1898.

[18] R. E. Liesegang. *Liesegang Photograph Archiv*, 37:321–326, 1896.

[19] F. E. Lloyd and V. Moravek. Further studies in periodic precipitation. *The Journal of Physical Chemistry*, 35(6):1512–1564, 1930.

[20] T. Isemura. Studies of rhythmic precipitates. *Bulletin of the Chemical Society of Japan*, 14:179–237, 1939.

[21] L. Badr and R. Sultan. Ring morphology and pH effects in 2D and 1D $Co(OH)_2$ Liesegang systems. *The Journal of Physical Chemistry A*, 113(24):6581–6586, 2009.

[22] T. Karam, H. El-Rassy, and R. Sultan. Mechanism of revert spacing in a $PbCrO_4$ Liesegang system. *The Journal of Physical Chemistry A*, 115(14):2994–2998, 2011.

[23] N. Kanniah, F. D. Gnanam, P. Ramasamy, and G. S. Laddha. Revert and direct type Liesegang phenomenon of silver iodide. *Journal of Colloid and Interface Science*, 80(2):369–376, 1981.

[24] M. Flicker and J. Ross. Mechanism of chemical instability for periodic precipitation phenomena. *The Journal of Chemical Physics*, 60(9):3458–3465, 1974.

[25] S. K. Smoukov, I. Lagzi, and B. A. Grzybowski. Independence of primary and secondary structures in periodic precipitation patterns. *The Journal of Physical Chemistry Letters*, 2(4):345–349, 2011.

[26] L. Mandalian and R. Sultan. Fractal structures in PbF_2/$Pb(NO_3)_2$ precipitate systems. *Collection of Czechoslovak Chemical Communications*, 67:1729–1742, 2002.

[27] A. Volford, F. Izsak, M. Ripszam, and I. Lagzi. Pattern formation and self-organization in a simple precipitation system. *Langmuir*, 23(3):961–964, 2007.

[28] R. Suganthi, E. Girija, S. Narayana Kalkura, H. Varma, and A. Rajaram. Self-assembled right handed helical ribbons of the bone mineral hydroxyapatite. *Journal of Materials Science: Materials in Medicine*, 20(0):131–136, 2009.

[29] J. Jackson, J. Mehl, and Neuendorf. *Glossary of Geology*. Springer, 2005.

[30] H. Meinhardt. *The Algorithmic Beauty of Sea Shells*. New York: Springer, 2009.

[31] R. E. Liesegang. *Selbstorganisation Chemischer Strukturen*. Ostwalds Klassiker der exakten Wissenschaften. Deutsch, 1999.

[32] S. Sadek and R. Sultan. Liesegang patterns in nature: A diverse scenery across the sciences. In I. Lagzi, editor, *Precipitation Patterns in Reaction-Diffusion Systems*, pages 1–43. Trivandrum, Research Signpost publications, 2011.

[33] M. B. Short, J. C. Baygents, J. W. Beck, D. A. Stone, I. Toomey, Rickard S., and R. E. Goldstein. Stalactite growth as a free-boundary problem: A geometric law and its platonic ideal. *Physical Review Letters*, 94(1), 2005.

[34] P. Y. Chan and N. Goldenfeld. Steady states and linear stability analysis of precipitation pattern formation at geothermal hot springs. *Physical Review E*, 76:046104, 2007.

[35] S. Kondo. The reaction-diffusion system: a mechanism for autonomous pattern formation in the animal skin. *Genes to Cells*, 7:535, 2002.

[36] P. Heaney and A. Davis. Observation and origin of self-organized textures in agates. *Science*, 269:1562, 1995.

[37] E. Ben-Jacob, O. Schochet, A. Tenenbaum, I. Cohen, A. Czirok, and T. Vicsek. Generic modelling of cooperative growth patterns in bacterial colonies. *Nature*, 368(6466):46–49, 1994.

[38] G. Nicolis and I. Prigogine. *Self-Organization in Nonequilibrium Systems: From Dissipative Structures to Order Through Fluctuations*. Wiley, 1977.

[39] S. Prager. Periodic precipitation. *The Journal of Chemical Physics*, 25(2):279–283, 1956.

[40] G. T. Dee. Patterns produced by precipitation at a moving reaction front. *Physical Review Letters*, 57(3):275–278, 1986.

[41] R. Sultan, P. Ortoleva, F. DePasquale, and P. Tartaglia. Bifurcation of the Ostwald-Liesegang supersaturation-nucleation-depletion cycle. *Earth-Science Reviews*, 29 (14):163–173, 1990.

[42] D. Smith. On Ostwald's supersaturation theory of rhythmic precipitation (Liesegang's rings). *The Journal of Chemical Physics*, 81(7):3102–3115, 1984.

[43] R. Feeney, S. L. Schmidt, P. Strickholm, J. Chadam, and P. Ortoleva. Periodic precipitation and coarsening waves: Applications of the competitive particle growth model. *The Journal of Chemical Physics*, 78(3):1293–1311, 1983.

[44] R. Sultan and P. Ortoleva. Periodic and aperiodic macroscopic patterning in two precipitate post-nucleation systems. *Physica D: Nonlinear Phenomena*, 63(1):202–212, 1993.

[45] W. Ostwald. *Lehrbuch der Allgemeinen Chemie*. Engelmann: Leipzig, Germany, 1897.

[46] C. Wagner. Mathematical analysis of the formation of periodic precipitations. *Journal of Colloid Science*, 5(1):85–97, 1950.

[47] Y. B. Zeldovich, G. Barenblatt, and R. Salganik. On the quasiperiodic precipitation of sediment under mutual diffusion of two substances (LiesegangâĂŹs rings). 140: 1281–1284, 1961.

[48] T. Antal, M. Droz, J. Magnin, Z. Racz, and M. Zrinyi. Derivation of the matalon-packter law for Liesegang patterns. *The Journal of Chemical Physics*, 109(21): 9479–9486, 1998.

[49] S. C. Mueller, S. Kai, and J. Ross. Periodic precipitation patterns in the presence of concentration gradients. 1. dependence on ion product and concentration difference. *The Journal of Physical Chemistry*, 86(20):4078–4087, 1982.

[50] D. Feinn, P. Ortoleva, W. Scalf, S. Schmidt, and M. Wolff. Spontaneous pattern formation in precipitating systems. *The Journal of Chemical Physics*, 69(1):27–39, 1978.

[51] I. M. Lifshitz and V. V. Slyozov. The kinetics of precipitation from supersaturated solid solutions. *Journal of Physics and Chemistry of Solids*, 19(1):35–50, 1961.

[52] S. Kai, S. C. Muller, and J. Ross. Measurements of temporal and spatial sequences of events in periodic precipitation processes. *The Journal of Chemical Physics*, 76 (3):1392–1406, 1982.

[53] E. S. Hedges and R. V. Henley. The formation of Liesegang rings as a periodic coagulation phenomenon. *Journal of the Chemical Society*, 0(0):2714–2726, 1928.

[54] A. A. Polezhaev and S. C. Muller. Complexity of precipitation patterns: Comparison of simulation with experiment. *Chaos: An Interdisciplinary Journal of Nonlinear Science*, 4(4):631–636, 1994.

[55] D. S. Chernavskii, A. A. Polezhaev, and S. C. Muller. A model of pattern formation by precipitation. *Physica D: Nonlinear Phenomena*, 54(1âĂŞ2):160–170, 1991.

[56] C. V. Raman and K. S. Ramaiah. The wave-like character of periodic precipitates. *Proc. - Indian Acad. Sci., Sect. A*, 9A:455–66, 1939.

[57] H. J. Arnikar and D. Meenamani. A tracer study of Liesegang rings. *Kolloid-Z.*, 189:57–9, 1963.

[58] H. B. Weiser. *Inorganic Colloidal Chemistry*, volume III. Wiley, New York, 1938.

[59] G. Venzl and J. Ross. Nucleation and colloidal growth in concentration gradients (Liesegang rings). *The Journal of Chemical Physics*, 77(3):1302–1307, 1982.

[60] S. C. Muller and J. Ross. Spatial structure formation in precipitation reactions. *The Journal of Physical Chemistry A*, 107(39):7997–8008, 2003.

[61] N. Palaniandavar, F. D. Gnanam, and P. Ramasamy. Diffusion controlled autocatalytic growth of revert periodic precipitation of cadmium sulphide in lyophillic colloid. *The Journal of Chemical Physics*, 80(7):3446–3450, 1984.

[62] J. Ross, A. P. Arkin, and S. C. Mueller. Experimental evidence for Turing structures. *The Journal of Physical Chemistry*, 99(25):10417–10419, 1995.

[63] A. M. Turing. The chemical basis of morphogenesis. *Philosophical Transactions of the Royal Society of London. Series B, Biological Sciences*, 237(641):37–72, 1952.

[64] V. Castets, E. Dulos, J. Boissonade, and P. De Kepper. Experimental evidence of a sustained standing Turing-type nonequilibrium chemical pattern. *Physical Review Letters*, 64(24):2953–2956, 1990.

[65] I. Lengyel, S. Kadar, and I. R. Epstein. Transient Turing structures in a gradient-free closed system. *Science*, 259(5094):493–495, 1993.

[66] G. Biosa, S. Bastianoni, and M. Rustici. Chemical waves. *Chemistry, A European Journal*, 12(13):3430–3437, 2006.

[67] P. De Kepper, V. Castets, E. Dulos, and J. Boissonade. Turing-type chemical patterns in the chlorite-iodide-malonic acid reaction. *Physica D: Nonlinear Phenomena*, 49(12):161–169, 1991.

[68] Q. Ouyang and H. L. Swinney. Transition to chemical turbulence. *Chaos: An Interdisciplinary Journal of Nonlinear Science*, 1(4):411–420, 1991.

[69] I. Lengyel, G. Rabai, and I. R. Epstein. Experimental and modeling study of oscillations in the chlorine dioxide-iodine-malonic acid reaction. *Journal of the American Chemical Society*, 112(25):9104–9110, 1990.

[70] K.-J. Lee, W. D. McCormick, J. E. Pearson, and H. L. Swinney. Experimental observation of self-replicating spots in a reaction-diffusion system. *Nature*, 369 (6477):215–218, 1994.

[71] H. Liu, J. A. Pojman, Y. Zhao, C. Pan, J. Zheng, L. Yuan, A. K. Horvath, and

Q. Gao. Pattern formation in the iodate-sulfite-thiosulfate reaction-diffusion system. *Physical Chemistry Chemical Physics*, 14(1):131–137, 2012.

[72] B. Belousov. *Collection of Short Papers on Radiation Medicine*. Medgiz, Moscow, 1959.

[73] A. N. Zaikin and A. M. Zhabotinsky. Concentration wave propagation in two-dimensional liquid-phase self-oscillating system. *Nature*, 225(5232):535–537, 1970.

[74] J. Carballido-Landeira, V. K. Vanag, and I. R. Epstein. Patterns in the belousov-zhabotinsky reaction in water-in-oil microemulsion induced by a temperature gradient. *Physical Chemistry Chemical Physics*, 12(15):3656–3665, 2010.

[75] Z. Racz. Formation of Liesegang patterns. *Physica A: Statistical Mechanics and its Applications*, 274(12):50–59, 1999.

[76] T. Antal, M. Droz, J. Magnin, and Z. Racz. Formation of Liesegang patterns: A spinodal decomposition scenario. *Physical Review Letters*, 83(15):2880–2883, 1999.

[77] R. Matalon and A. Packter. The Liesegang phenomenon. i. sol protection and diffusion. *Journal of Colloid Science*, 10(1):46–62, 1955.

[78] L. Galfi and Z. Racz. Properties of the reaction front in an A+B $\rightarrow$ C type reaction-diffusion process. *Physical Review A*, 38(6):3151–3154, 1988.

[79] J. W. Cahn and J. E. Hilliard. Free energy of a nonuniform system. i. interfacial free energy. *The Journal of Chemical Physics*, 28(2):258–267, 1958.

[80] J. W. Cahn. On spinodal decomposition. *Acta Metallurgica*, 9(9):795 – 801, 1961.

[81] C. K. Jablczynski. La formation rythmique des precipites: Les anneaux de Liesegang [rhythmic formation of the precipitates: Liesegang rings]. *Bulletin de la Societe Chimique de France*, 4:1592, 1923.

[82] H. W. Morse and G. W. Pierce. Diffusion and supersaturation in gelatine. *Physical Review (Series I)*, 17(3):129–150, 1903.

[83] M. Droz, J. Magnin, and M. Zrinyi. Liesegang patterns: Studies on the width law. *Journal of Chemical Physics*, 110:9618–9622, 1999.

[84] S. C. Muller, S. Kai, and J. Ross. Curiosities in periodic precipitation patterns. *Science*, 216(4546):635–637, 1982.

[85] K. M. Pillai, V. K. Vaidyan, and M. A. Ittyachan. Theory of Liesegang phenomena. *Colloid and Polymer Science*, 258:831–8, 1980.

[86] W. Daus and O. F. Tower. Colloidal behavior of the sulfides and hydroxides of cadmium and zinc. *The Journal of Physical Chemistry*, 33:605–12, 1929.

[87] B. M. Mehta and K. Kant. Periodic precipitation of cadmium sulfide. *Proceedings of the National Academy of Science, India, Sect. A*, pages 253–6, 1970.

[88] N. Palaniandavar, N. Kanniah, F. D. Gnanam, and P. Ramaswamy. Charge reversal in cadmium sulfide in diffusion controlled pattern formation process in agar gel. *Bulletin of Materials Science*, 7:105–10, 1985.

[89] B. A. Grzybowski and C. J. Campbell. Fabrication using programmed reactions. *Materials Today*, 10:38–46, 2007.

[90] W. Lu and C. M. Lieber. Nanoelectronics from the bottom up. *Nature materials*, 6 (11):841–850, 2007.

[91] M.-A. Han, S.-H. Jun, and Y. Kang. Effect of electrolyte on the shapes of Liesegang rings. *Journal of the Korean Chemical Society*, 52:356, 2008.

[92] A. Toramaru, T. Harada, and T. Okamura. Experimental pattern transitions in a Liesegang system. *Physica D*, 183:133–140, 2003.

[93] I. Bensemann, M. Fialkowski, and B. Grzybowski. Wet stamping of microscale periodic precipitation patterns. *The Journal of Physical Chemistry B*, 109(7):2774–2778, 2005.

[94] I. Bena, M. Droz, and Z. Racz. Formation of Liesegang patterns in the presence of an electric field. *The Journal of Chemical Physics*, 122:204502/1–204502/9, 2005.

[95] I. Lagzi. Controlling and engineering precipitation patterns. *Langmuir*, 28(7):3350–3354, 2012.

[96] Z. Shreif, L. Mandalian, A. Abi-Haydar, and R. Sultan. Taming ring morphology in 2d Co(OH)$_2$ Liesegang patterns. *Physical Chemistry Chemical Physics*, 6(13):3461–3466, 2004.

[97] S. L. Patil, R. D. Ladhe, P. K. Baviskar, B. R. Sankapal, et al. Ion exchange processed CdS nanorods in powder form using cadmium hydroxide nanowires by wet chemical route. *Journal of Scientific Review*, 2(2):91–95, 2010.

[98] I. Hecht, Y. Moran, and H. Taitelbaum. Reaction-diffusion front width anomalies in disordered media. *Physical Review E*, 73(5):051109, 2006. PRE.

[99] S. Van Vlierberghe, V. Cnudde, P. Dubruel, B. Masschaele, A. Cosijns, I. De Paepe, P. J. S. Jacobs, L. Van Hoorebeke, J. P. Remon, and E. Schacht. Porous gelatin hydrogels: 1. cryogenic formation and structure analysis. *Biomacromolecules*, 8(2):331–337, 2007.

[100] L. V. Turco. *Controlled Synthesis of Nanoparticles in Microheterogeneous Systems*. Springer, 2006.

[101] N. V. Hullavarad and S. S. Hullavarad. Optical properties of organic and inorganic capped CdS nanoparticles and the effects of x-ray irradiation on organic capped CdS nanoparticles. *Journal of Vacuum Science and Technology, A*, 26:1050–1057, 2008.

[102] I. Lagzi. Formation of Liesegang patterns in an electric field. *Physical Chemistry Chemical Physics*, 4(8):1268–1270, 2002.

[103] I. Lagzi and F. Izsak. Stochastic description of precipitate pattern formation in an electric field. *Physical Chemistry Chemical Physics*, 5:4144–4148, 2003.

[104] R. Sultan and R. Halabieh. Effect of an electric field on propagating $Co(OH)_2$ Liesegang patterns. *Chemical Physics Letters*, 332(34):331–338, 2000.

[105] I. Das, A. Pushkarna, and A. Bhattacharjee. New results on light-induced spatial bifurcation and electrical field effect on chemical waves in the mercury(ii) chloride-potassium iodide system in gel media. *The Journal of Physical Chemistry*, 94(26): 8968–8973, 1990.

[106] C. Wagner. Theorie der alterung von niederschlagen durch umlosen (Ostwald-reifung). *Zeitschrift fur Elektrochemie, Berichte der Bunsengesellschaft fur physikalische Chemie*, 65:581–591, 1961.

[107] M. Hillert. A solid-solution model for inhomogeneous systems. *Acta Metallurgica*, 9(6):525 – 535, 1961.

[108] C. Chevallard, M. Clerc, P. Coullet, and J. M. Gilli. Interface dynamics in liquid crystals. *Eur. Phys. J. E*, 1:179–188, 2000.

[109] C. Godreche. *Solids Far from Equilibrium*. Cambridge University Press, 1991.

[110] A. Stegner and J. E. Wesfreid. Dynamical evolution of sand ripples under water. *Physical Review E*, 60:R3487–R3490, 1999.

[111] M. Al-Ghoul, T. Ghaddar, and T. Moukalled. Pulse-front propagation and interaction during the growth of CdS nanoparticles in a gel. *The Journal of Physical Chemistry B*, 113(34):11594–11603, 2009.

[112] E. M. Foard and A. J. Wagner. Survey of morphologies formed in the wake of an enslaved phase-separation front in two dimensions. *Phys. Rev. E*, 85:011501, 2012.

[113] S. Cornell and M. Droz. Steady-state reaction-diffusion front scaling for mA+nB = 0. *Physical Review Letters*, 70(24):3824–3827, 1993. PRL.

[114] S. Thomas, I. Lagzi, J. Molnar, Ferenc, and Z. Racz. Probability of the emergence of helical precipitation patterns in the wake of reaction-diffusion fronts. *Physical Review Letters*, 110:078303/1–078303/5, 2013.

[115] A. Abi Mansour and M. Al-Ghoul. Vertex-based finite volume simulation of Liesegang patterns on structureless meshes. *Physical Review E*, 89:033303, 2014.

[116] J. R. Shewchuk. Delaunay refinement algorithms for triangular mesh generation. *Computational Geometry*, 22(1):21–74, 2002.

[117] J. Rahbani, A. R. Behzad, N. M. Khashab, and M. Al-Ghoul. Characterization of internal structure of hydrated agar and gelatin matrices by cryo-sem. *Electrophoresis*, 34(3):405–408, 2013.

[118] T. Mokalled. *Preparation of Cadmium Sulfide Nanoparticles in Gel Media: Experimental and Theoretical Study of a New Pulse Propagating System*. Thesis, 2010.

[119] T. Sugimoto, S. Chen, and A. Muramatsu. Synthesis of uniform particles of CdS, ZnS, PbS and CuS from concentrated solutions of the metal chelates. *Colloids and Surfaces A*, 135(1):207–226, 1998.

[120] V. Smyntyna, V. Skobeeva, and N. Malushin. The nature of emission centers in cds nanocrystals. *Radiation Measurements*, 42(4):693–696, 2007.

[121] C. Burda, X. Chen, R. Narayanan, and M. A. El-Sayed. Chemistry and of nanocrystals of different shapes. *Chemical Reviews*, 105(4):1025–1102, 2005.

[122] V. Kulvietis, G. Streckyte, and R. Rotomskis. Spectroscopic investigations of CdTe quantum dot stability in different aqueous media. *Lithuanian Journal of Physics*, 51:163–171, 2011.

[123] K. M. Mullaugh and I. Luther, George W. Spectroscopic determination of the size of cadmium sulfide nanoparticles formed under environmentally relevant conditions. *Journal of Environmental Monitoring*, 12:890–897, 2010.

[124] G. Tai, J. Zhou, and W. Guo. Inorganic salt-induced phase control and optical characterization of cadmium sulfide nanoparticles. *Nanotechnology*, 21(17):175601, 2010.

[125] J. Tabony, N. Glade, J. Demongeot, and C. Papaseit. Biological self-organization by way of microtubule reaction-diffusion processes. *Langmuir*, 18:7196–7207, 2002.

[126] E. O. Budrene and H. C. Berg. Dynamics of formation of symmetrical patterns by chemotactic bacteria. *Nature*, 376:49–53, 1995.

[127] S. A. Newman. Lineage and pattern in the developing vertebrate limb. *Trends in Genetics*, 4:329–32, 1988.

[128] S. A. Newman and H. L. Frisch. Dynamics of skeletal pattern formation in developing chick limb. *Science*, 205:662–8, 1979.

[129] Q. Ouyang and H. L. Swinney. Transition from a uniform state to hexagonal and striped Turing patterns. *Nature*, 352(6336):610–612, 1991.

[130] A. De Wit, P. Borckmans, and G. Dewel. Twist grain boundaries in three-dimensional lamellar Turing structures. *Proceedings of the National Academy of Sciences*, 94(24):12765–12768, 1997.

[131] H. Shoji, K. Yamada, D. Ueyama, and T. Ohta. Turing patterns in three dimensions. *Physical Review E*, 75:046212/1–046212/13, 2007.

[132] A. De Wit, G. Dewel, P. Borckmans, and D. Walgraef. Three-dimensional dissipative structures in reaction-diffusion systems. *Physica D: Nonlinear Phenomena*, 61(1):289–296, 1992.